Alma Mater Studiorum – University of Bologna

SCHOOL OF SCIENCE

Department of Industrial Chemistry "Toso Montanari"

Second cycle degree in

Low Carbon Technologies and Sustainable Chemistry

Classe LM-71 - Scienze e Tecnologie della Chimica Industriale

Kraft lignin depolymerization to added-value building blocks by electrooxidation over Ni and Cu electrocatalysts

Experimental degree thesis

CANDIDATE

Ilenia Giarnieri

SUPERVISOR

Chiar.ma Prof. Patricia Benito Martin

CO-SUPERVISOR

Dr. Claudio Gioia

Monica Nota

KEY WORDS

Kraft lignin

Electrocatalysis

Ni

Cu

Foam

Vanillin

ABSTRACT

Lignin is a natural by-product coming from lignocellulosic biomass. Due to its polymeric aromatic structure, it is becoming an attractive source of aromatic building blocks, but the complexity and the heterogeneity of this material makes its depolymerization challenging. Among the possible depolymerization treatments, electrocatalysis have been adopted in this work to depolymerize lignin in basic media and mild conditions, applying renewable electricity, by means of an electrocatalytic process. Four types of catalysts, based on open-cell foams, have been tested: Ni bare, Cu bare, calcined Ni and calcined Cu. All of them have been characterized chemical-physically by SEM, XRD and Raman and electrochemically by cyclic voltammetry. Their activities have been evaluated by comparing obtained yield of vanillin, acetovanillone and guaiacol, the most recurrent products. Ni bare displayed the highest total yield. The effects of applied potential and reaction time on total products yields were evaluated. The best operating conditions were found to be 0.7 V vs SCE applied potential and 10 minutes reaction time.

AIM OF THE WORK

In the attempt to reduce global CO_2 emissions and fossil fuels dependance, chemical industry could evolve by performing sustainable processes. The use of biomass is one of the possible solutions to environmental issues, by starting from a bio-source of chemicals and materials and performing carbon neutral processes.

Lignin is an important fraction of lignocellulosic biomass, currently burned to get energy, and it is a bio-source of aromatic building blocks, like vanillin, guaiacol and acetovanillone, which are employed in food, chemical, pharmaceutical and fragrance industries.

The aim of the thesis work is to depolymerize Kraft lignin structure into value-added building blocks by means of electrocatalysis and searching for the best operating conditions and catalyst type, trying to continue and optimize the previous thesis projects. Ni bare, Cu bare, calcined Ni and calcined Cu open-cell foam catalysts have been tested for lignin electrooxidation. The product mixture treatments and extraction procedure have been optimized and a quantification of the most recurring products was possible through GC-MS. Cyclic voltammetry and chronoamperometry experiments were conducted to study the catalytic activity and the unfolding of the reaction.

Index

1. Introduction

1.1 Climate change and fossil fuels dependance

Climate changes have always been existed periodically in the world history, as a sign of our planet activity. Currently we are affected by drastic changes in temperatures and ecosystem services, which are clearly observable in a shorter temporal window, probably because of man's activities that affect our environment. What took a back seat in the past, cannot be underestimated anymore in 2021. There is a feedback between climate and CO_2 (Fig. 1.1), in fact temperature increases together with CO_2 emissions, whose major responsible are nowadays fossil fuels dependance and all those activities related to them [1]. Carbon dioxide concentration into atmosphere was about 409.8 ppm in 2019, with a rate of 2,5 ppm for year. The measured concentration in the pre-industrial era was about 280 ppm [2].

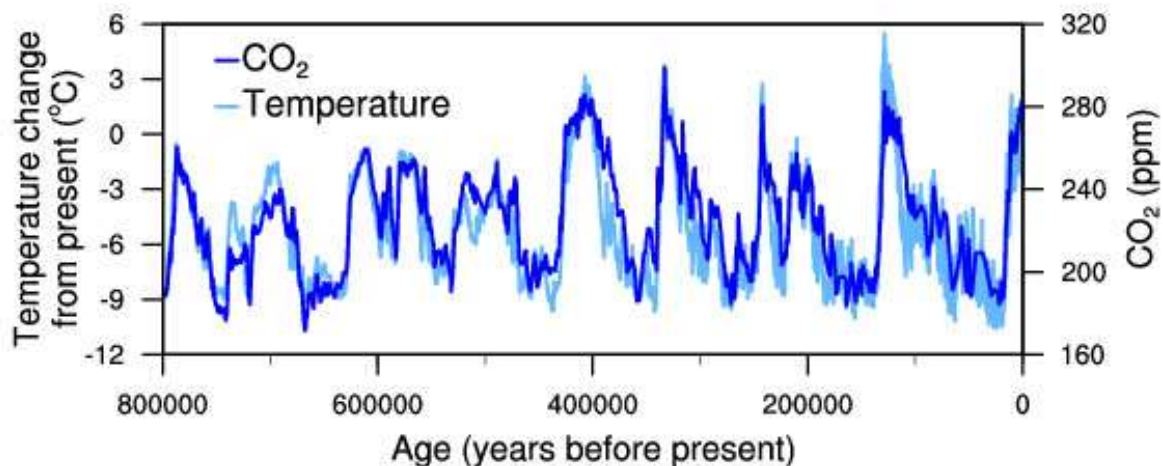*Figure 1.1 Temperature change (light blue) and carbon dioxide change (dark blue) measured from the EPICA Dome C ice core in Antarctica. [1]*

From 1901, the rate of increasing temperatures on the Earth was 0,7-0,9°C per century, but from 1975 it almost doubled to 1,5-1,8°C. In particular, in Italy, in the last 100th years there is an increase of 2°C [3]. In Figure 1.2, March temperature anomalies are reported, until 2020.

Global Land and Ocean

March Temperature Anomalies
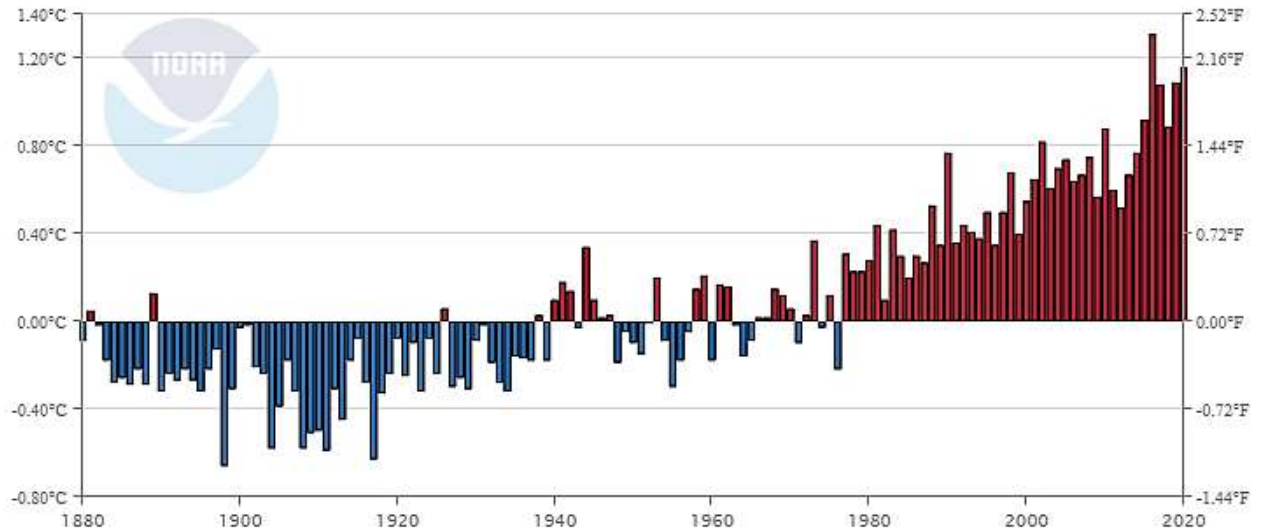
Figure 1.2 March temperature anomalies from 1880 to 2020, National Centers for Environmental Information – National Oceanic and Atmospheric Administration (Ncei-Noaa) [3]

We have just seen an anomalous trend for pollution and CO_2 emissions in the 2020, during lockdown months for Covid-19 emergency. We changed a lot our behavior in daily activities, obliged to stay at home and reduce at the strictly necessary the use of transports like cars and planes. It is a proof of the fact that to solve environmental problems we should change our way of thinking, together with a transformation of the industrial activities, when possible.
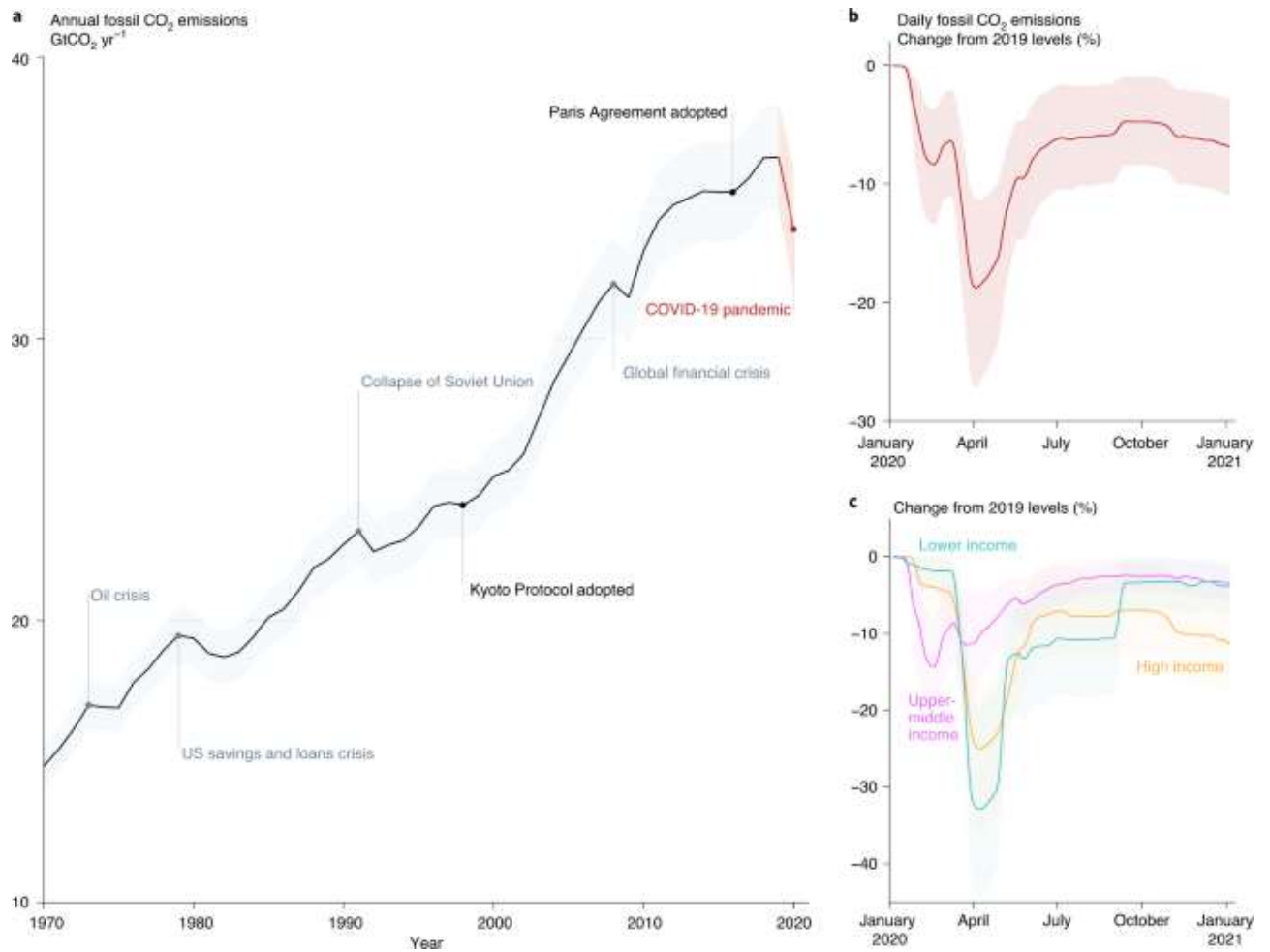
Figure 1.3 Fossil CO2 emissions in the post-COVID-19 era [4]

From the Figure 1.3 there is a clear decreasing trend for CO_2 emissions, related to the pandemic event, and moreover it can be seen how important it is to set goals and laws, like Kyoto Protocol and Paris Agreement. In this regard, ONU established sustainable development goals, that are a universal call for action as part of the 2030 Agenda for Sustainable Development (Fig 1.4) [5]. Moreover, new goals for carbon neutrality and economic growth are set in 2020 by the Green Deal between European countries.

Figure 1.4 Sustainable Development Goals [5]

An important target established by ONU summit is not to exceed average temperatures of 2°C with respect to pre-industrial values and thus global emissions should be limited to 1000 and 1500 billions of tons of CO_2 between 2000 and 2050. In 2001 there were 34 billions of tons of CO2, that was the 3% more than the previous year. From 2000 to 2011 420 billions of tons of CO2 were registered [2].

1.1.1 Greenhouse effect and GHG

Greenhouse effect is a natural phenomenon, taking place on our Earth surface, that controls the absorption of IR incoming radiation from the sun by means of greenhouse gases (GHG). The direct effect is the warming of Earth's surface and the troposphere. If GHG concentration increases, the result of the greenhouse effect would be an overall increase of temperatures, because the activity of these gases is overstimulated. The main GHG are CO_2, CH_4, N_2O, CCl_2F_2, $CHCl_2F_2$, CF_4, SF_6 and their effect depends on the concentration and on the global warming potential (GWP), defined as the contribution to the greenhouse effect with respect to CO_2, whose GWP is set to 1, as shown in Fig. 1.5

The main greenhouse gases

Greenhouse gases	Chemical formula	Pre-industrial concentration	Concentration in 1994	Atmospheric lifetime (years)***	Anthropogenic sources	Global warming potential (GWP) *
Carbon-dioxide	CO_2	278 000 ppbv	358 000 ppbv	Variable	Fossil fuel combustion Land use conversion Cement production	1
Methane	CH_4	700 ppbv	1721 ppbv	12,2 +/- 3	Fossil fuels Rice paddies Waste dumps Livestock	21**
Nitrous oxide	N_2O	275 ppbv	311 ppbv	120	Fertilizer industrial processes combustion	310
CFC-12	CCl_2F_2	0	0,503 ppbv	102	Liquid coolants. Foams	6200-7100 ****
HCFC-22	$CHClF_2$	0	0,105 ppbv	12,1	Liquid coolants	1300-1400 ****
Perfluoromethane	CF_4	0	0,070 ppbv	50 000	Production of aluminium	6 500
Sulphur hexa-fluoride	SF_6	0	0,032 ppbv	3 200	Dielectric fluid	23 900

Note : pptv= 1 part per trillion by volume; ppbv= 1 part per billion by volume, ppm v= 1 part per million by volume

Figure 1.5 The main GHG and their GWP [6]

The more CO_2 is produced, affecting greenhouse effect, the more the carbon cycle is altered. Since anthropogenic activities are creating more CO_2 emissions, the natural carbon cycle, in which forests and oceans act as sink for CO_2, is not able to balance carbon fluxes. In Figure 1.6, the entire natural and anthropogenic carbon cycle is illustrated, with the identification of sinks, sources and fluxes of carbon.
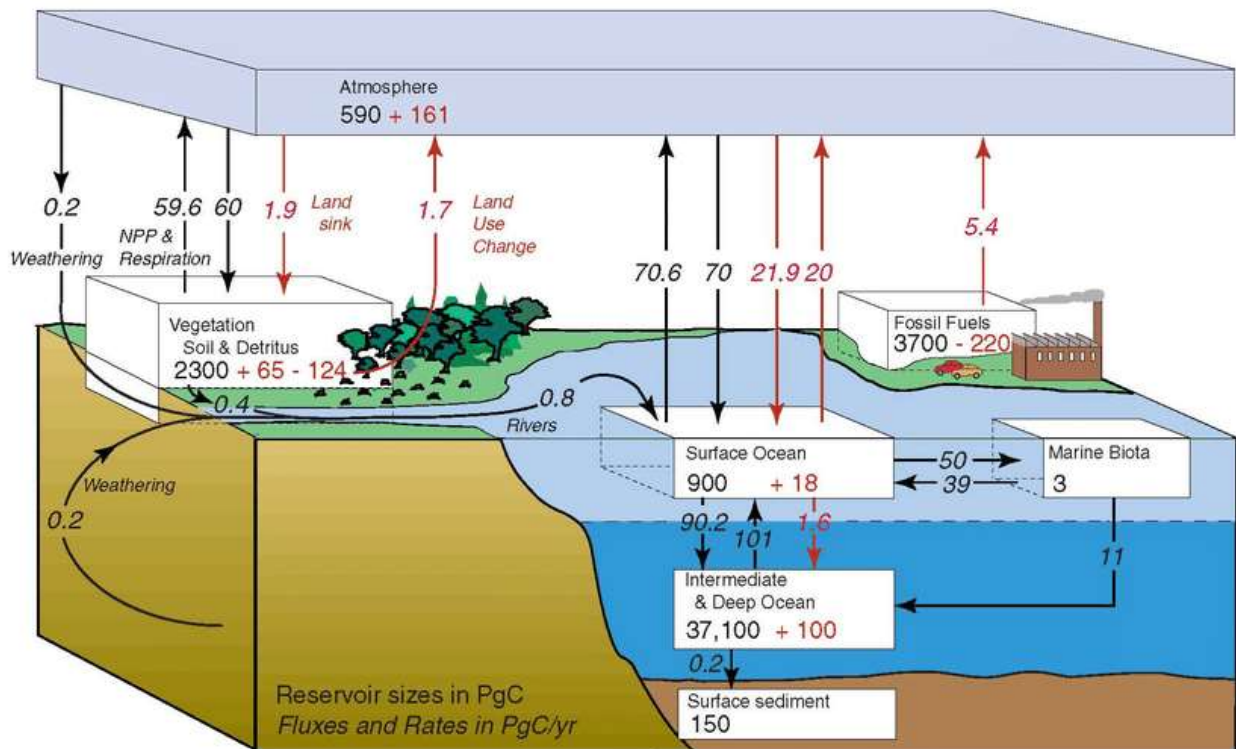
Figure 1.6 Carbon cycle with natural fluxes (black) and anthropogenic fluxes (red) of carbon. [7]

Sources of CO_2 can be natural like decomposition, ocean releases and respiration, and anthropogenic, like cement production, deforestation, land use, burning of fossil fuels and industrial activities.

1.1.2 CO_2 capture, storage and utilization

It is necessary to limit the increasing of CO_2 concentration into the atmosphere by searching for alternative sources to fossil fuels, reducing land use and deforestation, and/or by trapping CO_2, avoiding its release into the environment. Carbon capture and storage (CCS) is becoming a hot and interesting topic, but it is a hard task at the same time, because carbon dioxide should be trapped in a stable form, without damaging the surrounding environment.

Being oceans a potential sink for carbon dioxide, they should be considered in principle good candidates for CCS, but unfortunately they would be damaged by high CO_2 concentrations and by acidic pH that compromises the entire ecosystem. A good alternative for CCS is represented by salty aquifers that are not suitable anymore for drinkable water and became unusable, as shown in Figure 1.7.

Carbon utilization includes different ways to use or recycle captured carbon to produce economically valuable products [8]. The most common techniques for carbon utilization include:

- **CO_2 electrolysis** to formate, oxalate and methanol;
- **Carbon-neutral fuel** synthesis by using captured CO_2 as hydrocarbon source;
- **Chemical synthesis** of acetic acid, urea, PVC and polycarbonates;
- **Enhanced oil recovery** by injecting CO_2 into depleted oil fields to increase oil output;
- **Carbon mineralization** with alkaline reactants, such as magnesium oxide and calcium oxide, to form carbonates, bicarbonates, cements and other inorganic materials involved in construction sector.

CCS is suitable for carbon dioxide "end-of-life", but regarding the production of CO_2, biomass and alternative sources come into help. Replacing the burning of fossil fuels and thus the emissions of huge amounts of CO_2, there would be the chance to close the loop on elements cycle and to limit wastes. A lot of industries are pointing more and more to carbon neutrality processes, that means zero net emissions of CO_2.

Carbon Capture and Storage (CCS)

The distance between the power station and the CCS storage facility can extend to distances of over 500 kilometres

CO_2 is injected and stored underground

Impermeable cap-rock keeps CO_2 underground

The CO_2 is pumped to a depth of about 1.5 km or more

Depleted oil or gas reservoir

Natural saline aquifer

Inset right:
CO_2 becomes stabilised within the porous rock as it forms natural compounds with the surrounding brine and minerals
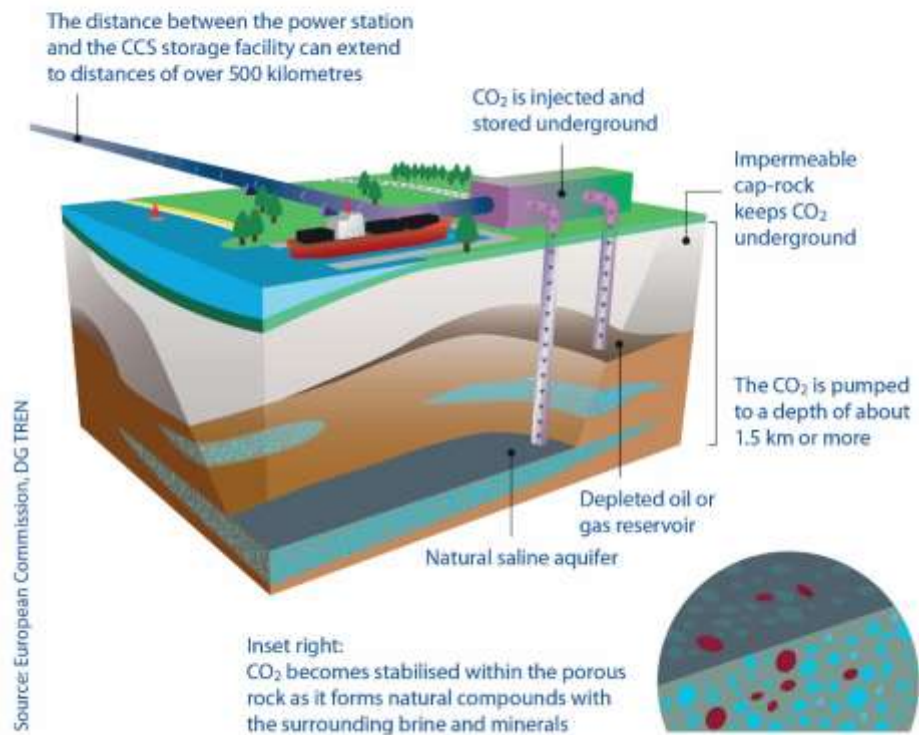
Figure 1.6 Carbon capture and storage [9]

1.2 Biomass and biorefinery

In the search for alternative sources to replace fossil fuels, biomass is a good candidate. Biomass refers to the mass of living organisms, including plants, animals and microorganisms, including both the above- and belowground tissues of plants [10]. Chemical energy contained into plants, in the form of sugars, derives directly from sunlight that is the main ingredient for photosynthesis (Fig. 1.8). Plants are autotrophs, because they can get energy autonomously from sun, feeding on CO_2 as carbon source and producing O_2 as co-product.
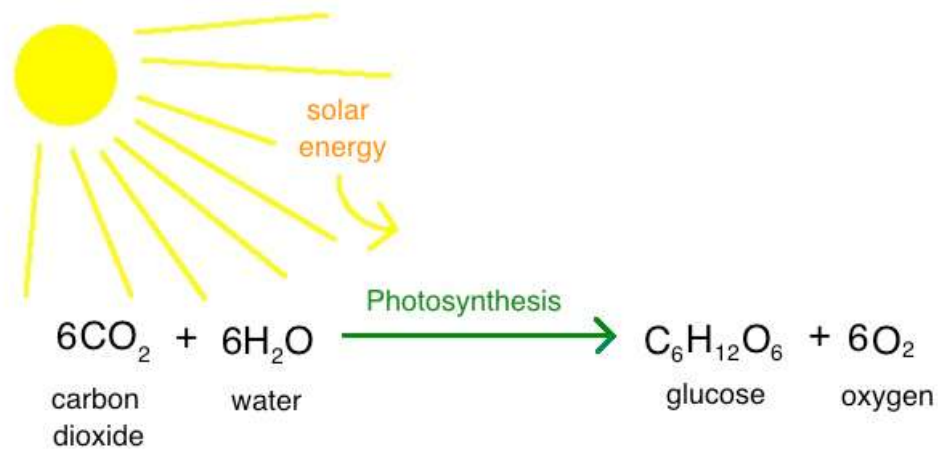
Figure 1.7 Scheme of Photosynthesis [11]

Microorganisms, instead, usually take energy and carbon source from organic or inorganic matter, representing the biomass for biotechnologies. In analogy with common refineries that use fossil fuels as raw materials, biomass is treated and exploited in the so called biorefinery (Fig. 1.10). The common definition of the term is: "Biorefining is the sustainable processing of biomass into a spectrum of marketable products and energy" [12]. It is a facility that comprehends all the processes concerning biomass conversion to building blocks and finally to value added products, biofuels and chemicals [13]. Biomass conversion processes can be divided into three groups: fermentative, chemical and thermochemical processes.

- **Thermochemical processes** aim at breaking down the starting material into smaller molecules and can make use of different types of biomass source. The most common thermochemical processes are gasification, pyrolysis, liquefaction and combustion [14].

- **Fermentative processes** are performed by microorganisms that are forced to follow a fermentation metabolism in particular conditions, producing the compound of interest. Many fermentative processes are exploited in the production of ethanol, lactic acid, 1,4-butanediol starting from sugars to obtain biofuels and polymers.

- **Chemical processes** involve the use of chemical reactants to modify the structure of the starting material, usually characterized by a higher oxygen content with respect to fossil fuels. The most common chemical processes are

hydrolysis, hydrogenation, dehydration, halogenation, C-C coupling and deoxygenation.

The concept of biorefinery evolved in time with different available technologies and searches, thus biorefineries have been divided into three main types, based on the used feedstocks, on the generated intermediates, on the conversion processes and the status of the technology.

- More established biorefineries start from one feedstock material, have a fixed process capability and produce a single primary product, like biodiesel from vegetable oil, pulp and paper mills and the production of ethanol from corn grain.
- The second type of biorefinery, usually connected to less established markets, start from one feedstock but produce various products, like chemicals from starch.
- The last type of biorefinery can utilize different feedstocks and processes to obtain different resulting products and it includes sub-classes: Whole-crop biorefinery, Green biorefinery, Lignocellulosic biorefinery, Two-platform concept biorefinery.

Another classification of biorefineries is based on the chemical nature of feedstocks.

- **Triglyceride biorefinery** converts vegetable oils, animal fats, oil from algae and cooking wastes, through a transesterification pathway mediated by a base, acid or biocatalyst, co-producing glycerol, an added value compound.
- **Sugar and starchy biorefinery** deals with the fermentation of sugars and starch, coming from sugar beet, sugar cane, wheat, corn and maize, to ethanol production.
- **Lignocellulosic biorefinery** utilizes wood, straw and grasses with variable composition of cellulose, hemicellulose and lignin, to obtain a wide spectrum of products through different approaches [15].

Attained building blocks can be named on the base of carbon atoms number in their structure: C6, C5, C4, C3, C2, C1 (Fig. 1.9).
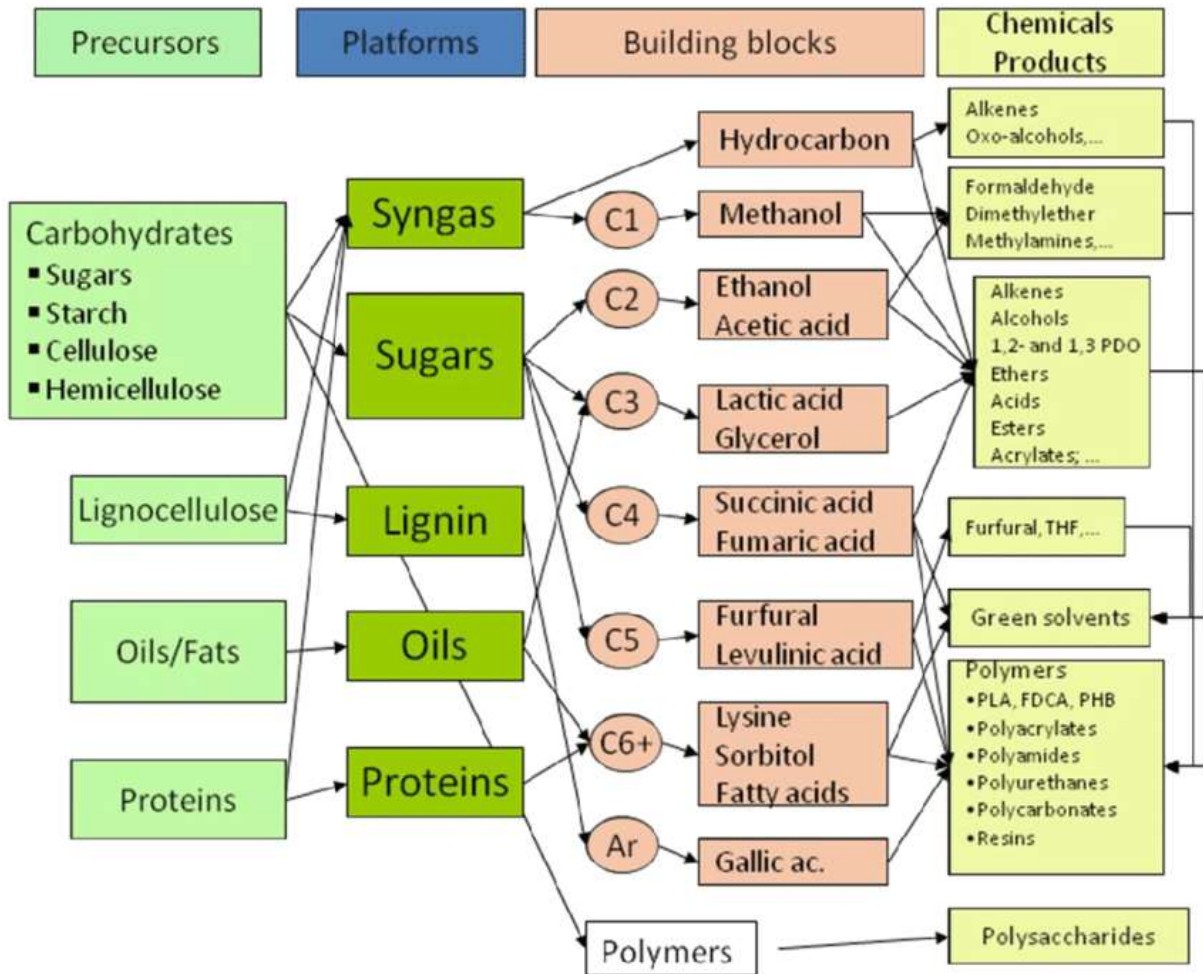
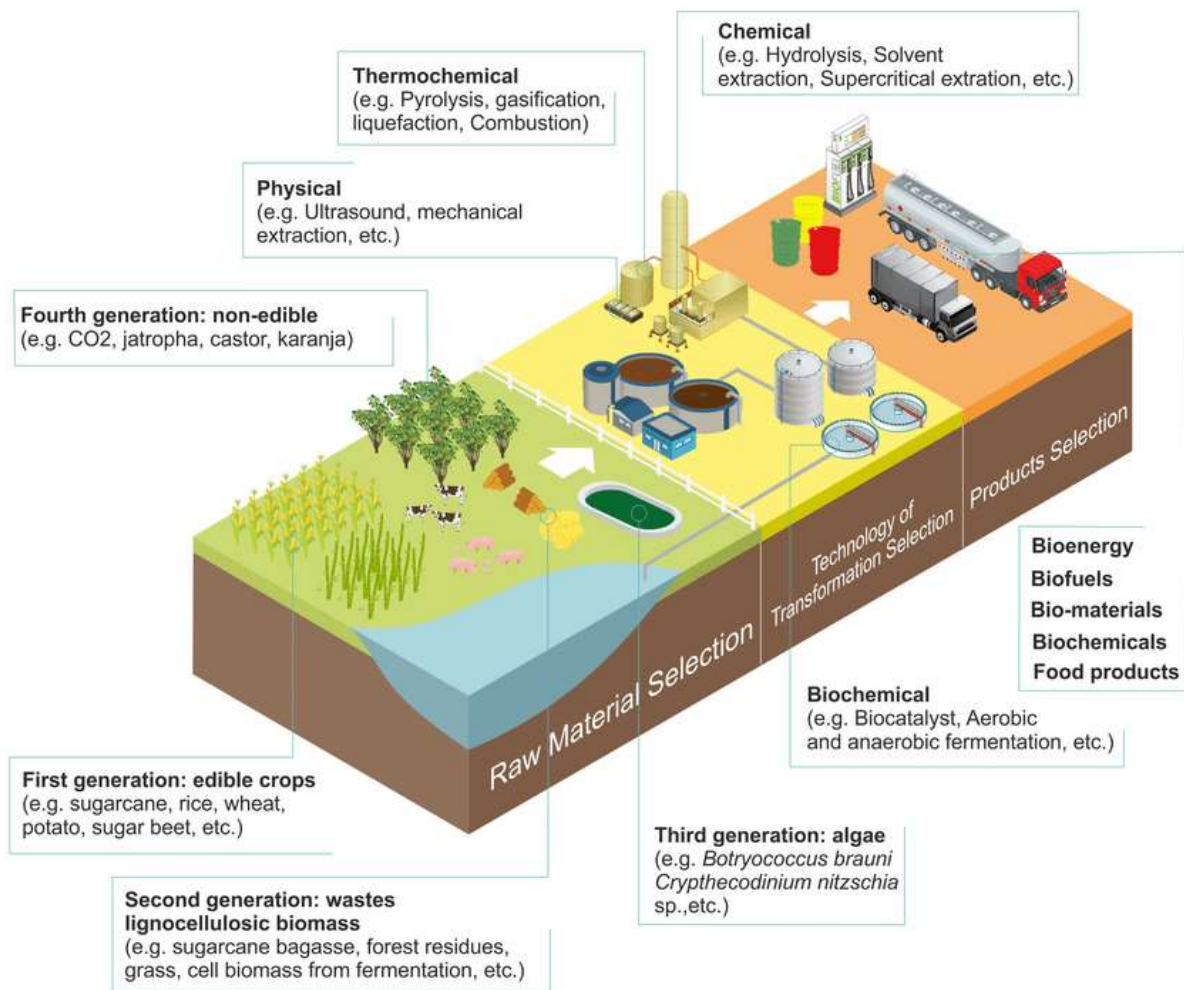*Figure 1.8 The main building blocks [16]*

Figure 1.9 Biorefinery [14]

In order to use biomass in a sustainable way, it should satisfy some requisites, connected to the competitiveness with fossil fuels and to the feasibility of the entire process. The main characteristics are the production of a high-quality product with the highest possible yield at the minimum cost, and the food-uncompetitiveness. Given these two prerequisites, there are other important factors to be considered: the availability all over the year and the variations during seasons, the added costs and the time related to the agricultural practices like harvesting, irrigation, fertilization and finally the transport and the storage of the semi-finished product.

Biomass as raw material is a sustainable route to produce relevant products, anyway it is not simple to perform a fully sustainable process from the beginning to the end, satisfying the prerequisites and obtaining an economically competitive product. Shifting from biomass to waste biomass, there are more chances to achieve sustainability and

close the loop on elements. Different types of waste can be suitable for this purpose, because in most processes there is the accumulation of waste, by-products and co-products: forestry and agricultural residues, agro-industrial and industrial waste such as black liquor, sewage, municipal solid waste and food processing waste [17].

1.2.1 Lignocellulosic biomass

Lignocellulose is the main component and supporting tissue of plant cell wall, which is widely distributed in crop residues such as corn stover, wheat straw, wood chips, dead branches, fallen leaves and grasses, and its total amount accounts for 30%–50% of the total dry weight of plants [18]. Its composition varies depending on the source; its average is made of about 50% cellulose, 24% hemicellulose, 20% lignin, 0,1% vegetable oils, 1% starch, 0,1% other sugars and 4,8% proteins and other compounds. Figure 1.11 shows lignocellulosic material structures.
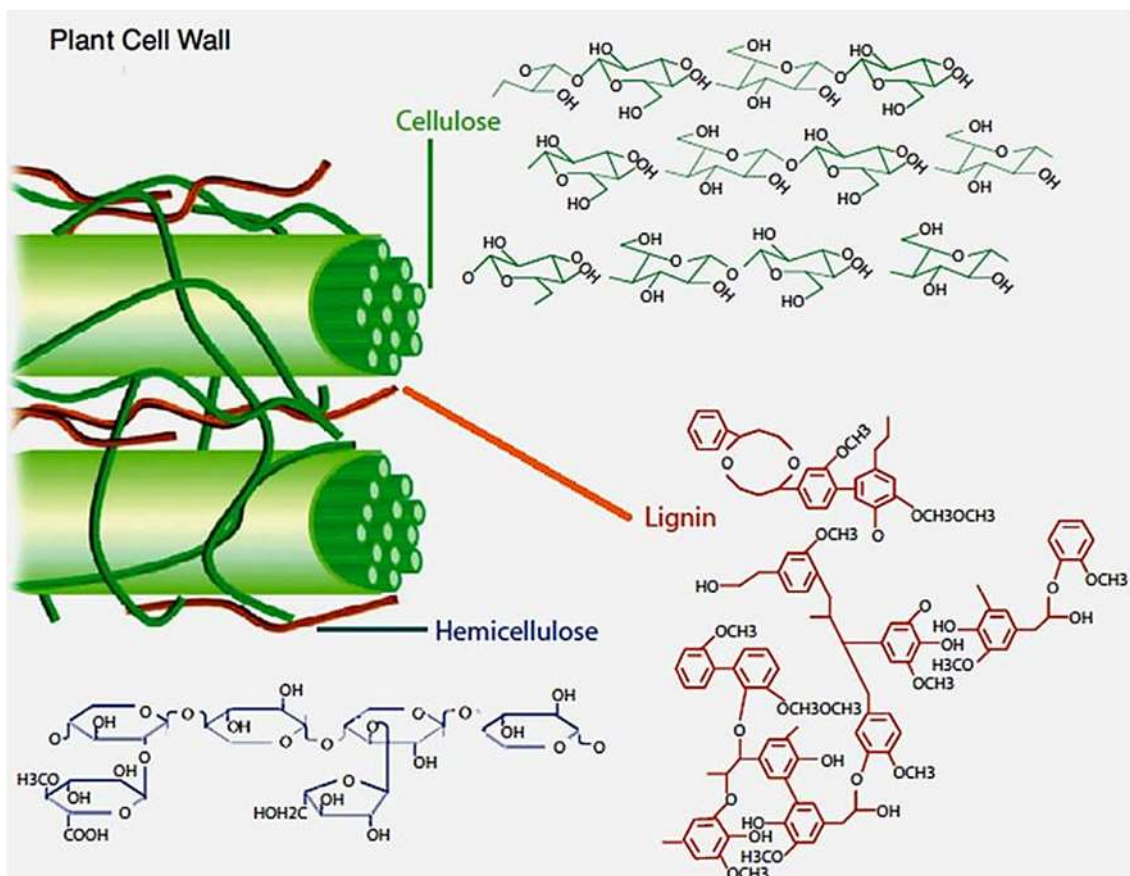

Figure 1.10 Lignocellulosic biomass [19]

- **Cellulose** is a natural not food-competitive polymer, made of glucose repeating units, which create rigidity, order and high degree of crystallinity. D-glucose

monomers are linked together by β-1,4 glycosidic bonds. The presence of the pyranose ring and the chair conformation confers linearity, stiffness and stability to the structure. Cellulose is insoluble in water and in common organic solvents, because of the presence of hydrogen bonding networks that must be broken to dissolve and treat this material. Thermal treatments are not possible, because cellulose would decompose before melting, hence some modifications have to be applied, obtaining regenerated cellulose (films and fibers) or cellulose derivatives (ethers, esters).

- **Hemicellulose** is a branched polysaccharide consisting of shorter sugar chains with respect to cellulose. Besides six-carbon rings like α-D-galactose and β-D-mannose, five-carbon sugars make up most of the hemicellulose structure: β-D-xylose and α-L-arabinose. Unlike cellulose, hemicellulose is easily hydrolyzed by acids or bases and by enzymes. From its depolymerization both C5 and C6 sugars can be obtained.

- **Lignin** has a very complex and heterogeneous polymeric structure, whose primary monomers are p-coumaryl alcohol, coniferyl alcohol and sinapyl alcohol in different ratios from source to source. Lignin has not a defined repeating unit, because there is no constancy in its structure, composition, linkages and molecular weight. Lignin confers the hydrophobic properties to plant cell wall, being composed by aromatic compounds called phenylpropanoid units which fill the spaces between cellulose, hemicellulose and pectin components and are linked with ester, phenyl and covalent C-C bonds. Lignin allows for water and nutrient transport, as well as structural support and protection against pathogens and insects. Pre-treatments for lignin exploitation can be summarized as follow: the extraction refers to the separation of lignin from biomass mixture, the fractionation is the process of lignin leaving the biomass cell wall, the precipitation is the actual separation from solvent and then fragmentation, considered as the breaking of lignin in added-value molecules. In Fig. 1.12 monolignols and monomeric units of lignin are reported, with the presence of metoxy and hydroxyl functional groups.
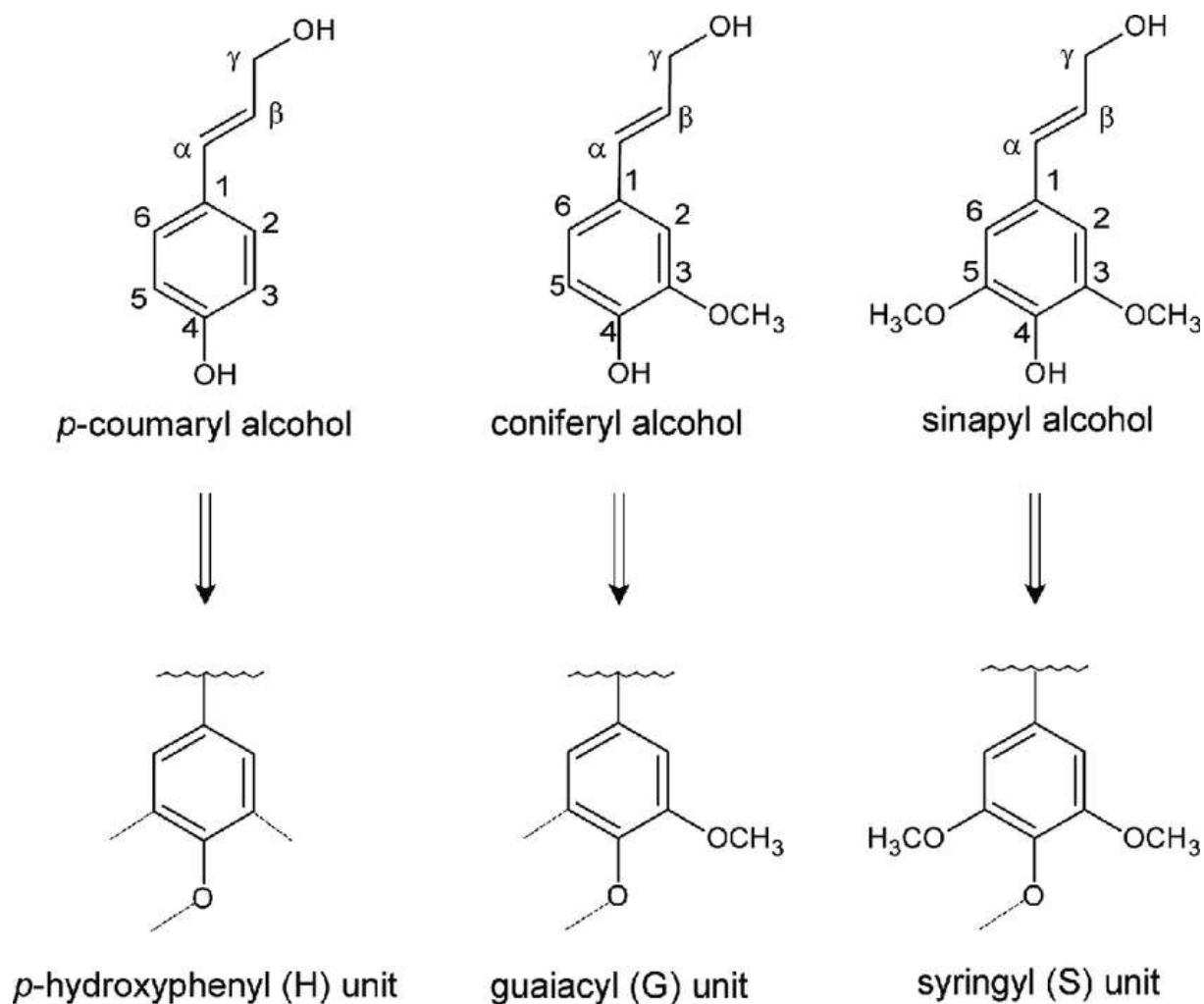
Figure 1.11 Chemical structure of monolignols and the corresponding building blocks in lignin. [20]

Lignocellulosic biomass conversion is more challenging than sugars, starch and oils, probably because of the heterogeneity of the composition and its main building units. The valorization of this biomass type starts with a pretreatment that leads to cellulose, hemicellulose and lignin separation. While cellulose and hemicellulose are used by traditional biorefineries to produce platform chemicals, lignin is usually burned to get energy [15].

1.2.2 Lignin as natural by-product

Lignin is currently burned to produce energy and its potential to obtain added value aromatic compounds is not fully exploited. The principal aim in lignocellulosic biomass treatment is to separate other components from cellulose, which already has an

established market. Thus, lignin is practically a costless aromatic biowaste coming mainly from lignocellulosic biomass treatment and from pulp industry.

Lignin can be classified, depending on its plant origin, into hardwood, softwood and grass lignin and, depending on the applied treatment, into Kraft, Soda, lignosulfonate and organosolv [21].

- **Hardwood** lignin: high syringyl-to-guaiacyl ratio (S/G)
- **Softwood** lignin: only guaiacyl units (G)
- **Grass** lignin: low syringyl-to-guaiacyl ratio (S/G)

In Fig. 1.3 different sources of lignin are compared based on the obtained monomer yield. Depolymerization of hardwood lignin results in higher aromatic monomer yields because this feedstock generally displays high syringyl-to-guaiacyl monolignol ratios. Syringyl unit has 3 and 5 aromatic ring positions prevented from C-C bond formation and higher portion of cleavable β-O-4 linkages [22].
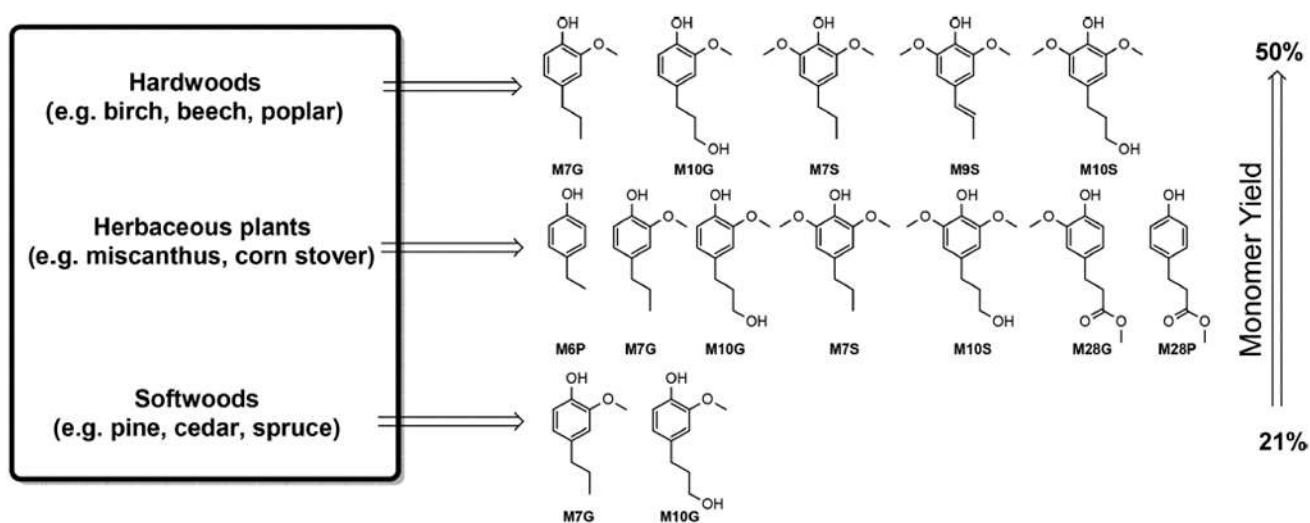

Figure 1.12 Structures of phenolic monomers derived from native lignin of different sources. (M7G= 4-propylguaiacol, M10G= 4-propanolguaiacol, M7S= 4-propylsyringol, M9S= 4-allyl-2,6-dimethoxyphenol, M10S= 4-propanolsyringol, M6P= 4-ethylphenol, M28G= methyl 3-(4-hydroxy-3-methoxyphenyl)propionate, M28P= methyl 3-(4-hydroxyphenyl)-propionate) [22]

- **Kraft** lignin is obtained through a separation process that starts from the reaction of wood, Na2S, NaOH at 165-175°C for 2-4 hours in autoclave. Then, the obtained pulp is transferred into another autoclave to separate cellulose from the black liquor, containing lignin. The liquor is concentrated and the separation of a sulfur-containing lignin is made. Kraft lignin is soluble in alkaline

solutions and molecular weight values are in the range of 1500 and 25000 g/mol^{-1} [39]

- **Soda** pulping lignin comes from the heating of biomass with alkaline aqueous solution at a temperature of 160°C, without the utilization of sulfur compounds. Lignin is precipitated and separated by acidification of the medium. The so-obtained lignin is characterized by an average molecular weight (Mw) of 1000–3000 g mol^{-1} [39]

- **Lignosulfonates** are water soluble lignin obtained through sulfite pulping, based on the acid cleavage of ether bonds at 140-160°C in presence of sulfide or bisulfide salts of ammonium, magnesium, sodium, or calcium. Due to the nature of the process, the obtained lignin contains sulfur in the form of sulfonate groups in variable amounts (3–8 %). Therefore, this form of lignin is highly water soluble within a broad pH range [19]. Sulfite lignin can reach high average molecular weight with Mw fluctuating between 1000 to 140000 [39]. Lignosulfonates are used as additives in concretes, paints and agricultural products.

- **Organosolv** process is the most recent pulping procedure that involves organic solvents to solubilize and separate lignin.

Even if lignin is now suitable for niche applications, there are efforts in its valorization to produce carbon fibers, elastomeric and thermoplastic polymers, membranes and aromatic compounds [15]. New routes for lignin valorization can be developed by functionalizing its structure and creating lignin derivatives, starting from a cheaper raw material with respect to fossil fuels. Important properties of lignin can be exploited in the manufacturing of products, such as mechanical strength, hydrophobicity, thermal stability and antioxidant action [21].

1.3 Lignin valorization to added-value products

The interest toward lignin exploitation comes from its abundance and from the search for alternative resources on the planet [21a]. Lignin is the greatest source of aromatic building blocks in nature, hence different routes of depolymerization to break down the starting material were developed, such as thermic, thermochemical, catalytic and

biochemical treatments. Depolymerization behavior is strictly connected with the types of linkages that make up the overall structure, strongly dependent on the source. The most common linkages, shown in Figure 1.14, are β-O-4, β-β, β-5, 4-O-5, 5-5. The main depolymerization techniques aim at fracture β-O-4, because it makes up about the 50% of all linkages in native hardwood and softwood lignin [21a]. A representative structure of lignin with its main linkages is shown in Figure 1.15. In particular, the β-O-4 is a ether bond between an aromatic ring and the lateral carbon chain of another aromatic ring; the β-β is a C-C bond that connects two furan rings; 5-5 is a C-C bond between two aromatic rings in 5 position; 4-O-5 is a ether bond in which an oxygen connects the carbon 4 and 5 of two aromatic rings; β-5 is a C-C bond between the 5 position of an aromatic ring and the lateral chain of another. Considering the common substructure of all monomers, the final lignin macromolecule usually incorporates a variety of functional groups, including methylphenyl ethers, aliphatic and aromatic hydroxyl groups as well as carbonyl residues [39].
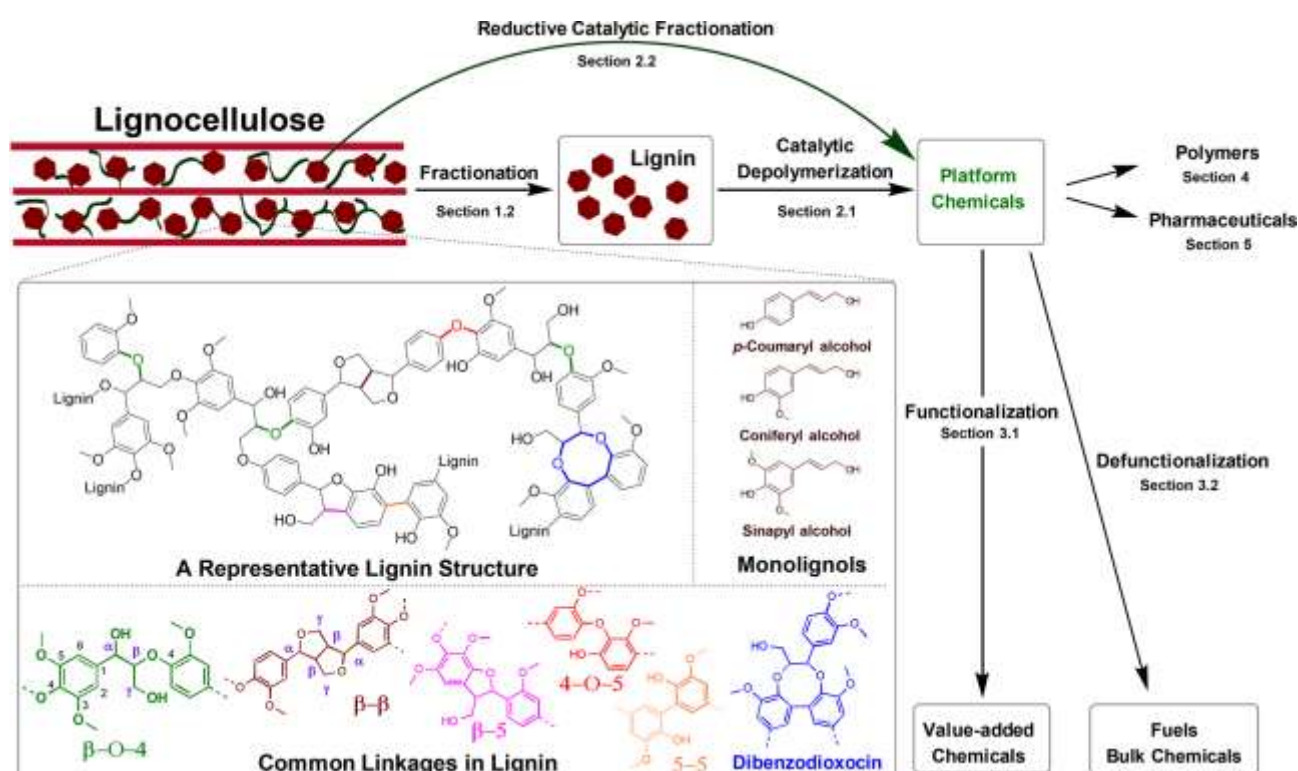

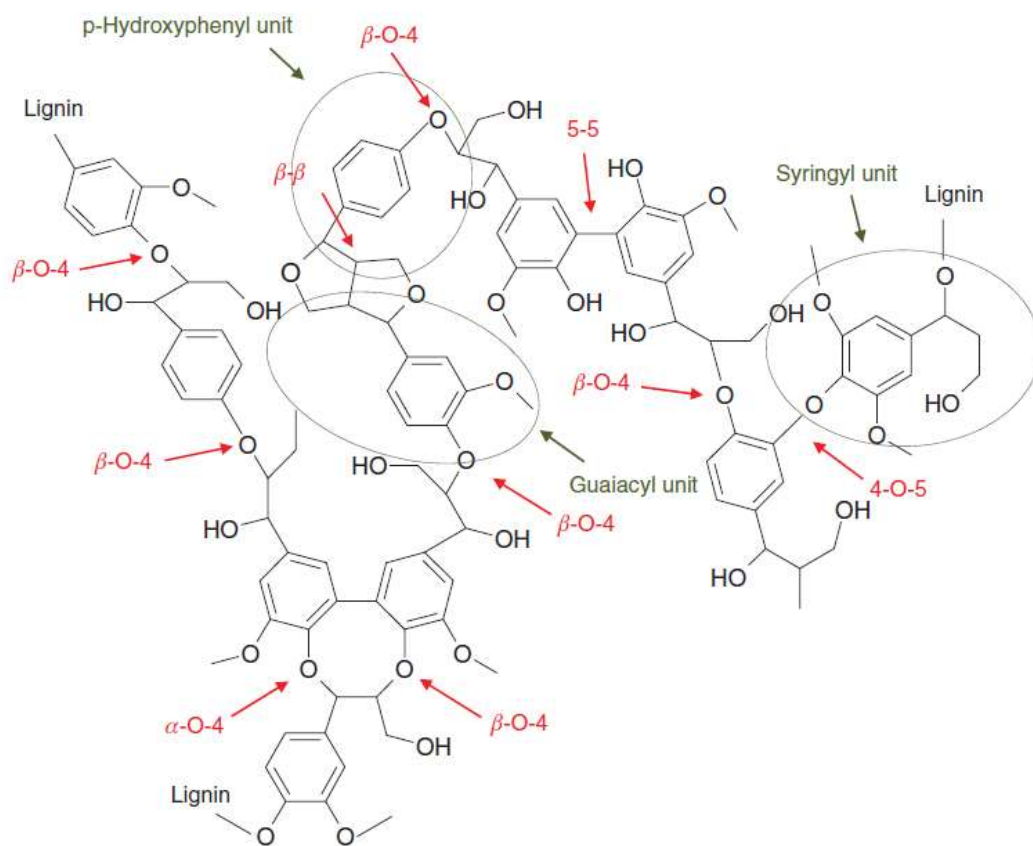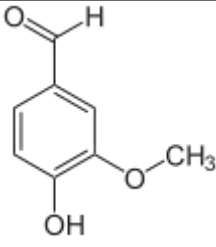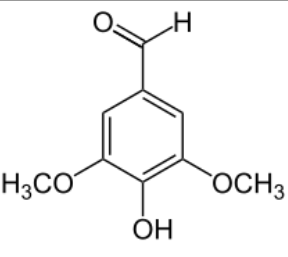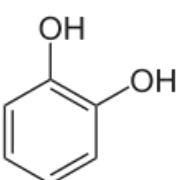Figure 1.14 Catalytic fractionation and common linkages in lignin [21a]

21
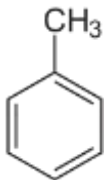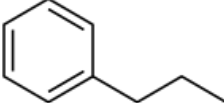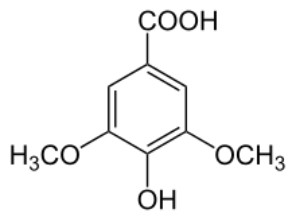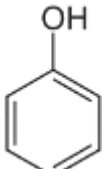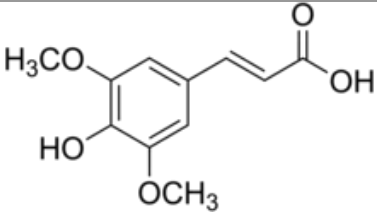
Figure 1.15 Representative structure of lignin [22]

The main achievable building blocks are vanillin, syringaldehyde, catechol and its derivatives, toluene, propylbenzene, syringic acid, phenol, guaiacol, acetovanillone, ferulic acid, sinapic acid and similar structures, depending on the applied treatment, working temperature and lignin typ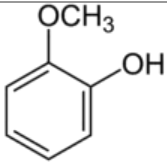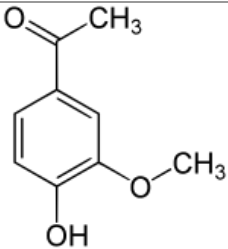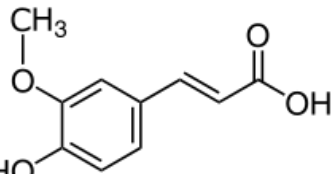e. The most likely depolymerization mechanisms, such as hydrogenolysis, hydrodeoxygenation and oxidation reactions are reported in Fig. 1.16. The so-obtained aromatic monomers can rearrange and form added-value building blocks, listed in Table 1, with their structures and some applications. Depolymerization in oxidative conditions is useful to obtain a wide pool of functionalities: the benzylic carbons and the α-alcohols of the lignin backbone can be easily attacked and converted into carbonyl compounds [39].

Table 1 Achievable building blocks from lignin

Structure	Applications
Vanillin	• Flavoring agent, usually in sweet foods • Fragrance industry, in perfumes, and to mask unpleasant odors or tastes in medicines and cleaning products
Syringaldehyde	• Bioactive properties, used in pharmaceuticals, food, cosmetics, textiles, pulp and paper industry
Catechol	• 50% of the synthetic catechol is consumed in the production of pesticides • Precursor to fine chemicals such as perfumes and pharmaceuticals
Toluene	• Industrial feedstock • Precursor to benzene and xylene • Solvent for paints, paint thinners, silicone sealants, many chemical reactants, rubber, printing ink, adhesives (glues), lacquers, leather tanners, and disinfectants
Propylbenzene	• Nonpolar organic solvent in various industries, including printing and the dyeing of textiles • Manufacture of methylstyrene
Syringic acid	• Pharmaceutical properties such as anti-oxidant, anti-microbial, anti-inflammation, anti-cancer and anti-diabetic
Phenol	• Important industrial commodity as a precursor to many materials and useful compounds • Conversion to precursors for plastics • Precursor to a large collection of drugs

23

Guaiacol		• Precursor for the synthesis of other compounds • Reagent for the quantification of peroxidases • Precursor to flavouring agents, such as eugenol
Acetovanillone		• Used in the treatment of atherosclerosis to prevent the activity of NADPH oxidase activity • Investigated for the treatment of asthma
Ferulic acid		• Precursor in the manufacture of other aromatic compounds • Ubiquitous in the plant kingdom • Used as a matrix for proteins in MALDI mass spectrometry analyses
Sinapic acid		• Matrix for MALDI due to its ability to absorb laser radiation and to donate protons (H+) to the analyte of interest

Catalytic Depolymerization of Lignin
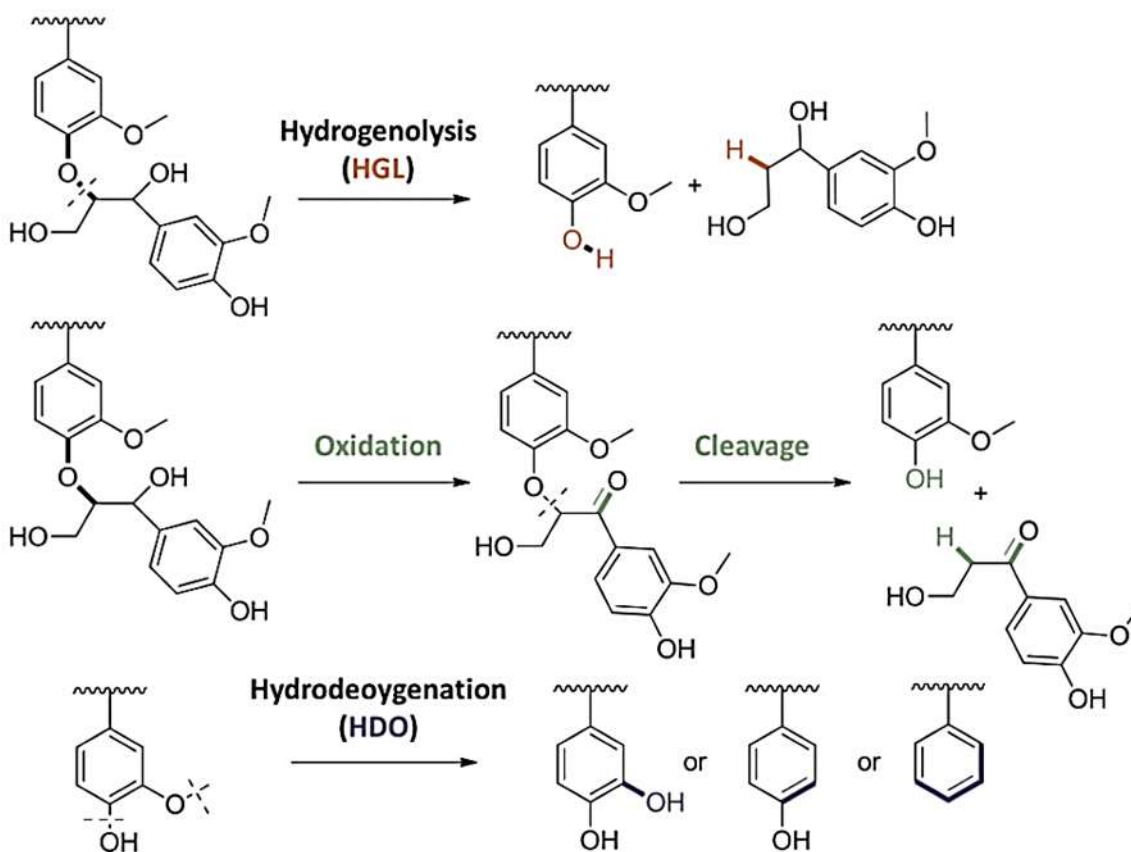
Figure 1.16 Classical pathways for lignin depolymerization [39]

Figure 1.17 Proposed mechanism for C-O cleavage of oxidized lignin model [39]

In Figure 1.17, a possible mechanism of an oxidized lignin model compound is reported, achieving important functionalities of the most common building blocks.

1.3.1 Depolymerization processes of lignin

Depolymerization of lignin, also called delignification, can proceed through oxidative pathways with oxygen, hydrogen peroxide or peroxyacids, exploiting the already available techniques for papermaking industry for pulp bleaching. Oxidative species

are very reactive, thus a lot of products can be obtained such as aldehyde, alcohols and carboxylic acids, but high selectivity is required to avoid overoxidation and, if radicals are present, products yield may be reduced. Reductive approaches should efficiently break C-O bonds and usually the product mixture is less complex than oxidative treatments, with increasing selectivity for target aromatic compound. On the other hand, competitive ring hydrogenation reactions may cause a reduction in selectivity [21a]. The role of the catalyst is very important in both of them because the cleavage of C-O bond is metal dependent. The main supported catalysts for this purpose are made of Ru, Pd, Rh and Ni on activated C or Al_2O_3. Examples of catalytic oxidation and reduction are reported below.

- **Oxidation** of lignin usually leads to highly functionalized chemicals.

  Recent use of **Polyoxometallates** (POMs) as catalysts for lignin oxidation was reported by Rohr and co-workers [38], to convert Kraft lignin into aromatics, mainly vanillin. They treated lignin in a MeOH-H2O (4:1) mixture at 170 °C under O2 (10 bar) with a H3PMo12O40 catalyst and obtained a 70% conversion of initial lignin. The main products were 7%wt vanillin:methylvanillate (ratio 1:1) and oligomeric compounds.

  Zhao et al. [40] reported the depolymerization of different lignin types using H5PMo10V2O40 as catalyst under conditions similar to those of the previous work, (190 °C, MeOH-H2O 9:1), pH of reaction mixture 0.93, O2 20 bar. The main impact on process efficiency was found to be the solvent mixture ratio. Authors noticed that increasing methanol fraction, the product mixture was richer in alcohols and oily fraction, like aldehydes, carboxylic esters, diesters. Methanol acts as promoter for oxidation through radical formation and as capping agent preventing degradations or recondensation [41].

  Another work compared the oxidative depolymerization of alkali lignin by tungsten- or molybdenum-based POMs, at 175 and 225 °C. They obtained carboxylic acids such as formic, acetic and succinic acid, attesting for an overoxidation of the intermediate aromatic compounds. Authors did not observe the presence of aromatic compounds, because they only used pure water as reaction medium. The presence of co-solvents would have prevented over oxidation [41].

- **Perovskites** of general formula ABO3 are employed as catalysts for hydrocarbons oxidation due to the redox behavior of the metals. Lin and Liu and coworkers [42] evaluated various perovskites for oxidative depolymerization of enzymatic extracted lignin from steamexploded cornstalk. Perovskite catalysts were found to improve both lignin conversion and production of aromatics, especially with catalysts containing Cu. However, yields of vanillin and syringaldehyde decreased after a relatively short reaction time (0.5-1 h), probably because of the formation of redox metallic couples by adsorption of oxygen species at the surface of the perovskites [41].

- One of the most common **metal oxides** for lignin oxidative depolymerization is CuO, which shows good activity but not particularly high selectivity. Zhu and coworkers [43] reported the use of ReOx supported on γ-Al2O3 to produce vanillin from Kraft lignin in molten phenol as solvent. The use of phenol is arguably green, but it led to high selectivity towards vanillin and could prevent over oxidation. Yield of vanillin was around 7.5 %wt.

- **Mixed metal oxide** catalysts represent an interesting approach in this field. Barakat and coworkers [44] described the use of various CoFeO mixed metal oxides, varying Co:Fe ratios. Among the catalysts, Co1.8Fe1.2O4-Co0.8Fe1.2O3, demonstrated the best performance, with resulting mixture of aromatic molecules in 10-20%wt in which aldehydes (mainly syringaldehyde) are the main compounds observed, using water or water/methanol mixture as reaction medium.

  Jeon et al. [45] studied the alkaline wet oxidation of lignin over Cu-Mn oxide catalysts to produce vanillin at reaction temperature of 120-180°C, using H2O2 as oxidizing agent. They choose the best ratio Cu:Mn to obtain the highest yield possible of the target product and to avoid over oxidation to vanillic acid. A reaction pathway was proposed, with Cu1.5Mn1.5O4 as catalyst and assuming coniferyl alcohol as starting material. As shown in Figure 1.18, hydrogen peroxide is dissociatively adsorbed onto the catalyst surface and decomposed to oxygen species, that would convert coniferyl alcohol to vanillin. The higher the Cu loading, the higher will be the possibility of over oxidation to vanillic acid.
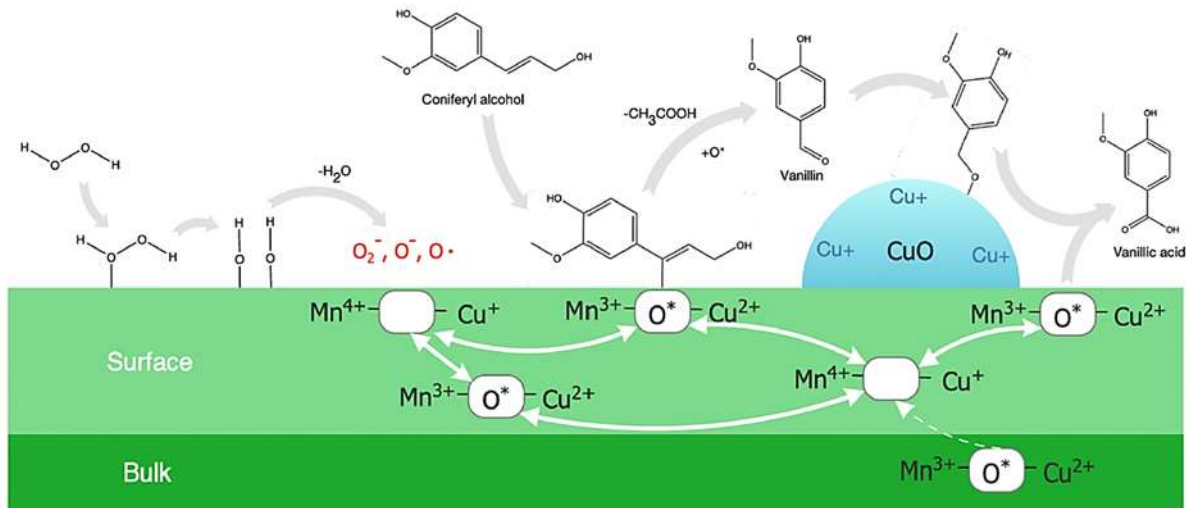
Figure 1.18 Proposed mechanism for lignin catalytic oxidation over Cu-Mn oxide [45]

- **Reduction** processes are more likely to form alkylphenolics and BTX. Besides the cost, many studies reported that **noble metal catalysts** have high hydrogenation activity, converting phenolic compounds into naphtenes and cyclohexanols. **Fe** and **Cu-based** catalysts show lower activity but are usually efficient at milder conditions and can work without added H2 gas. Different bimetallic oxides and sulfides catalyst based on Co, Ni, Mo and W were studied. In particular, **metal sulfides** are effective in oxygen removal from biomass-derived components through a deoxygenation to non-oxygenated aromatics [41].

- **Biochemical** treatments aim at obtaining a specific target compound by means of bacteria or fungi, that will follow their metabolic pathway converting and decomposing lignin in mild conditions. Pseudomonas putida was used by Beckham and co-workers to obtain medium-chain length polyhydroxyalkanoates [22].

1.3.2 Vanillin production

Vanillin (4-hydroxy-3-methoxybenzaldehyde, Table 1) is an aromatic compound widely used in food industry, as additive flavor agent but also as vulcanization inhibitor, antifoaming agent and chemical precursor. Natural vanillin is extracted from the seed pods of Vanilla Planifolia, in the β-D-glucoside form [24]. It is biosynthetized by

phenylpropanoid pathway, starting from L-phenylalanine, and through cytochrome P450 enzyme cinnamate 4-hydroxylase that introduces the para hydroxyl group [25]. The traditional fossil-based process starts from benzene catalytic oxidation to guaiacol, that is further oxidized to vanillin. Synthetic, natural and bio-vanillin differ from the original source, that could be fossil-based, naturally obtained from vanilla beans and bio-based from plants, like lignin. There is also a difference in their prices, since natural extract costs 1800$/kg and synthetic 15$/kg. The oxidation of lignosulfonates to vanillin by oxygen is quite challenging because of the complex structure of the raw material. Moreover, aromatic aldehydes are particularly sensitive to drastic oxidative conditions, because peroxyl radicals, which are intermediates in the oxidation by oxygen, react fast with vanillin leading to oxidative degradation [46].

Borregaard process from lignosulfonates (Fig. 1.19) produces vanillin from the black liquor of Kraft pulping, that is collected into the lignin processing plant and the oxidation pathway is conducted in alkaline medium at 160°C on Cu-based catalyst. Membrane separation and ion exchange are utilized to separate phenolic compounds, vanillin (7%wt) and similar structures. The entire process accumulates a lot of impurities that require further purification and separation, resulting in about 160 tonnes of waste per ton of vanillin. Starting from a bio-source does not necessarily means performing a sustainable process if it accumulates waste and requires numerous steps.
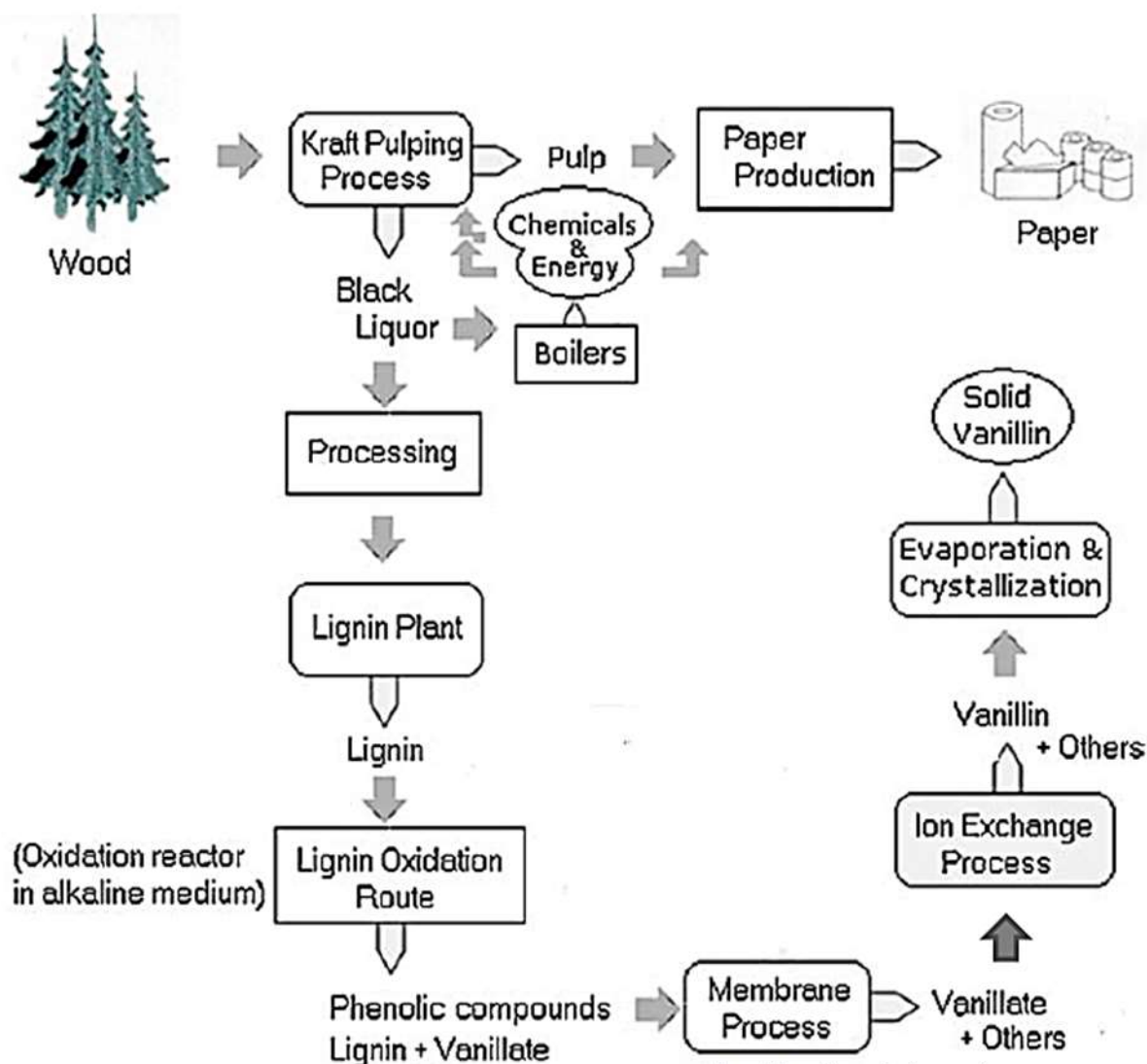
Figure 1.19 Borregaard process scheme [47]

Vanillin contains three reactive functional groups, hence it can easily undergo different types of reactions [25a]. The aldehyde can cause condensation reactions and, if the hydroxyl group is protected, vanillic acid is obtained through oxidation. Oxidation of vanillin can be conducted both under alkaline media and by enzymes such as xanthine oxidase and peroxidase. Vanillin is highly oxidized in presence of oxygen in alkaline solution, especially at higher temperatures, and oxidation rate depends on vanillin concentration. The influence of oxygen concentration is significative on the rate only for pH<12 [25a]. Constant et al. [48] studied the behavior of vanillin in aqueous medium and oxidative conditions, to understand if vanillin could be considered as a model compound for studies on lignin depolymerization. They reported possible reaction

pathways (Fig. 1.20) to vanillic acid, quinonic intermediates, dialcohols, dimers and diacids, hence vanillin can bring to a wide variety of important added-value molecules.
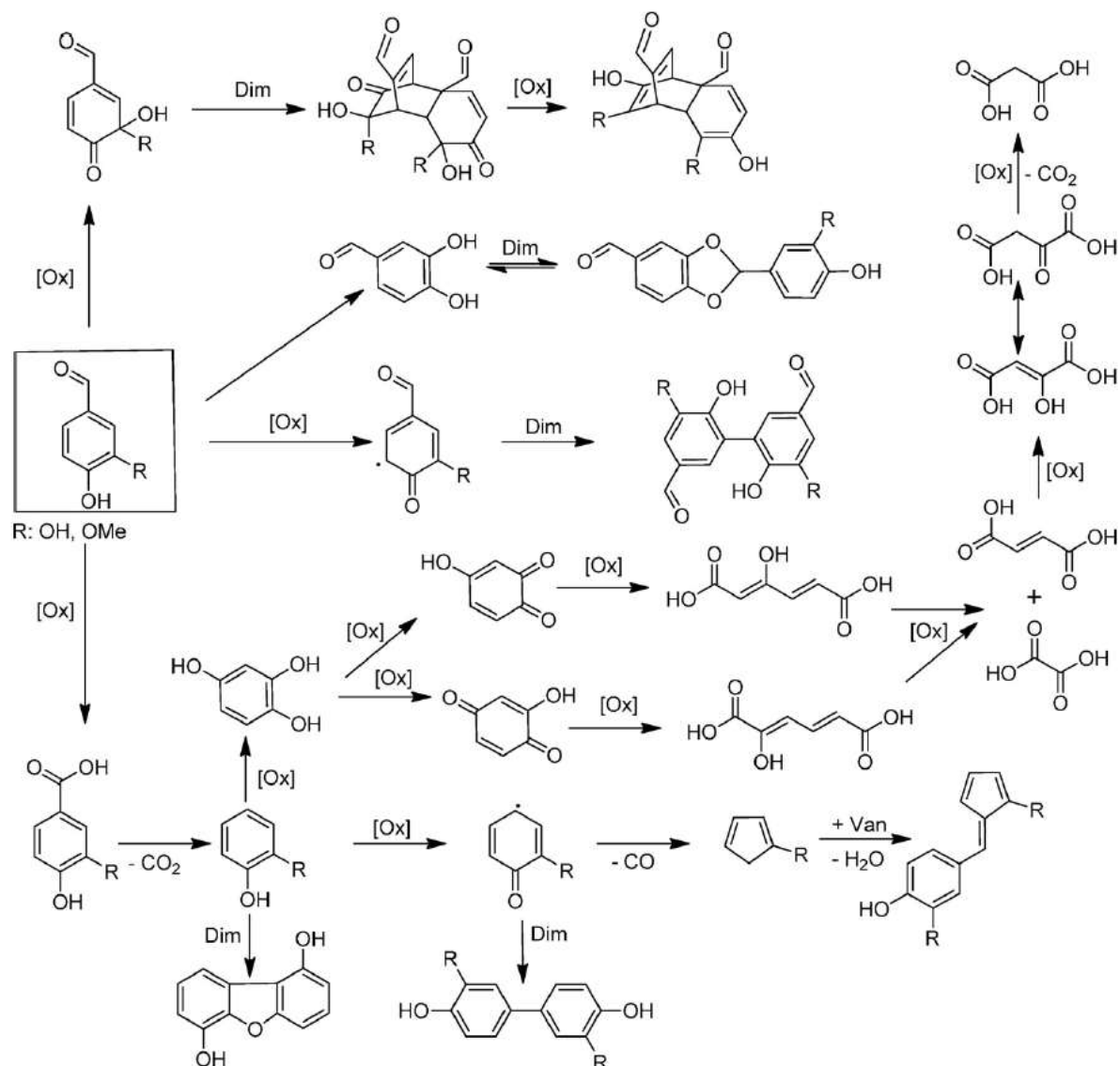

Figure 1.20 Possible reaction pathways in oxidative treatment of vanillin (Ox=oxidation, Dim=dimerization) [48]

1.4 The importance of the catalysis for lignin depolymerization

In the necessity to reduce environmental impacts and avoiding the releasing of hazardous substances, the green chemistry comes to industrial sector's aid, through the setting of green tools such as the 12 green principles (Fig. 1.21) and the green metrics. Sustainable and green chemistry in very simple terms is just a different way of thinking about how chemistry and chemical engineering can be done [26].

Examining the 12 principles, there is a particular interest into the 9th one: catalysis, that can group all the others in itself.

Catalysis is born as an alternative to stoichiometric reactions to reduce the production of byproducts and undesired pathways. It is an important tool to avoid waste generation, trying to maximize the incorporation of all materials used in the process into the final product [26]. Catalysis is a crucial tool for lignin depolymerization because it enhances the use of mild conditions of temperature, pressure and reaction environment and it gives the possibility of select the right properties for a catalyst, finding a good compromise between selectivity and activity.

Figure 1.21 The 12 Principles of Green Chemistry [26]

1.4.1 Renewable electricity as an important energy source

A process can be defined as green if it satisfies the 12 principles and it has optimal values of green metrics (Atom Economy, Percentage Yield, Reaction Mass Efficiency, Environmental Factor). These tools alone are not enough to define a sustainable process, that should be analyzed from cradle-to-grave considering all direct and indirect impacts on the environment, usually through the adoption of Industrial Ecology and a life cycle thinking.

Catalysis can certainly create a green process, but to achieve sustainability other aspects of production phases must be examined, such as the energy source. Starting from renewable energy sources, impacts to environment are reduced a lot because there's not dependence on fossil fuels in the primary phases of production and, ideally, during the overall process. Wind, solar, geothermal, hydrothermal energy and biomass can be adopted to obtain clean and renewable electricity and to achieve the energy feedstock for a photocatalytic, electrocatalytic or photoelectrocatalytic process.

1.4.2 Electrocatalysis basis

Electrocatalysis is a branch of electrochemistry and of catalysis that deals with the effect of the electrode material on the rate and the mechanism of electrode reactions. The electrocatalyst is involved in the acceleration of electrochemical reactions, proceeding in mild conditions of pressure and temperature, together with renewable electricity sources. The electrocatalyst changes the potential at which oxidation and reduction processes are observed, lowering the activation energy, thus facilitating the passage of electrons at the electrode surface. The applied potential is never equal to equilibrium potential, but a surplus should be applied. This **overpotential** (described by eq. 1 and 2) is due to: activation energies of the electrode reactions, concentration profiles at the electrode due to mass transport limitations and ohmic loss.

$$E_{CELL} = E_{CELL}^0 + \eta_{AN} + \eta_{CAT} + \eta_{\Omega} \quad \text{(eq. 1)}$$

(E_{CELL}= cell potential; E_{CELL}^0= equilibrium cell potential; η_{CAT}= cathodic overpotential; η_{AN}= anodic overpotential; η_{Ω}= ohmic loss).

In general, the overpotential is defined as the difference between the applied electrode potential and the equilibrium potential:

$$\eta = E - E_{eq} \qquad \text{(eq. 2)}$$

(η= overpotential; E= electrode potential; E_{eq}= equilibrium potential).

The solution applies a resistance to the passage of the charges, therefore substances that increase the conductivity of the solution are added and they are called supporting electrolytes. Electrolytes stability depends on the solvent type and on the potential range: outside the window stability they decompose leading to side reactions.

The equilibrium potential is described by **Nernst equation** (eq. 3), relating the cell potential to the concentration ratio of oxidized and reduced species in solution:

$$Eeq = E^{0^1} + \frac{RT}{nF}[MN1]ln\frac{C\ ox}{C\ red} \qquad \text{(eq. 3)}$$

(Eeq= equilibrium potential; E^{0^1}= formal potential; R= universal gas constant; T= temperature; F= Faraday constant; n= transferred electrons in the reaction; $ln\frac{C\ ox}{C\ red}$= concentration ratio of oxidized and reduced species).

The choice of electrode material should be based on the minimization of activation energies of electrode reactions. The ohmic loss derives from cell connections and from the solution which applies a resistance to charge transfer, causing a potential drop that can be improved by the utilization of a three electrodes cell, made of a working electrode, a reference electrode, a counter electrode, a potentiostat and a lugging capillary that gets reference and working electrode as closest as possible, as shown in Figure 1.22.
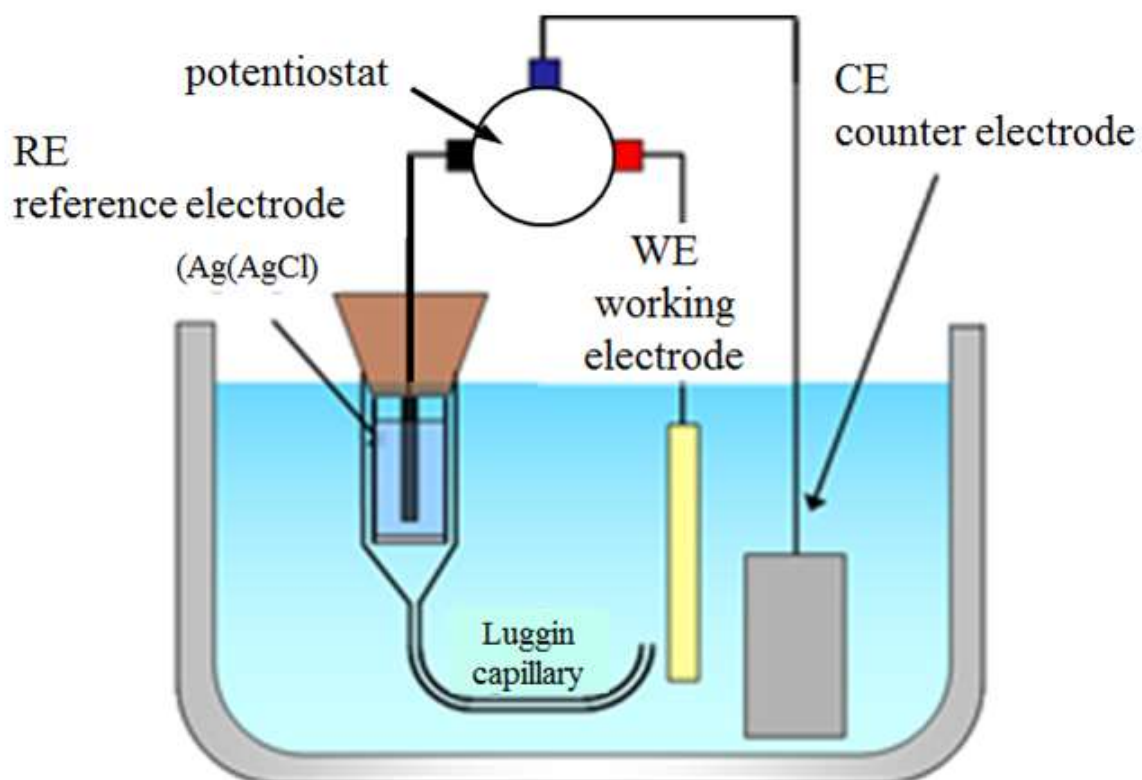
Figure 1.22 Three-electrode set-up [27]

The scale up of a three-electrode cell to real applications results in electrochemical reactors, like the slurry reactor (Fig. 1.23) reported by Wijaya et al. to electrocatalytically reduce lignin model compounds [51].
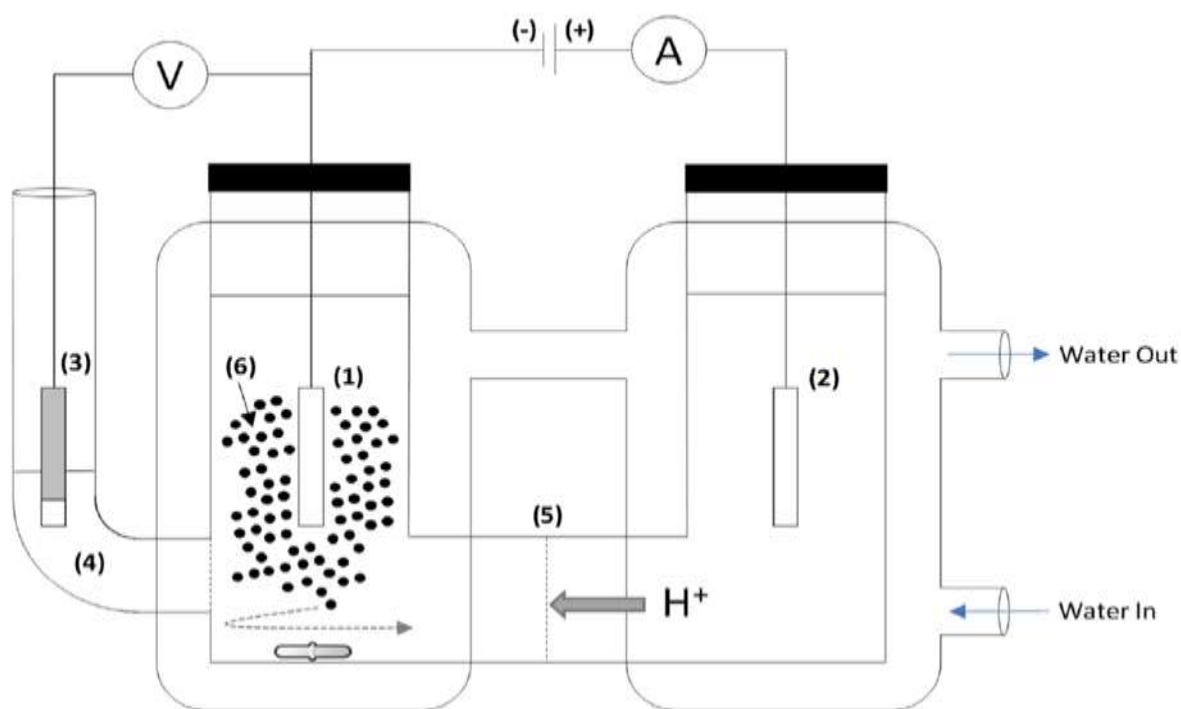
Figure 1.23 Electrochemical reactor setup for hydrogenation-hydrolysis of phenolic compounds: (1) cathode, (2) anode, (3) reference electrode (Ag/AgCl/3 M KCl), (4) fritted side compartment (Luggin probe) for reference electrode filled with 3 M KCl, (5) cation exchange membrane (Nafion-117), (6) catalyst [51]

Analogously to conventional catalysis, an electrocatalyst can be heterogeneous or homogeneous, bulk or supported, mechanically and chemically stable, with high active surface area. Moreover, it should be electrochemically stable and electrically conductive. In addition to traditional techniques to characterize a catalyst, its electrochemical properties are analyzed by voltammetry.

Faraday law puts in relation the charge and amount of product formed. The number of electrons is stoichiometrically linked to the chemical reaction (eq. 4).

$$Q = I \cdot t = nF \frac{N}{MM} \quad \text{(eq. 4)}$$

(Q= charge; I= current; t= time; n= stoichiometric number of electrons transferred; F= Faraday constant; $\frac{N}{MM}$= mass of the deposited material).

Such relation is only true for Faradaic processes, or a process in which charges are transferred within the interface electrode electrolyte. Conversely non-Faradaic

processes involve reactions that change the electrode-electrolyte interface (like adsorption and absorption).

The region of charges at the interface electrode-electrolyte is called electrical double layer (Fig. 1.24), composed by several sub-layers:

•   the **Inner Helmholtz plane** contains solvent molecules and other specifically adsorbed species;

•   the **outer Helmholtz plane** contains non-specifically adsorbed solvated ions;

•   the **diffuse layer** is created by the thermal mixing of the solution.
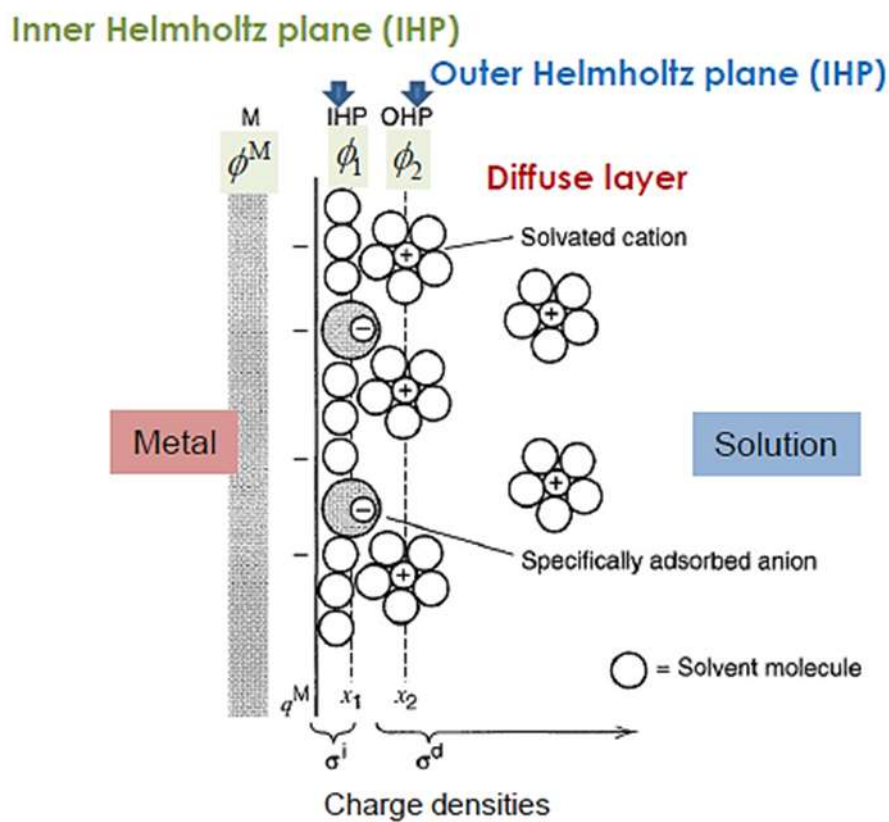

Figure 1.24 Electrical double layer with a negatively charged metal electrode [28a]

Since Faradaic processes are caused by a change in potential that allows redox reactions and charge transfer generates a current, the plot of I in function of V can be constructed, called response after excitation curve (Fig. 1.25).
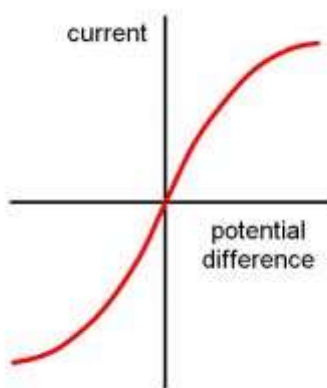
Figure 1.25 Current vs Potential curve [49]

Faraday law shows that charge transfer is connected to the quantity of product, while to define how fast such product is formed, reaction rate is utilized, defined as the change of the moles of reactant overtime to achieve the current flowing and hence the product formation. Since a potential must be applied, the rate not only depends on the current but also on the potential. When the standard electrochemical potentials of the species in solution are equal, the activation barrier will be symmetrical. If a potential to drive a redox reaction is applied, the electrochemical potential of the species will be modified, resulting in an asymmetrical energy barrier (Fig 1.26).
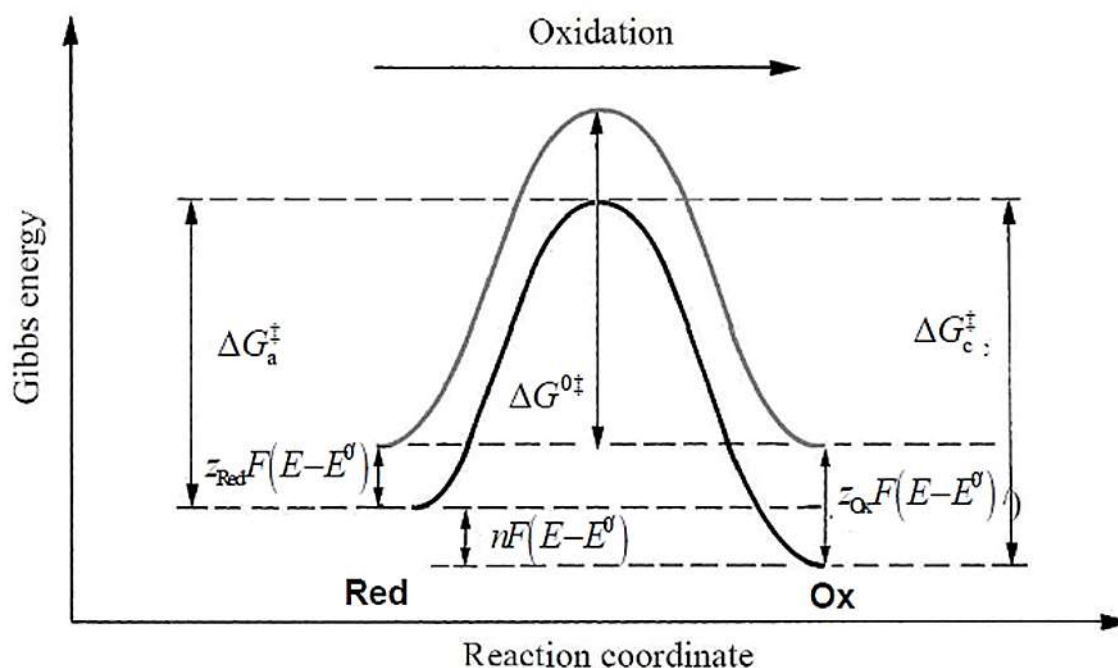

Figure 1.26 Energy barrier of redox species in solution [50]

The rate of the electrochemical reaction depends on the potential which in turns depends on the current. The **Butler-Volmer** equation (eq. 5) expresses these relationships:

$$I = Io\left[\exp\left(\frac{\alpha nF\eta}{RT}\right) - \exp\left(\frac{-(1-\alpha)nF\eta}{RT}\right)\right] \quad \text{(eq. 5)}$$

(I= current; Io= exchange current; α= charge transfer coefficient; η= overpotential; F= Faraday constant; R= gas constant; T= temperature; n= stoichiometric number of electrons transferred).

Io, exchange current, is the anodic current and the absolute value of the cathodic current that cross the interface at equilibrium. It depends on the standard reaction rate constant k° and on the concentration of the redox species.

From the Butler-Volmer equation (eq. 5), the total current is related to:

- **k°** which is the standard rate constant related to Gibbs energy and shows the Arrhenius temperature dependence
- **αnFη** which is the variation of energy barrier, related to the applied potential

It can be concluded that the rate constant of an electrochemical reaction depends on both the contributions. If there are equilibrium conditions, the Butler-Volmer falls into the Nernst equation and so the thermodynamic describes the equilibrium conditions while the kinetic describes how to reach and maintain the equilibrium. The Butler-Volmer can predict the current resulting from an overpotential.

In **Tafel plots** (eq. 6), the Butler-Volmer equation is used in the form of the logarithm of the current plotted versus the overpotential. Tafel plots allow the extraction of kinetic parameters, such as the exchange current density jo.

$$\log(i) = \log(io) + \frac{\eta}{b} \quad \text{(eq. 6)}$$

Where b (Tafel slope) $= \pm\frac{RT}{\alpha nF}$, a measure of how fast the current increases against overpotential.

1.4.3 Electrocatalysis for lignin valorization

Electrocatalysis could be the tool to conduct a green and sustainable process by means of a catalyst and renewable electricity and to depolymerize lignin at room temperature and pressure, namely, under milder conditions with respect to other catalyzed processes. Anyway, the surface-catalyzed and unselective nature of this depolymerization type brings to a big influence of the electrode structure and to yield reduction by overoxidation phenomena [28]. Both oxidation and reduction can be achieved, the choice between the two pathways depends primarily on the reactant itself, on its reactivity and on the target products.

The polymeric structure of lignin can be broken down both by oxidative and reduction pathways. The oxidative mode aims at increasing oxygen content in the final product, through a transfer of electrons from lignin to the anode material, while reduction proceeds through electrons transfer from cathode to lignin, obtaining hydrogen- and carbon-rich products (lignin oil) [29]. In Figure 1.27 different electrocatalytic pathways are shown:

an indirect electrocatalytic process proceeds with the help of a mediator, that is oxidized/reduced by the electrode, and lignin would be finally oxidized/reduced indirectly;

direct oxidation and reduction involve the direct transfer of electrons between the electrode and lignin;

the combination of the anode for lignin oxidation and the cathode for lignin reduction creates a hybrid electro-oxidation and reduction;

through electrical-chemical combination, lignin is directly electrooxidized on the anode and chemically oxidized by the electro-generated reactive oxygen species (ROS) [29].
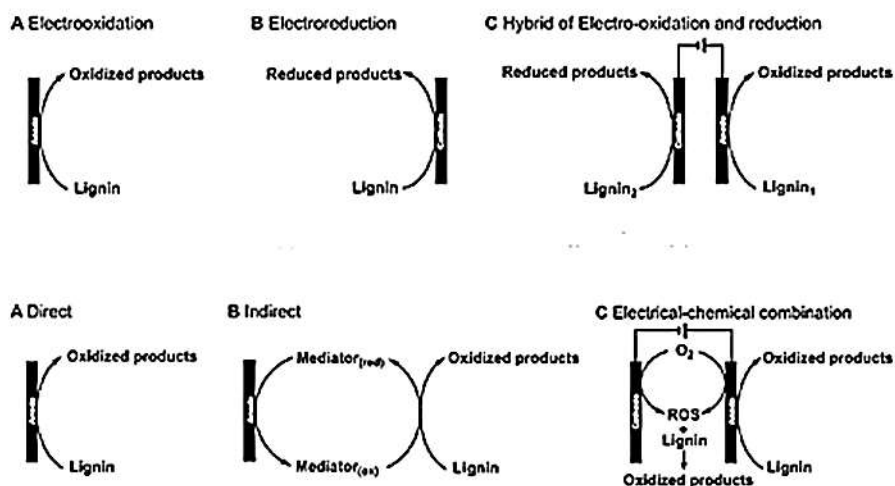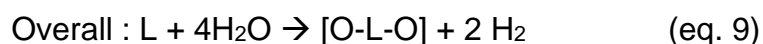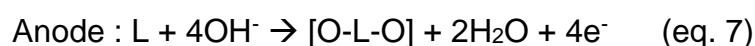
Figure 1.27 Electrocatalytic pathways: Electrooxidation, Electroreduction, Electrooxidation + reduction, Direct and indirect oxidation, Electrical-chemical combination [29]

Electrooxidation of lignin includes several phenomena such as lignin functionalization, depolymerization, intermediates oxidation, overoxidation and polymerization. C-O bound and C_α-C_β in β-O-4 linkages are found to be successfully cleaved by electrocatalysis. During anodic oxidation of lignin occurs in aqueous environment, development of hydrogen through electrolysis is observed at the cathode at a lower potential than the normally required for HER. Hence, Oxygen evolution (OER) is suppressed at such potential [29]. Equations 7-9 show lignin electrooxidation and simultaneous H2 evolution:

$$\text{Anode} : L + 4OH^- \rightarrow [O\text{-}L\text{-}O] + 2H_2O + 4e^- \quad \text{(eq. 7)}$$

$$\text{Cathode} : 4H_2O + 4e^- \rightarrow 4OH^- + 2\,H_2 \quad \text{(eq. 8)}$$

$$\text{Overall} : L + 4H_2O \rightarrow [O\text{-}L\text{-}O] + 2\,H_2 \quad \text{(eq. 9)}$$
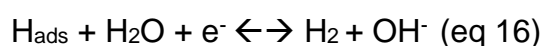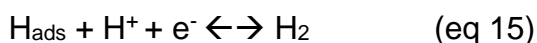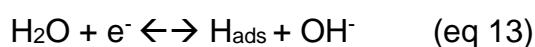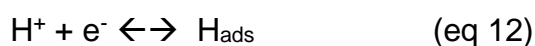
The anode material and structure play key roles in the process. The electrode should be stable towards anodic corrosion and catalytically active for lignin depolymerization. Transition metals such as Ni and Co, metal alloys with Fe and Ti, metal oxides like IrO2, PbO2, SnO2 have been used [29]. The transfer of a single electron from the anode in aqueous environment generates a hydroxy radical. The interaction between hydroxy radicals (*OH) and the electrode is crucial for a selective and efficient lignin oxidation: free radicals in solution could fully oxidize to CO2 organic species deriving from lignin depolymerization. Anyway, if radicals are strongly adsorbed by electrode

41

surface, they will oxidize the metal that acts as a mediator and a more selective oxidation of organic species will be achieved [29].

Electroreduction of lignin is not so commonly employed as oxidation, but it represents a useful pathway to reduce issues with overoxidation. Electrocatalytic hydrogenolysis of lignin feedstock is one of the most promising approaches for a selective depolymerization, integrating the reduction of protons (eq. 10) and the hydrogenation of organic compounds at the cathode, while oxygen evolution (eq. 11) is observed at the anode [29].

$$2H^+_{(aq)} + 2e^- \rightarrow H_{2(g)} \qquad \text{(eq. 10)}$$

$$2H_2O_{(l)} \rightarrow O_{2(g)} + 4H^+ + 4e^- \quad \text{(eq. 11)}$$
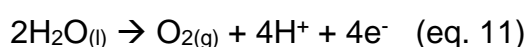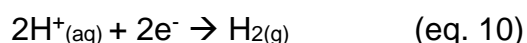
The steps for cathodic reduction of water involve the formation of adsorbed H (Volmer step eq. 12-13), the combination of two H to form H_2 (Tafel step eq. 14) and the concerted hydrogen production (Heyrovsky step eq. 15-16)

$$H^+ + e^- \leftrightarrow H_{ads} \qquad \text{(eq 12)}$$

$$H_2O + e^- \leftrightarrow H_{ads} + OH^- \qquad \text{(eq 13)}$$

$$2\,H_{ads} \leftrightarrow H_2 \qquad \text{(eq 14)}$$

$$H_{ads} + H^+ + e^- \leftrightarrow H_2 \qquad \text{(eq 15)}$$

$$H_{ads} + H_2O + e^- \leftrightarrow H_2 + OH^- \quad \text{(eq 16)}$$

In electrocatalytic hydrogenolysis of lignin, HER by Tafel and Heyrovsky steps is avoided though the generation of chemisorbed hydrogen species on the electrocatalyst at lower overpotential. The synergy between electrocatalyst and electrolyte solution aims to maximize Faradaic efficiency, hence electrons are used for hydrogenation/hydrogenolysis of feedstock over HER [51]. H_{ads} species can react with lignin, cleaving C-O single bonds [29]. The equation 17 shows a simplification of hydrogenolysis of a lignin residue L-C-OH, containing a C-O bond.

$$L\text{-}C\text{-}OH + H_{ads} \rightarrow L\text{-}C + H_2O \text{ (eq 17)}$$
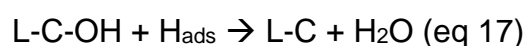
Hydrogenation is associated with addition of chemisorbed hydrogen to aromatic rings after hydrogenolysis of ether linkages. The main occurring phenomena are hydrogenation to cyclic alcohols and cycloalkyl ethers. Cathodic electrodes based on

Hg, Ni Raney, Cu, Ru, Pd have been tested [29]. Figure 1.28 shows some of the achievable products from hydrogenolysis of a lignin model compound. Conditions for an effective hydrogenation/hydrogenolysis process are:

• Availability of electrons on the catalyst particles

• Efficient reduction of protons to generate Hads

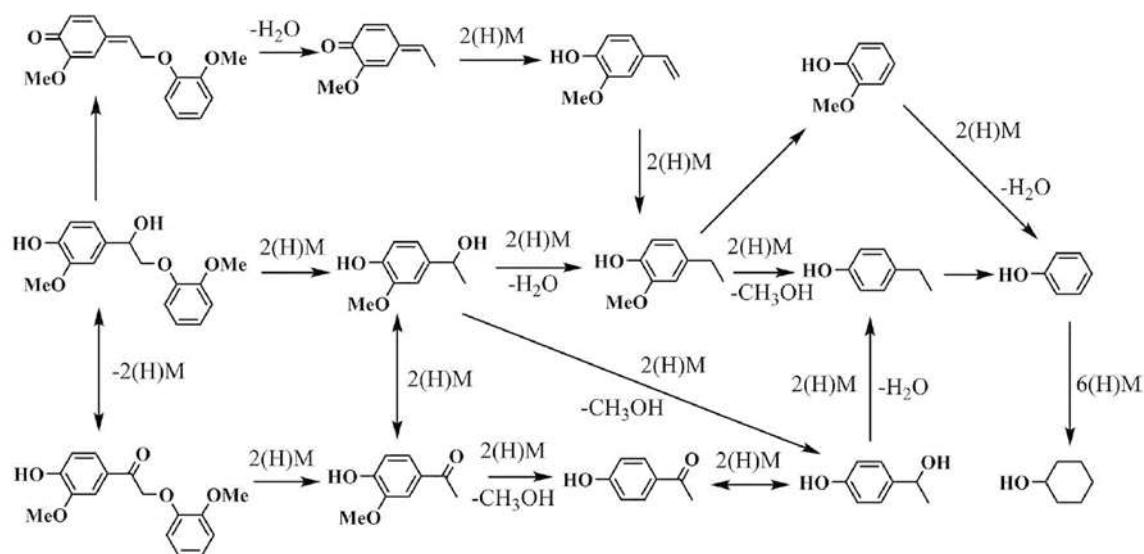• Contact between reactant feedstock and catalyst particles [51].

Figure 1.28 Reaction pathways for possible products in the electrocatalytic hydrogenolysis of a lignin model compound [29]

D. Schmitt et al. reported an experimental work on lignin oxidation combining electrocatalysis below 100°C in aqueous electrolytes and product recovery through a basic anion exchange resin to selectively separate low molecular weight phenols [30]. Different Ni- and Co-based anodes were tested, resulting in a preference for vanillin as main product and obtaining different yields, as shown in Figure 1.29. The selected temperature of 80°C was chosen according to higher yields of vanillin.

Entry	Anode	UNS-#	Alloy base	Yield of vanillin (1) / wt %
1	Ni	–	–	0,7
2	Monel 400k	N04400	Ni	0,7
3	Nichem 1151	–	Ni	1,0
4	Co	–	–	1,4
5	Stellite 21	W73021	Co	1,8

Figure 1.29 Influence of the anode material on electrochemical degradation of lignin [30]

Besides the three-electrode cell, other setups and reactors can be used for lignin depolymerization, such as the semi-continuous reactor (Fig. 1.30) reported by S. Stiefel et al. [31], achieving electrochemical lignin conversion and membrane filtration. This is made by two polymethylmethacrylate (PMMA) anodic and cathodic casings, separated by an anion exchange membrane. When the lignin solution enters the reactor, a flow distributor homogenizes it. Four nickel electrode materials with different morphologies and volume-specific surface areas have been tested and inserted planar in the chambers: a flat plate, a wire netting, unstructured fleece material and a foam-like material [31]. Authors found out that the foam-like electrode material, with higher electrode area, shows the strongest depolymerization of lignin.
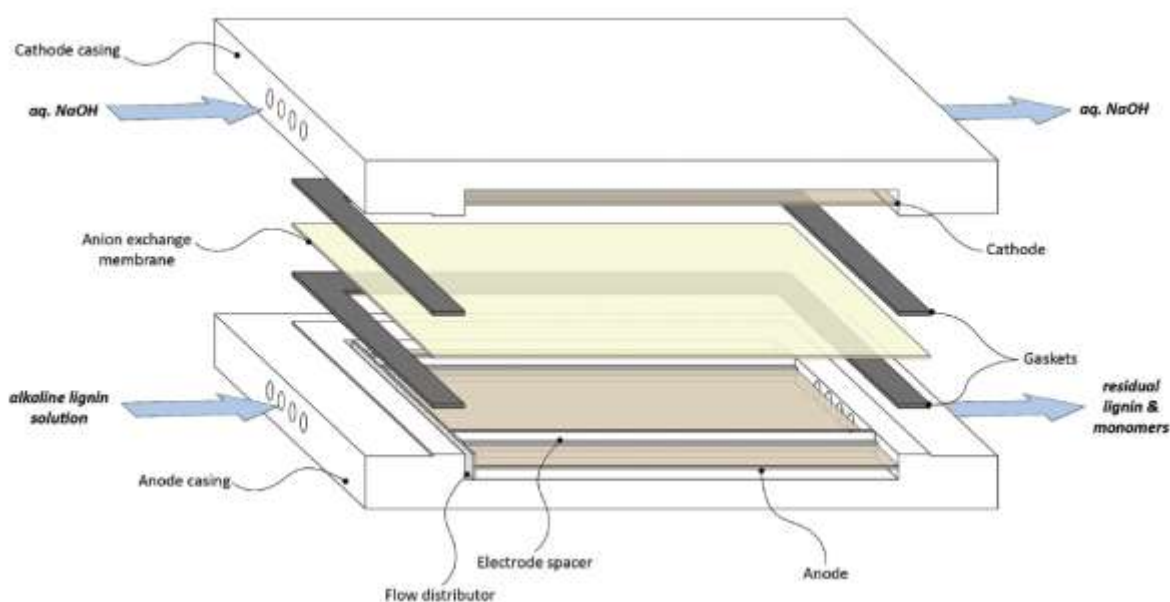

Figure 1.30 Cross section scheme of the electrochemical reaction for the continuous cleavage of lignin [31]

An interesting work [32] regarding the electrochemical oxidation of lignin on a Pt/Co alloy electrocatalyst shows the behavior of depolymerization products concentration with time. The most stable products increase their concentration with oxidation time, as shown in Figure 1.31, while other compounds participate in proceeding chemical or electrochemical reactions and their concentration decreases with time. This means that oxidation time, together with the applied potential, plays a crucial role in the oxidation or reduction of a starting material, especially with lignin, whose complex structure would break and rearrange randomly. To increase selectivity toward a target

molecule, an accurate selection of **reaction time**, **electrode material**, **current density**, **applied potential**, **temperature**, **concentration of starting feedstock** and **pH** should be done.

Lignin oxidation product concentrations (ppm).

Oxidation product	Oxidation time (min)		
	83	1200	2700
2,4-dimethyl-1-heptene	0.07	0.12	0.26
Heptane	0.42	0.49	0.50
2-methoxy-phenol	0.60	0.54	0.73
Phenol	0.08	–	–
2,6-dimethyl-nonane	0.06	–	–
Vanillin	8.45	7.43	9.83
Apocynin	1.96	1.62	2.49
1,3-bis(1, 1-dimethylethyl)-benzene	0.14	0.21	0.41
2,4-di-tert-butylphenol	0.18	0.47	0.44
1-(4-hydroxy-3,5-demethoxyphenyl)-ethanone	0.23	–	0.23
4-methyl-benzaldehyde	–	0.17	–

Figure 1.31 Lignin oxidation products concentrations over time [32]

Wijaya et al. [51] studied the electrocatalytic hydrogenation-hydrogenolysis (ECH) of phenolic molecules in the stirred slurry reactor reported in Fig. 1.23 (paragraph 1.4.2), using carbon-supported catalysts (Pt/C, Ru/C, Pd/C). They evaluated the correlation between electrocatalytic activity, electrode active surface sites, electrolyte, pH and potential. Neutral-acid (H2SO4 – NaCl) catholyte-anolyte pair was the best configuration to maximize the Faradaic efficiency for ECH. 0.2 and 0.5 M concentrations of electrolytes were tested at a constant current density and temperature [51].

• In case of Pt/C, the guaiacol conversion increased with the anolyte proton concentration (acidic pH). At pH>9, direct ring saturation route was predominant, while at pH<2, the demethoxylation step was favoured. Operating at higher catholyte concentration, guaiacol conversion was reduced.

• In contrast, with Ru/C and Pd/C, catholyte pH changes did not affect the product distribution. Guaiacol conversion was found to be higher with Pt/C catalyst [51].

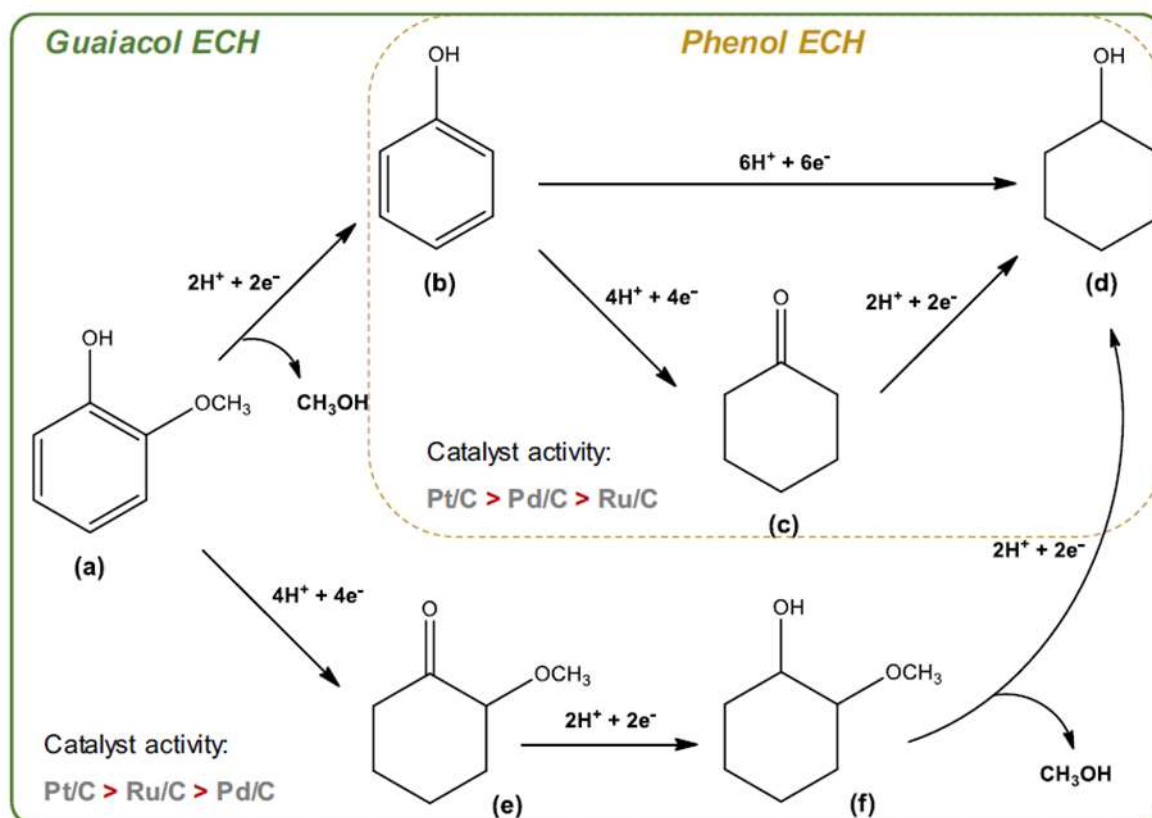Reaction pathways for ECH of guaiacol and phenol are reported in Fig. 1.32.

Figure 1.32 Guaiacol and phenol reactivity in ECH: a= guaiacol, b= phenol, c= cyclohexanone, d= cyclohexanol, e= 2-methoxycyclohexanone, f= 2-methoxycyclohexanol, and methanol as the byproduct [51]

Bawareth et al. conducted lignin oxidative depolymerization in an electrochemical batch reactor equipped with 3D nickel electrodes, with high active surface. A Swiss Roll electrode assembly was hosted in an acrylic glass tube, with a length of 15 cm and an inner diameter of 1.2 cm. Two rectangular pieces of nickel foam electrodes were assembled in the reactor, connected by two nickel wires and separated by a polymer spacer. The electrodes are rolled up together to obtain the Swiss Roll assembly (Fig. 1.33), inserted in the glass tube. Kraft lignin is dissolved in NaOH 1M and 100 mL of lignin solution (5g/L) are passed across the reactor with a flux of 50 mL/min, at room temperature and 3.5 V potential for 7 hours [52].
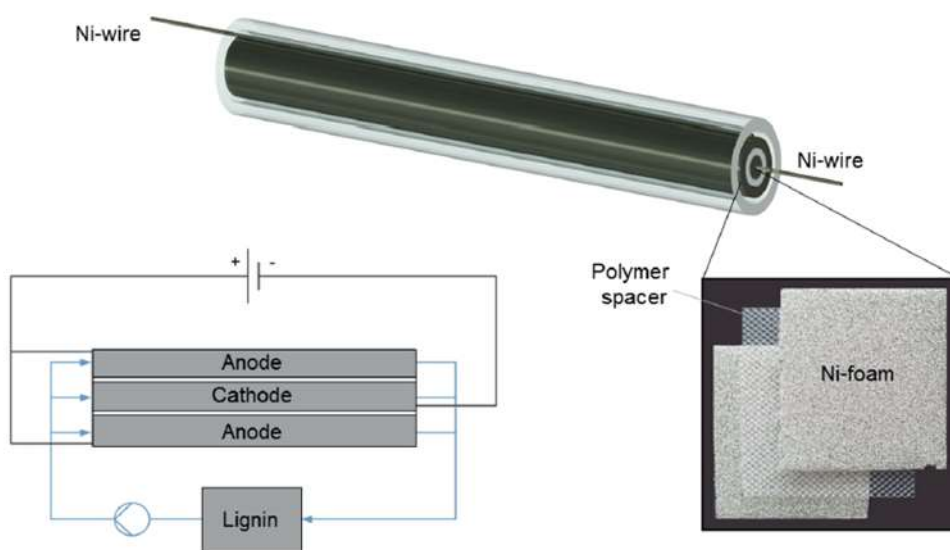
Figure 1.33 Swiss Roll electrochemical reactor [52]

Together with the production of chemicals, cogeneration of hydrogen is a meaningful target in the lignin exploitation processes. It could represent a renewable route for hydrogen production, with reduced costs through the application of lower energy input and with an economic gain through value-added products sale. To enhance surface area of the catalyst and mass transport of species, O. Movil et al. [33] used non-precious nanoparticle electrocatalysts for lignin oxidation in alkaline media, in a typical three-electrode cell. They worked with NiCo/C, Ni/C and Co/C electrocatalysts, a Pt counter electrode, a Hg/HgO reference electrode and lignin solution in NaOH 0.1M. Cyclic voltammograms at scan rate of 0.02 V and Linear sweep voltammograms were recorded. NiCo/C electrocatalyst was chosen because lignin oxidation current in presence of Ni/C and Co/C decreased rapidly as a sign of products adsorption on the active surface of the catalysts, limiting the catalytic activity. To verify lignin oxidation, FTIR and UV-Vis spectra were compared with unoxidized lignin [33].

Wessling et al. integrated the electrochemical depolymerization of Kraft lignin with the product separation through an electrochemical membrane reactor. The products are separated by an overpressure on the anode side, the membrane permeates low molecular weight molecules and retains high molecular weight lignin. Kraft lignin was dissolved in NaOH 1M and delivered to the anode compartment [53]. The system was used in semi-continuous mode. A scheme of the membrane reactor is reported in Fig. 1.33.
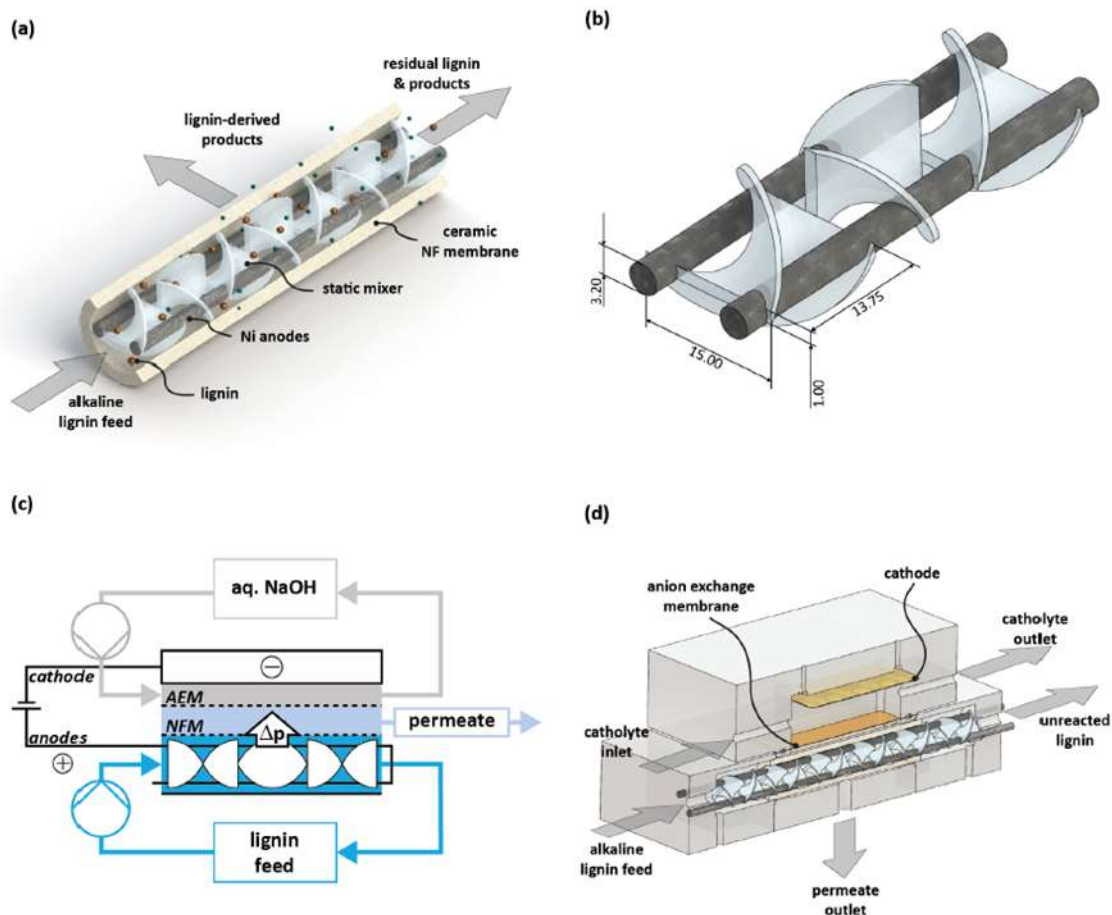
Figure 1.33 Electrochemical membrane reactor: (a) scheme with product removal; (b) electrode and mixer unit; (c) complete experimental setup; (d) cross section of the module [53]

Given the lignin complexity, some works start from a lignin model compound, containing the most common moieties, to study lignin depolymerization behavior. An example is reported by Kim et al. [34], in which copper-catalyzed oxidative cleavage of the C-C bonds of β-alkoxy alcohols and β-1 compounds is examined. Obtained results from model compounds as starting materials would not reflect lignin behavior, that is involved in polymerization-depolymerization and rearrangement phenomena. In addition to that, the dependance on pH and solvent-affinity would be different because the overall structure and composition is not representative. Surely model compounds can identify some moieties reactivity, but lignin structure creates too many variables with respect to working conditions.

1.5 Issues with biomass-derived processes

In addition to operational problems related with biomass, like seasonality and transport, economic challenges should be faced to create an established market based on biomass and biorefineries. The starting prices of the feedstock materials are usually so high that production facilities are only established locally, near the source, leading to a centralization of biomass projects [35]. Frequent fluctuations in prices would not encourage investors to take part because of a high market risk, low yields per material weight and high pre-treatments costs. Social challenges are connected to the living and working conditions of the local citizens, to the land use issue and overexploitation of the land, leading to ecosystem loss, soil nutrients depletion and soil activity loss [36]. The shifting from laboratory scale to industrial scale of biomass processes highlights the energy density issue (Fig. 1.34), because biomass is a crude and high-water content material.
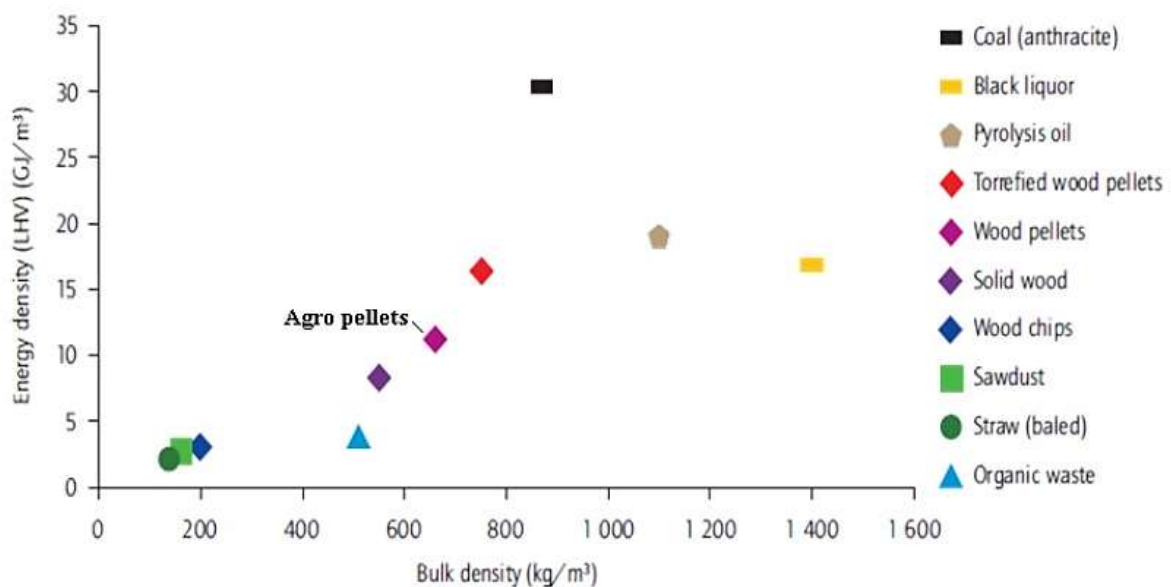

Figure 1.34 Bulk density and energy density of different feedstocks [37]

The establishment of a new market for biomass utilization necessarily involves the shifting from a petroleum-based economy to a bio-based one. Being petroleum the biggest competitor to natural sources, investors are more likely to choose an already established and safe route, with reduced investment costs. The majority of problems would be reduced by adopting waste biomass, crop and agroforestry residues and waste streams as feedstocks.

2. Experimental part

2.1 Materials and reagents used

The list of materials and reagents used for the entire process, from catalyst pre-treatments to final analyses, are reported in Table 2.1.

Table 2.1 List of materials and reagents

Compound	Physical state	PM (g/mol)	Purity %	Supplier
NaOH	Pellets	40	98	Sigma-Aldrich
Kraft lignin	Powder	10000	96	Sigma-Aldrich
Nickel metal foam	Macroporous solid			Alantum
Copper metal foam	Macroporous solid			Alantum
HCl	Water solution	36.46		Sigma-Aldrich
Isopropanol	Liquid	60.09	100	Sigma-Aldrich
Sulfuric acid	Liquid	98.08	96	Sigma-Aldrich
Ethyl acetate	Liquid	88.10	99.8	Sigma-Aldrich
n-Hexanol	Liquid	102.16	99	Sigma-Aldrich
DMSO	Liquid	84.17	99.8	Euristop

2.2 Electrocatalyst preparation and pre-treatments

Nickel and **copper** open cell foams, with geometrical area of 2,64 m^2, 10 mm x 10 mm x 1,6 mm, were used as electrocatalysts as received or after calcination, 400°C for 1 hour for copper and 500°C for 1 hour for nickel foams. Catalyst samples are listed in Table 2.2 with calcination conditions and applied treatments.

Table 2.2 Catalyst samples

CATALYST	CALCINATION	TREATMENTS
Ni bare	/	HCl 1M + isopropanol + UPP water
Cu bare	/	HCl 1M + isopropanol + UPP water
Calcined Ni	500°C 1 hour	UPP water
Calcined Cu	400°C 1 hour	UPP water

The foam pieces were electrically connected to a potentiostat by Pt or Cu wires for Ni and Cu, respectively.

Cu and Ni bare foams were pre-treated before CV scans by washing them in HCl 1M solution to remove surface oxides, then in isopropanol and finally in UPP water to remove contaminants and acid residues. Calcined foams were pre-treated only with water to remove contaminants from their surfaces.

2.3 Catalyst characterization techniques

Electrocatalysts are characterized by Scanning Electron Microscopy (SEM), X-ray Diffraction (XRD) and Raman techniques.

Scanning Electron Microscopy (SEM) - Energy Dispersive X-ray Spectrometry (EDS)

Scanning electron microscopy (SEM) is used to magnify details of a solid material and study its surface morphology. The electron beam is a high energy incident electron probe, or primary electron beam, condensed by electromagnetic lenses and transmitted through the sample. The physical phenomenon significant for image formation is coherent and incoherent scattering. Signals from secondary electrons or back-scattered electrons are produced by a process of impact ionization [54].

In Figure 2.1 different signals from electron beam are reported. **Secondary electrons** provide topographical information and are generated from the surface by inelastic interactions. **Backscattered electrons** are higher in energy than secondary ones and

result from elastic interactions between the material and the electron beam. Bigger atoms can better diffuse backscattered electrons, recording higher signals. The number of backscattered electrons is proportional to the atomic mass of the atoms, hence there is the possibility to differentiate different phases of the material. As a result, brighter and darker regions will be highlighted by this technique. Energy dispersive X-ray spectrometry (**EDS**) allows the determination of the surface composition.
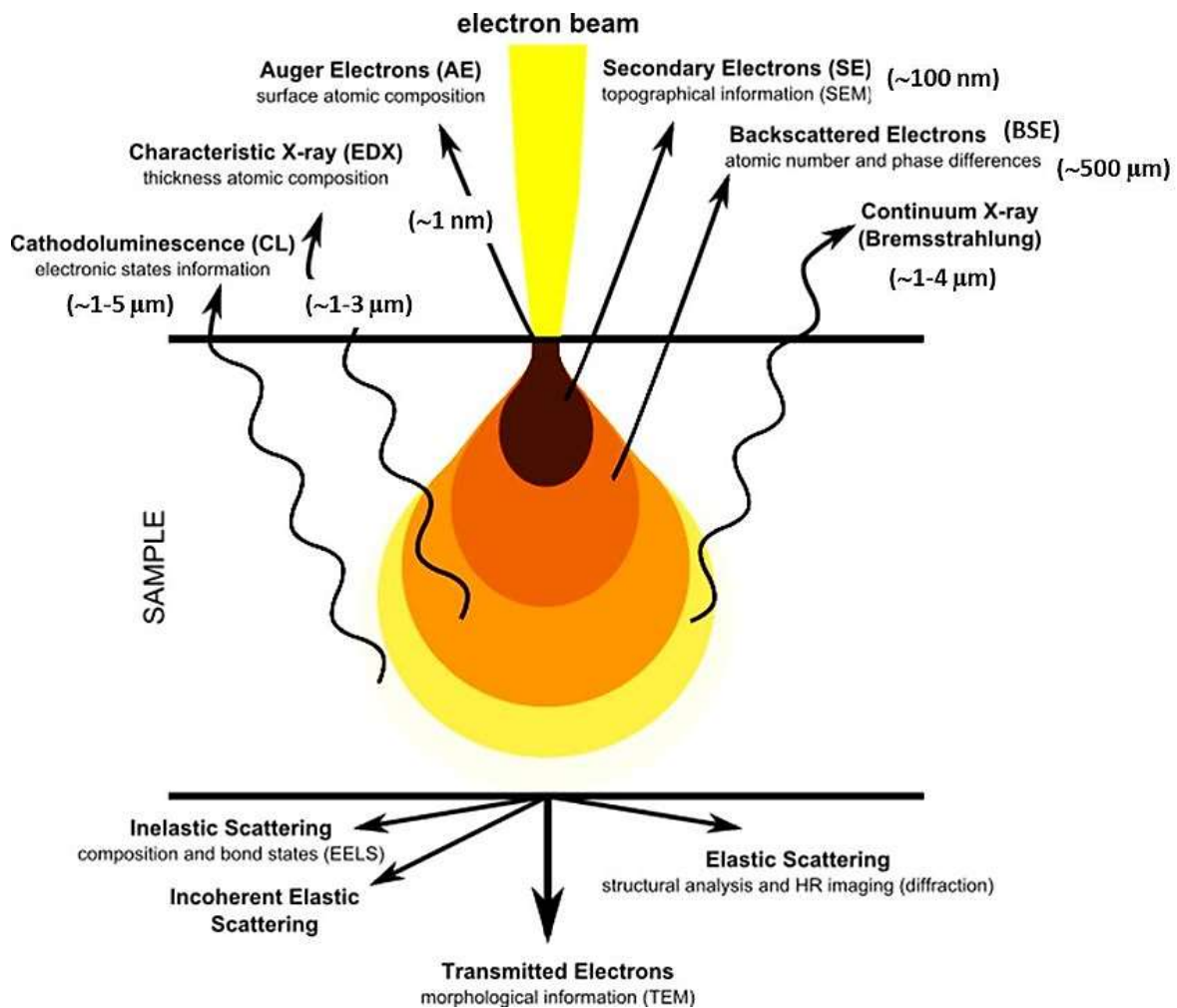

Figure 2.1 Signals emitted by the interaction electron beam – material. [55]

X-ray Diffraction (XRD)

X-ray diffraction (XRD) is an analytical technique used for the study of the nature and crystallinity of a solid material. It is mainly identified as a qualitative technique, but signals are proportional to the amount and crystallinity of a substance present in the sample [56]. The technique consists of a monochromatic X-ray incident beam that generates a diffraction phenomenon (Fig. 2.2), described by Bragg's law (eq. 18):

$$n\lambda = 2dsen(\theta) \qquad \text{(eq. 18)}$$

(λ = wavelength of incident radiation; n = diffraction order; d = distance between grid planes; θ = angle of incidence of the beam of the grid).
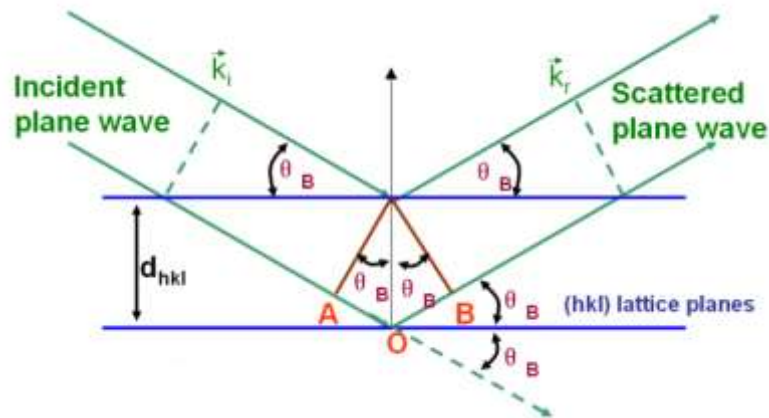
Figure 2.2 X-ray diffraction phenomenon [57]

XRD analysis for electrocatalysts characterization are performed by Bragg_Brentano X'pertPro Penalytical diffractomer with copper anode as source of X-radiation with 0,06° step size and acquisition time of 60 s per step in 3 - 81° 2θ range.

Raman Spectroscopy

Raman spectroscopy is used to provide a structural fingerprint, based on inelastic scattering phenomenon, known as Raman scattering, generated from a laser source in the range of visible, near infrared or near ultraviolet. The impact of the energy source excites the molecular vibrations that allow the sample identification, obtaining a spectrum with characteristic signals or "bands" [58]. The Raman shift (Figure 2.3) is the energy difference between the incident light and scattered light [59].
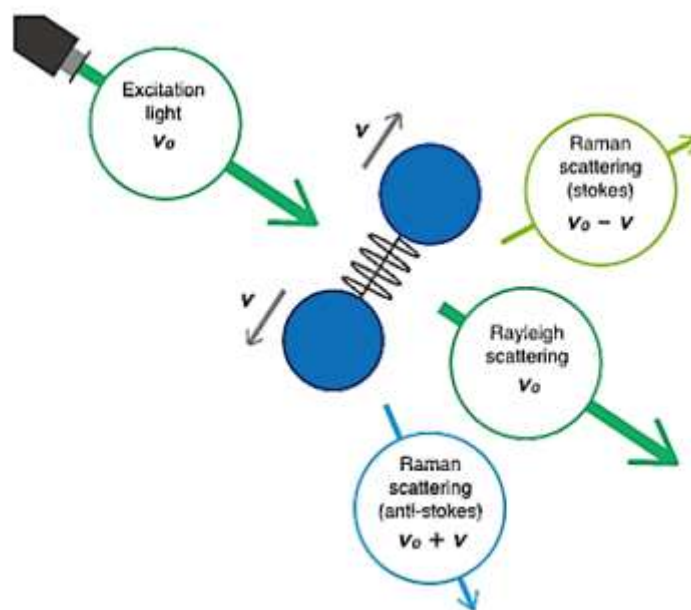
Figure 2.3 Raman scattering [59]

The instrument used is Renishaw RM1000 with a green laser (Ar + 514.5 nm) and 50x magnification. Spectra were recorded between 2000 and 100 cm^{-1}.

2.4 Cyclic voltammetry (CV)

Electrochemical studies of the electrocatalyst were conducted through cyclic voltammetry technique into a three-electrode glass cell, shown in Figure 2.4.
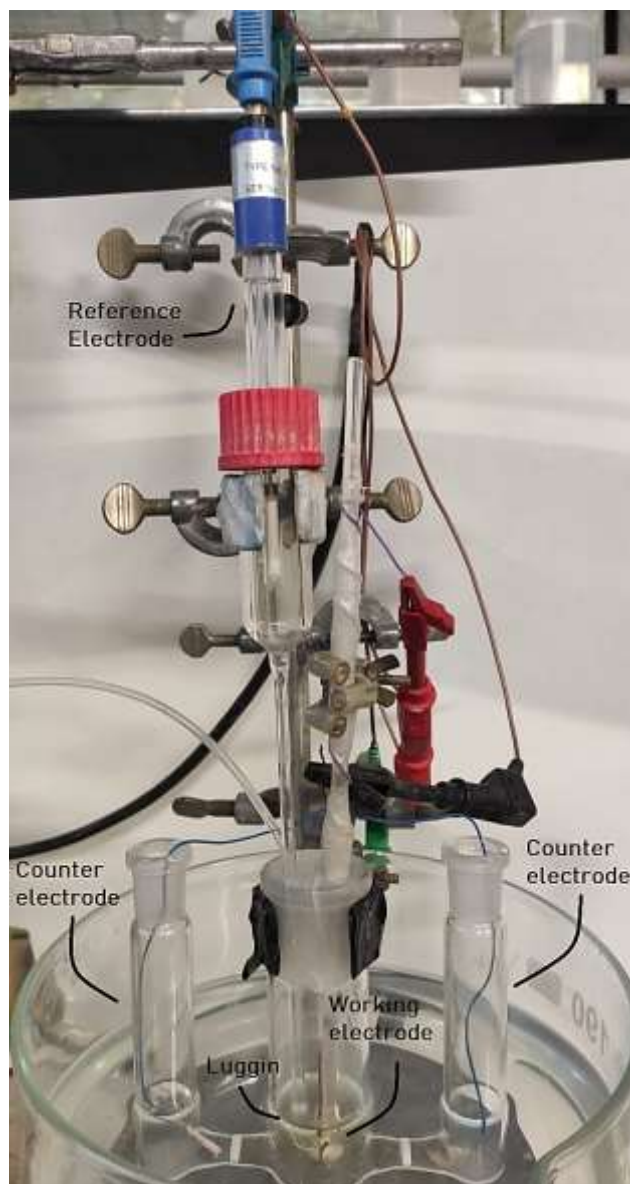
Figure 2.4 Electrochemical three-electrode cell

In the lateral compartments are placed platinum wires as counter electrodes, while in the central compartment a luggin connected to the calomel reference electrode and the working electrode, presented in paragraph 2.2. Between the three compartments there are two porous glass frits that separate the liquid solutions and enhance the passage of ions within the cell. The function of the luggin is to put in contact the reference and the working electrode, reducing ohmic losses. Electrodes are connected to a potentiostat, Metrohm Autolab PGSTAT204, to control the potential between the counter and the working electrode. The solutions of sodium hydroxide and lignin are purged with N_2 to remove oxygen before to pour them into the cell.

Cyclic voltammetry (CV) is an electrochemical method whose excitation signal is a triangular linear potential ramp that can be repeated, creating a cycle. The response I-E curve has a particular shape, shown in Figure 2.5, assuming a facile kinetic reaction.
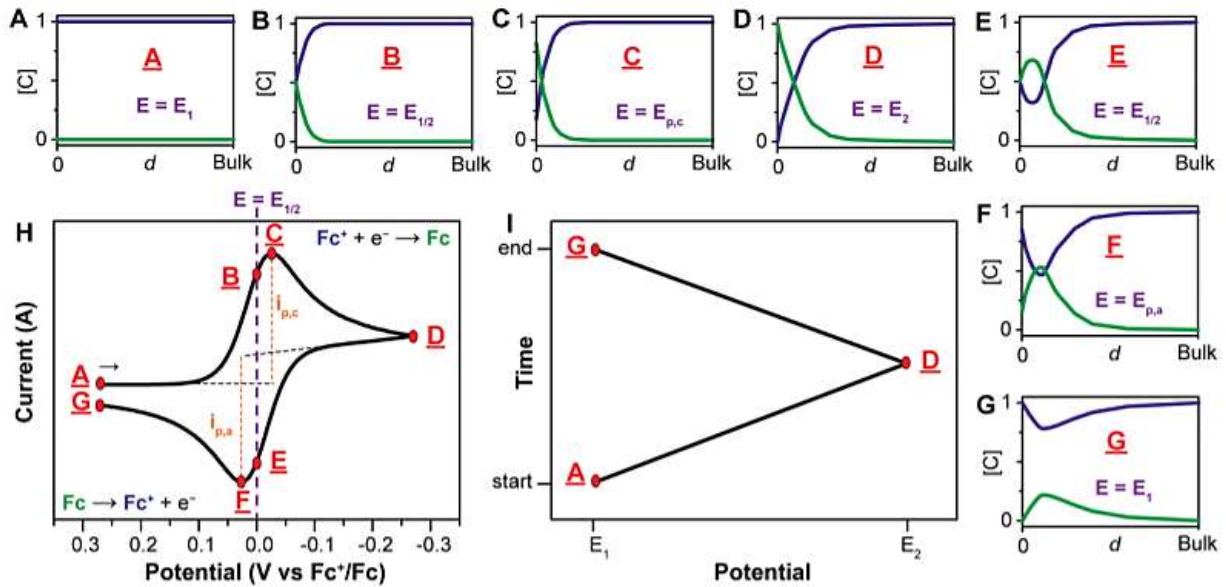

Figure 2.5 Cyclic voltammetry scan of a facile kinetic reaction and details of characteristic peaks [60]

To understand this particular shape of the response curve, there is the need to state that the Nernst equation (eq. 3) fixes the surface concentrations of oxidized and reduced species, while the flux of redox species from the solution bulk to the electrode surface depends on the concentration gradients. The current at the working electrode is higher when the concentration gradient is steep, on the contrary current decreases when concentration gradient flattens. The observable peaks in the CV scans are the result of oxidation and reduction at the maximum possible [60].

Randles and Sevcik equation (eq. 19) describes that the peak currents are proportional to the concentration of the redox species in solution and to the square root of the scan rate:

$$I_p = 0.4463 * nFAc(\infty)\sqrt{\frac{nFD}{RT}} * \sqrt{v} \qquad \text{(eq. 19)}$$

(I_p = peak current; n = electrons number; F = Faraday constant; A = electrode surface area; $c(\infty)$ = analyte concentration in the bulk; D = analyte diffusion coefficient; $\sqrt{v}$ = square root of the scan rate; R = universal gas constant; T = temperature).

Depending on the reversibility of the reaction, different cyclic voltammograms will be obtained. In reversible systems, that obey thermodynamic relationships, the equilibrium is established at any time at the electrode surface. Irreversible systems are characterized by a missing reduction peak after oxidation, or vice versa. In quasi-reversible systems the concentration ratio does not follow the Nernst equation, but the voltammograms look like reversible case at slow scan rates.

2.5 Chronoamperometry (CA)

Chronoamperometry is an electrochemical method that utilizes a potential step (Fig. 2.6) to reach a potential where a reduction or oxidation occurs and records the current response versus time. Usually, current decays within time and approaches zero, because a concentration gradient and a flux of species from the solution bulk to the electrode surface are created, until the complete reduction or oxidation, assuming a facile kinetic. The thickness of the diffusion layer grows over time in the direction of the solution bulk.
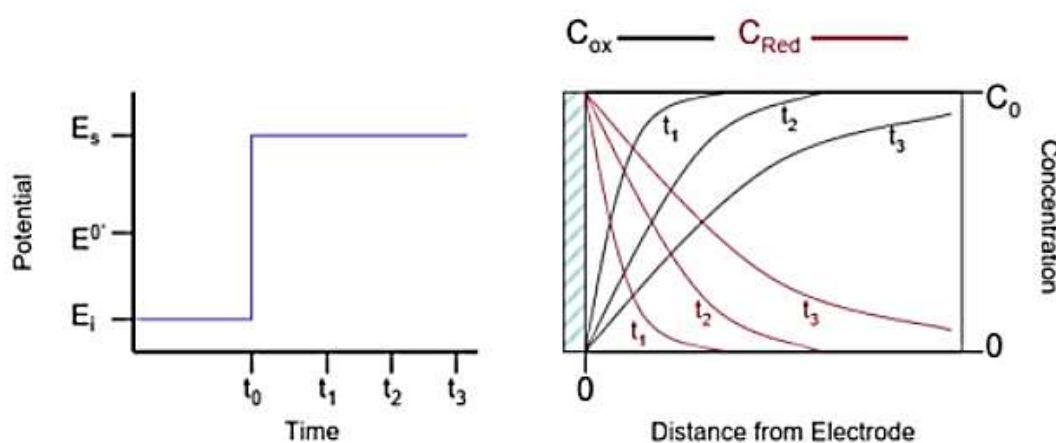

Figure 2.6 Potential step excitation and recorded current in chronoamperometry. [61]

The current is described by the Cottrell equation (eq. 20):

$$I(t) = \frac{nFA\sqrt{D}c(\infty)}{\sqrt{\pi}} * \frac{1}{\sqrt{t}} \quad \text{(eq. 20)}$$

($I(t)$ = current; n = number of electrons; F = Faraday constant; A = electrode area; D = diffusion coefficient; $c(\infty)$ = analyte concentration in the bulk; t = time).

2.6 Catalytic cycle

The catalytic cycle is conducted at room temperature (T=25°C) and atmospheric pressure. It is composed by:

- Three **cyclovoltammetry** scans in 25 mL of NaOH 1M in the central compartment and the same solution into the lateral ones to obtain the same liquid height (Fig. 2.4), between -0.4 V and 1 V vs SCE, with scanning rate of 5 mV/s;

- Three **cyclovoltammetry** scans in 25 mL of 10 g/L Kraft lignin solution in NaOH 1M in the central compartment and NaOH 1M solution into the lateral ones to obtain the same liquid height, between -0.4 V and 1 V vs SCE, with scanning rate of 5 mV/s;

- **Chronoamperometry** of 25 mL of 10 g/L Kraft lignin solution in NaOH 1 M, between 0.4-0.8 V vs SCE, with constant agitation of 1000 rpm and reaction time between 10-60 minutes, with NaOH 1 M solution in the lateral compartments;

- Three **cyclovoltammetry** scans in 25 mL of NaOH 1M in the central compartment and the same solution into the lateral ones to obtain the same liquid height (Fig. 2.4), between -0.4 V and 1 V vs SCE, with scanning rate of 5 mV/s;

- Three **cyclovoltammetry** scans in 25 mL of 10 g/L Kraft lignin solution in NaOH 1 M in the central compartment and NaOH 1M solution into the lateral ones to obtain the same liquid height, between -0.4 V and 1 V vs SCE, with scanning rate of 5 mV/s.

2.7 Extraction procedure

At the end of the chronoamperometry, the product mixture (25 mL) is poured from the central compartment of the cell to two falcons, where it is acidified with 2 mL of sulfuric acid 96%, to reach a pH<1. Shaking the falcon tubes and putting them into the centrifuge for 20 minutes at 4500 rpm, lignin precipitates on the bottom, leaving a liquid supernatant (S1) on the surface.

The supernatant is collected to be extracted with ethyl acetate, while the slimy lignin precipitate is put again in centrifuge, at the same conditions, with the addition of 20 mL of ethyl acetate. The so-obtained solution is filtered with Buchner to collect the solid lignin residue and the EtAc-soluble liquid (S2). The choice of ethyl acetate as solvent is linked with the extraction of aromatic molecules, with low molecular weight, to be efficiently treated and analyzed. In Figure 2.7, a schematization of the post-reaction process is reported.
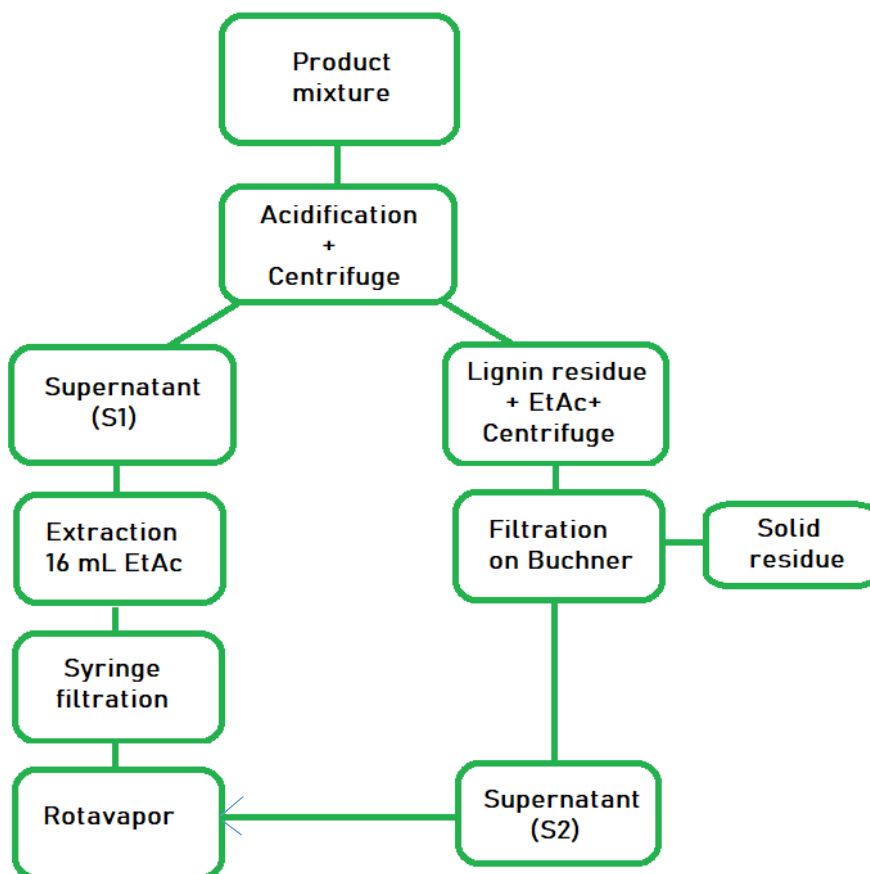
Figure 2.7 Scheme of post-reaction mixture treatments

The extraction procedure of the supernatant S1, that has been separated from the lignin precipitate, consists of three liquid-liquid extraction with 16 mL of ethyl acetate each. The liquid organic fraction is always filtered through a 0.45 μm syringe filter, in order to be analyzed with GC-MS and to eliminate possible aggregates.

After collecting the organic phases of the first (S1) and the second (S2) supernatant, they are poured into round flasks to be concentrated by rotavapor. During the solvent evaporation, it is very important to not completely remove the solvent, because molecules present in the product mixture will arrange together, forming solid aggregates. Hence, the liquid solutions are concentrated in 5mL of ethyl acetate.

The solid residue obtained after filtration on Buchner is weighted to calculate lignin conversion percentage.

2.8 Gas Chromatography - Mass Spectrometry (GC-MS)

The organic phases of S1 and S2 (Fig. 2.7) are analyzed through GC-MS technique, using n-Hexanol as internal standard to reduce errors due to the manual injection system. GC is a chromatography analytical technique in gas phase, in which the mobile phase is made by a carrier gas that flows into a column containing the stationary phase. The column is heated to a selected temperature to enhance the volatilization of the analytes, usually through temperature gradients to obtain enough resolution of final peaks in the spectrum. The amount of eluted analyte is plotted against the retention time, a measure of how long the molecule is retained by the stationary phase [62].

Gas chromatography has been coupled with a mass spectrometer detector (GC-MS). It ionizes and fragments analyte molecules, hence ions with different charge and mass are achieved, and the detector will recognize them depending on their mass/charge ratio (m/z). The resulting vertical lines spectrum allows reconstruction of the analyte molecule through identification of fragments, according to their atomic mass.

The instrument used is Agilent Gas Chromatograph 6890N series coupled to an Agilent Technologies 5973 Inert mass spectrometer with EI filament ionization system and quadrupole mass analyzer. The column is capillary, Agilent HP5, composed of 5% phenyl and 95% dimethyl-polysiloxane, with 30 m length and 1.025 mm diameter. The samples were manually injected with a 0.5 μL aliquote, maintaining a flow of 1 mL/min and starting from an injection temperature of 50°C for 3 minutes and then following a temperature ramp of 5°C/min up to 270°C. The selected method lasts 30 minutes and applies a pressure of 52 kPa. The analytes identification was carried out by the instrument's software, which compares the spectra with those present in the NIST library. Quantification through internal standard was made by constructing a calibration line for every analyte of interest, plotting the ratio of the analyte peak area over standard peak area against analyte concentration.

3. Results and discussion

Analyses on starting material, catalysts and electrooxidation reaction products are reported in this chapter, starting from pre-reaction chemical-physical and electrochemical catalyst characterization, then electrocatalytic reaction and finally post-reaction catalyst characterization.

3.1 Chemical-physical characterization of fresh catalysts

A comparison between Cu bare, calcined Cu, Ni bare and calcined Ni before reaction is conducted in this paragraph, through SEM images that show catalyst topography, XRD analysis and Raman spectroscopy for structural characterization. Both secondary electron and back-scattered electron images have been used, at different magnification.

Ni and Cu bare images at low magnification in Fig. 3.1 show similar morphologies, while at higher magnification in Fig. 3.2 Cu bare is characterized by some holes, where Ni bare presents swellings, due to the production method. EDS analyses (Fig. 3.3) conducted in selected regions of the catalysts did not evidence the presence of oxygen species, but only metal particles.
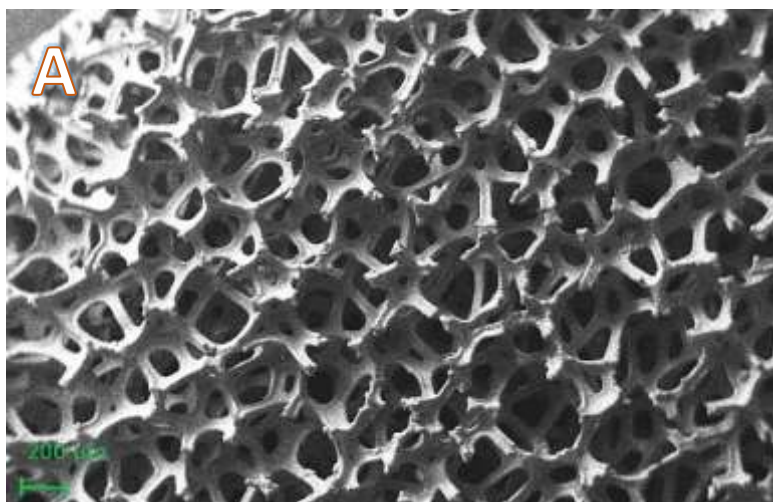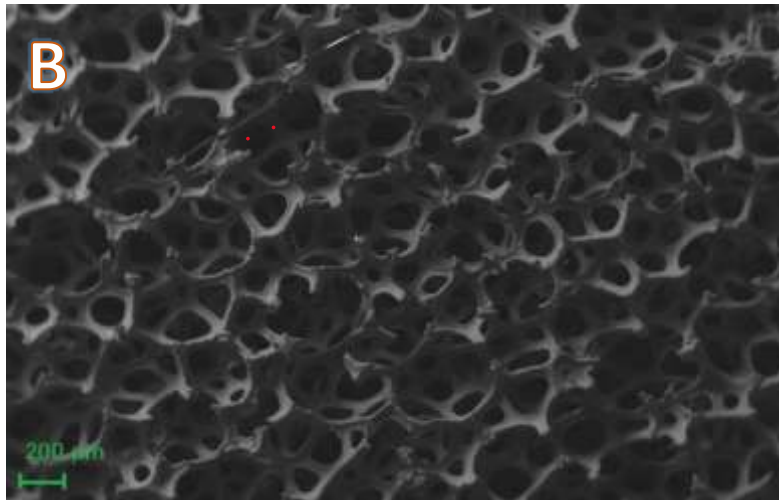
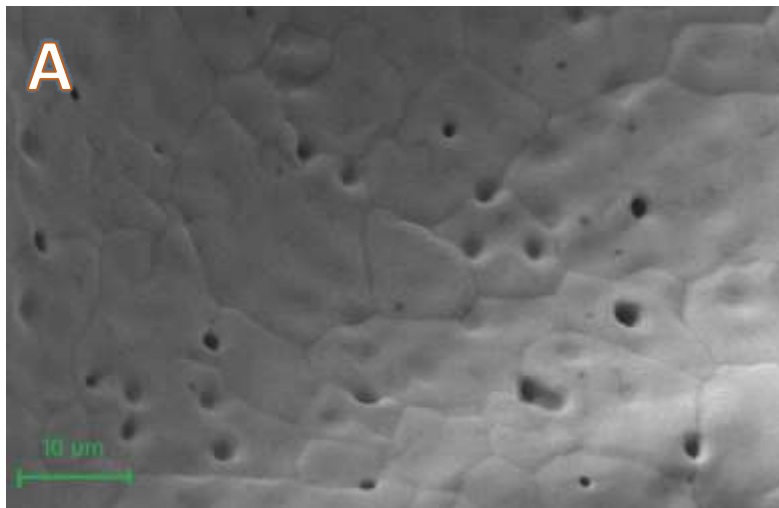*Figure 3.1 Cu (A) and Ni bare (B) secondary electron SEM images*
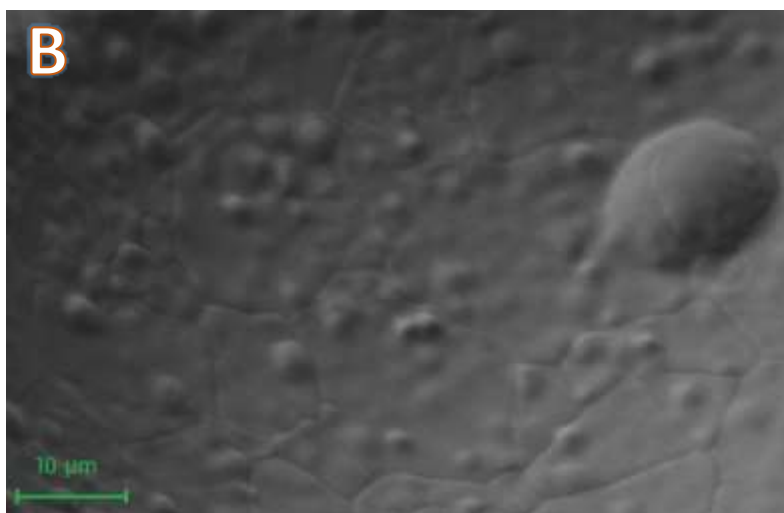
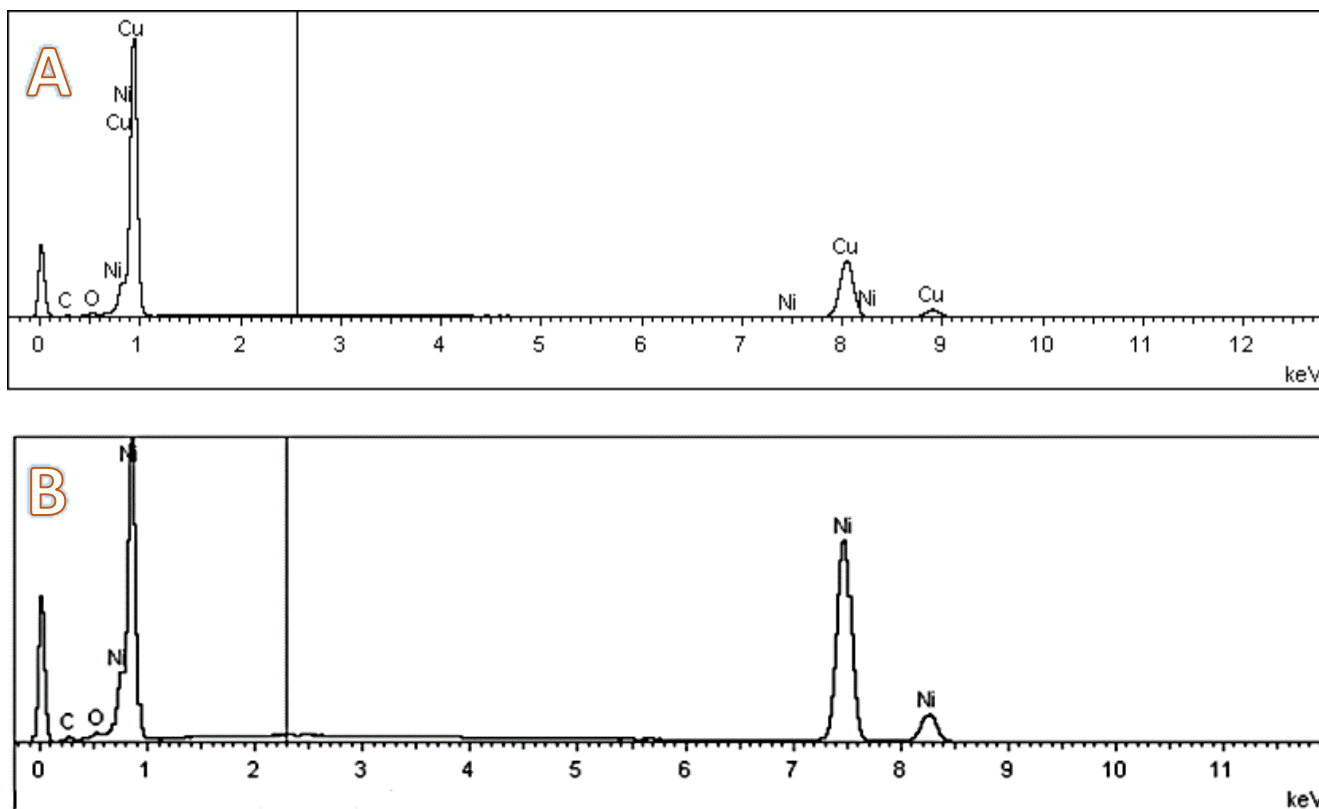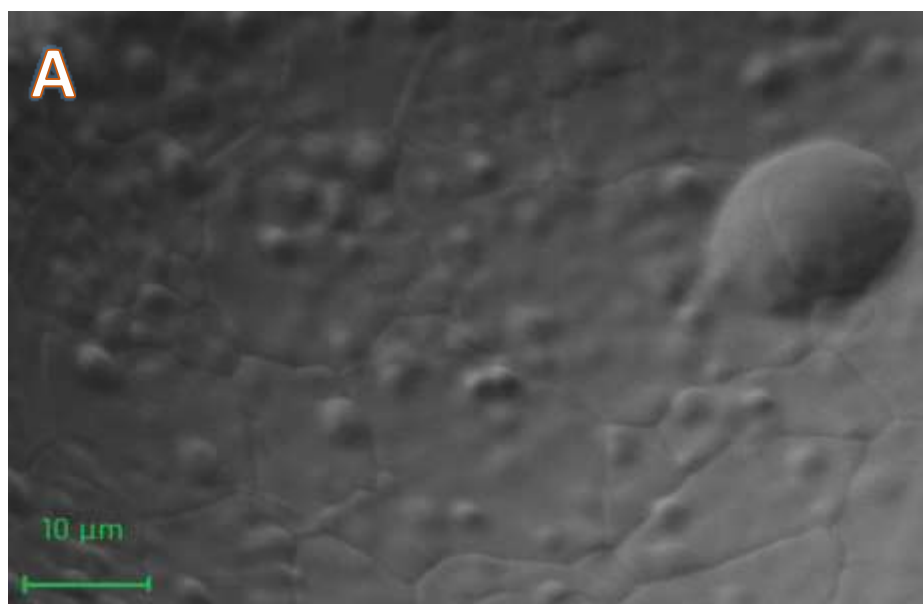*Figure 3.2 Cu (A) and Ni bare (B) secondary electrons SEM images*

Figure 3.3 EDS analyses of selected regions of Cu bare (A) and Ni bare (B) catalysts

Remarkable differences between non-calcined and calcined foams can be effectively noticed by comparing secondary electrons SEM images, shown in figures 3.4 and 3.5. Calcined Cu foam shows needle-like structures on their surface and calcined Ni foam shows bubble-like structures, because of the presence of oxides.

Figure 3.4 Cu bare (A) and calcined Cu (B) secondary electrons SEM images.
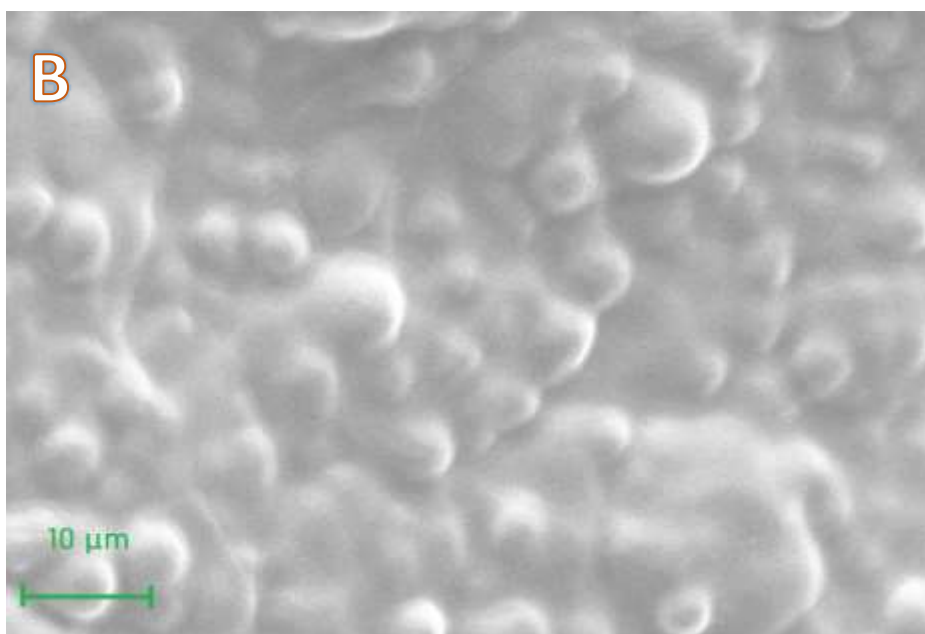
Figure 3.5 Ni bare (A) and calcined Ni (B) secondary electrons SEM images.

XRD characterizations on calcined foams in Figure 3.6 detected the presence of oxidized species. Comparing the pattern for calcined Cu and Cu bare, additional crystalline phases were identified for the calcined foam, which refer to CuO and Cu_2O formation [64] [65]. The presence of Cu_2O is predominant with respect to CuO. Cu bare pattern contains typical signals for the metal species. Ni bare XRD characterization shows the reflections of Ni^0 (45, 51 and 79 2θ°), while calcined Ni contains additional weak reflections corresponding to NiO. Raman characterizations on calcined foams have been reported in Figure 3.7. Calcined Ni foam Raman spectrum confirms the presence of NiO by identifying bands at 546 cm^{-1} and 1497 cm^{-1}. By analyzing Raman spectrum of calcined Cu foam, bands referred to copper oxides were identified at 293 and 620 cm^{-1} [66].
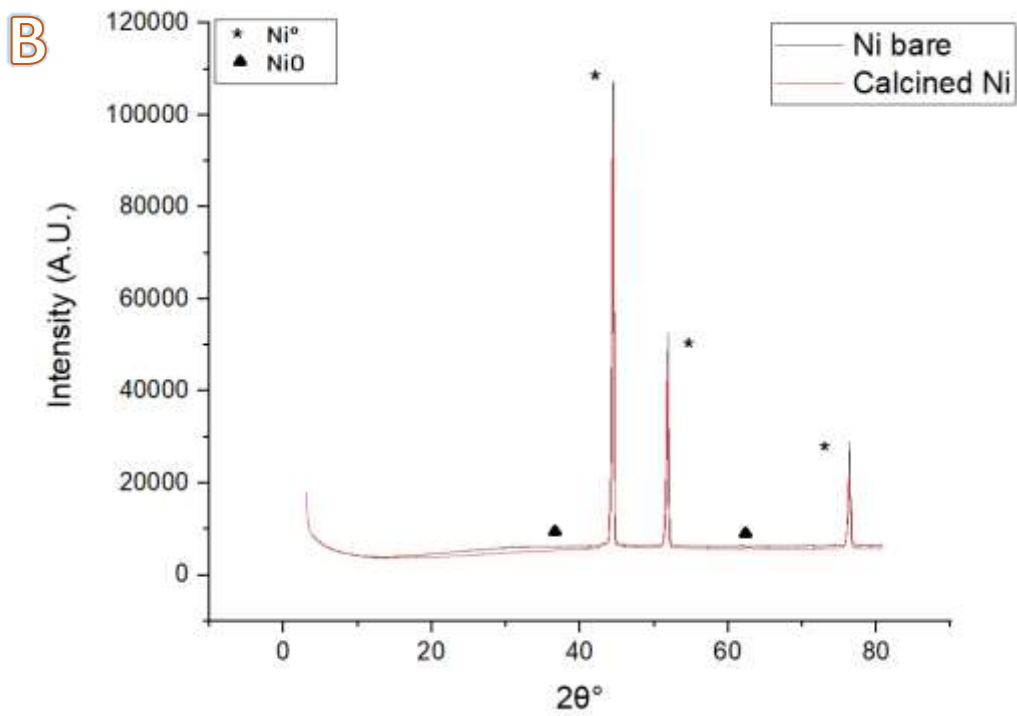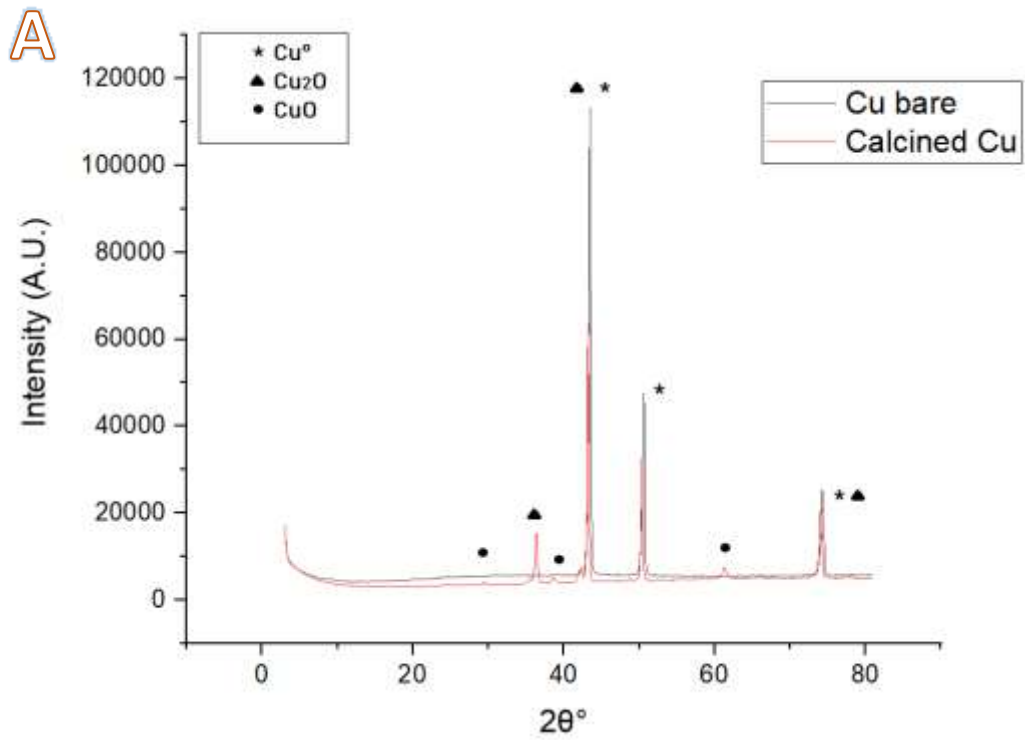
Figure 3.6 Calcined Cu and Cu bare XRD comparison (A). Calcined Ni and Ni bare XRD comparison (B).
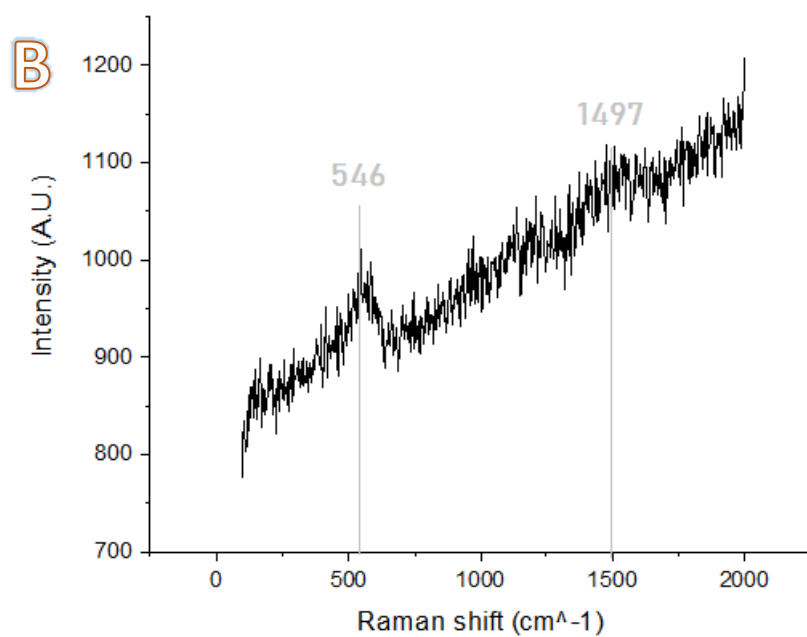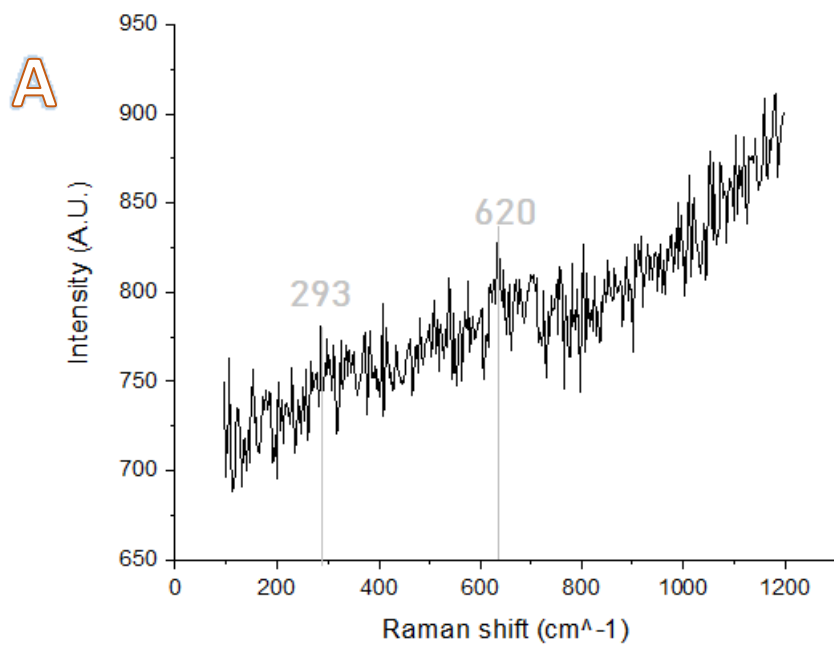
Figure 3.7 Raman characterization of pre-reaction calcined Cu (A). Raman characterization of pre-reaction calcined Ni foam (B).

3.2 Electrochemical characterization of fresh catalysts

Cyclovoltammetry technique is utilized to characterize the catalysts before reaction, adding first NaOH 1M and then lignin solution in the electrochemical cell. The pre-reaction procedure is reported in Chapter 2.

CV scans in NaOH 1M performed with Cu bare, Ni bare, calcined Cu and calcined Ni are compared each other (Fig. 3.8) to study the behavior of the electrocatalyst with respect to oxygen evolution reaction (OER) and to identify different oxidation peaks depending on the electrocatalyst. The onset of the OER in alkaline medium (equation 21) was observed at 0.5 V with Ni foam catalysts and a peak related to Ni^{2+}/Ni^{3+} (equation 22) couple around 0.35 V was also recorded. For Cu foam catalysts, the onset was shifted towards 0.6 V and a peak around -0.2 V was observed, because of Cu/Cu^+ oxidation (equation 23). Both the CV scans reach the oxidation plateau around 0,17 A/m^2, due to the recording limit of the instrument.

$$4OH^- \rightarrow O_2 + 2H_2O + 4e^- \qquad \text{(eq. 21)}$$

$$Ni(OH)_2 + OH^- \rightarrow NiOOH + H_2O + e^- \quad \text{(eq. 22)}$$

$$2Cu + 2OH^- \rightarrow Cu_2O + H_2O + 2e^- \qquad \text{(eq. 23)}$$
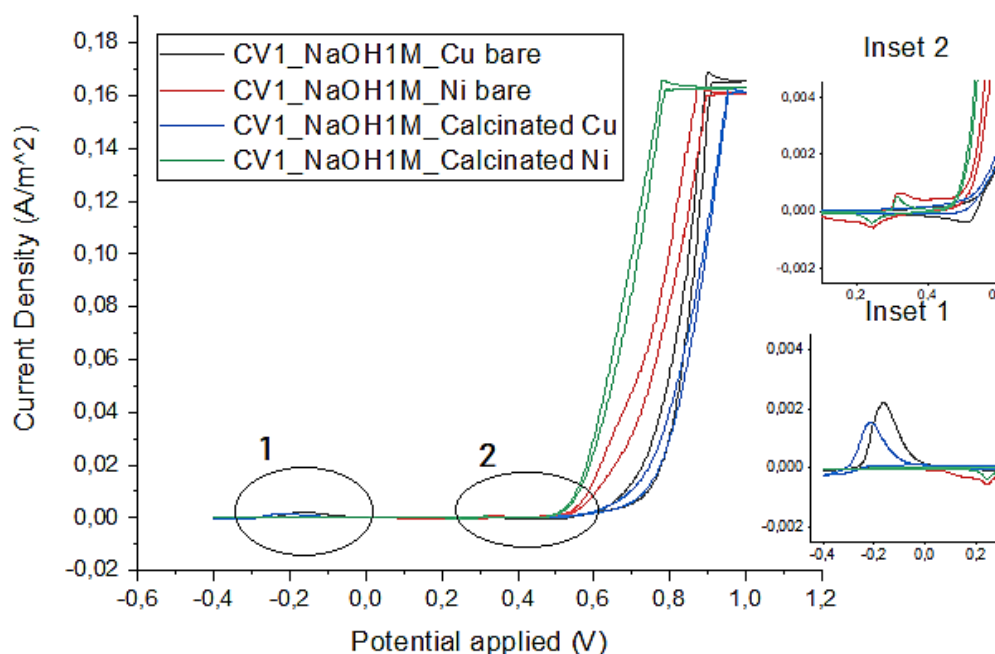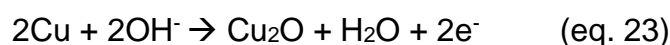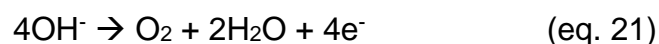

Figure 3.8 Pre-reaction cyclovoltammetry of Cu bare (black), Ni bare (red), Calcined Cu (blue) and Calcined Ni (green) in NaOH 1M.

The same procedure and catalysts comparison were done for CV scans in lignin solution (Fig. 3.9). Common features for Ni-based and Cu-based catalysts were confirmed in lignin solution with respect to NaOH environment. In addition to the previous peaks, around 0.4 V there is lignin oxidation crest that can be noticed by comparing Inset 2 of Figure 3.8 with Inset 2 of Figure 3.9. Ni-based catalysts onset is observed at 0.5V and characteristic Ni^{2+}/Ni^{3+} peak at 0.35V. The onset in presence of Cu catalysts is shifted to 0.6V and Cu/Cu^+ couple at -0.2 V, as noticed in NaOH CVs.
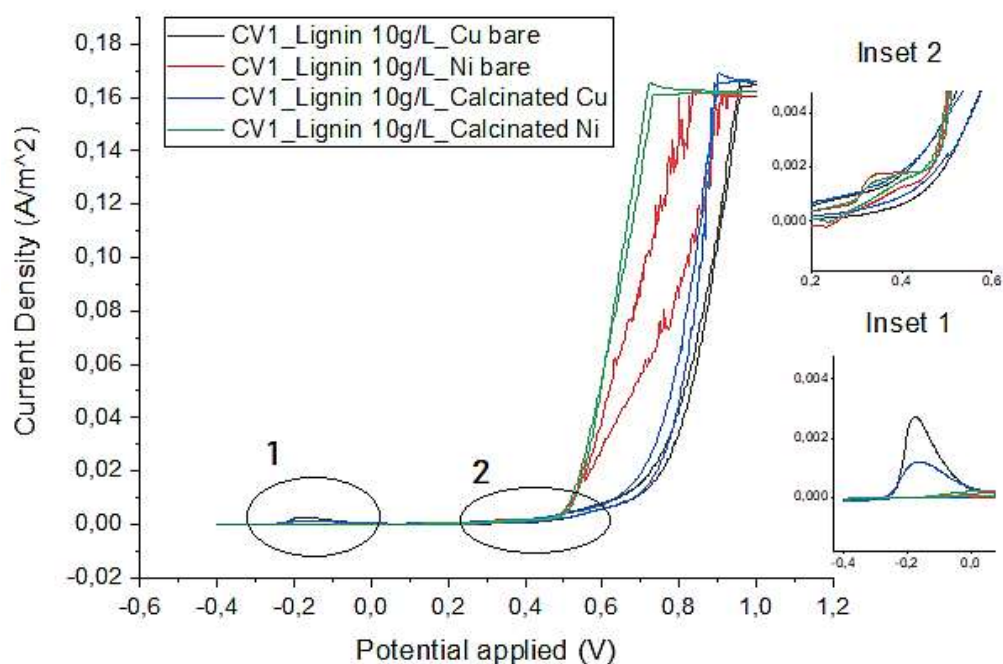

Figure 3.9 Pre-reaction cyclovoltammetry of Cu bare (black), Ni bare (red), Calcined Cu (blue) and Calcined Ni (green) in Lignin 10g/L.

3.3 Electrooxidation of Kraft lignin

Anodic potential values from 0.4 to 0.8 V vs SCE were tested for different reaction times of 60, 30 and 10 minutes, though chronoamperometry in 25 mL of lignin 10 g/L, as already described in Chapter 2.

The organic phase of reaction product was analyzed by GC-MS to quantify the most recurring products: vanillin, guaiacol, and acetovanillone. Yields of products were evaluated with respect to catalyst types and reaction conditions, and they were reported in Table 3.1 and Table 3.2 for 0.6 and 0.5 V vs SCE respectively.

Cu bare and calcined Cu catalysts were used to conduct lignin electrooxidation at 0.6 V vs SCE, varying the reaction time from 60 to 30 minutes (Table 3.1). Cu bare electrocatalyst did not produce detectable amount of guaiacol and acetovanillone at such reaction conditions. Since no observable changes in total products yield were observed with calcined Cu by lowering reaction time, 30 minutes were chosen due to time-saving reasons and to previous experimental thesis results.

Table 3.1 Lignin electrooxidation results at 0.6 V vs SCE

TIME	CATALYST	VANILLIN w/w%	GUAIACOL w/w%	ACETOVANILLONE w/w%	TOTAL w/w%
60 min	Cu bare	0.12	/	/	**0.12**
60 min	Cu calcined	0.18	0.18	0.81	**1.17**
30 min	Cu calcined	0.14	0.31	0.72	**1.17**

The potential was changed to 0.5 V vs SCE, resulting in improved vanillin, guaiacol and acetovanillone yields at reaction time of 30 minutes, with calcined Cu and Ni, reaching respectively a total yield of 1.23 and 1.65 w/w%. The samples listed in Table 3.2 were used to compare catalysts activity at the same reaction conditions of 30 minutes and 0.5 V vs SCE. These are not the best working conditions, hence a comparison between the four catalysts under not ideal parameters is possible and it is illustrated in Figure 3.10. With Cu bare catalyst no acetovanillone was detected, obtaining the smallest total yield of all. A yield increase was observed with calcined Cu, followed by calcined Ni catalyst. The better results were obtained by Ni bare catalyst (Ni bare > calcined Ni > calcined Cu > Cu bare).

Calcined Cu total yield was improved from 1.23 w/w% to 1.67 w/w% by decreasing reaction time to 10 minutes at 0.5 V vs SCE.

Table 3.2 Lignin electrooxidation results at 0.5 V vs SCE

TIME	CATALYST	VANILLIN w/w%	GUAIACOL w/w%	ACETOVANILLONE w/w%	TOTAL w/w%
30 min	Cu calcined	0.23	0.25	0.75	**1.23**
30 min	Ni calcined	0.3	0.51	0.84	**1.65**
30 min	Cu bare	0.18	0.14	/	**0.32**
30 min	Ni bare	0.39	0.75	0.59	**1.74**
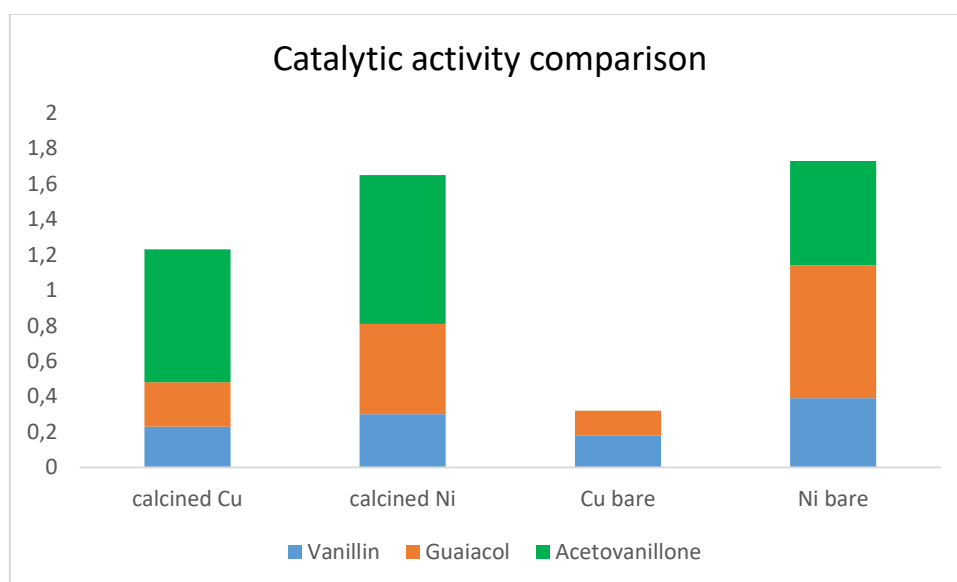
Figure 3.10 Catalytic activity comparison through products yields after chronoamperometry of lignin solution (10g/L) at 0.5 V and 30 minutes

Blank tests were performed to understand how lignin depolymerizes itself without applying current, in contact or not with the catalytic foam. The eventual catalyst was put in contact with NaOH 1M solution, then with lignin 10 g/L, to simulate the catalytic cycle, without applying current. Table 3.3 shows GC-MS results on the organic phases of blank tests. It can be deduced that lignin is able to be depolymerized in NaOH solution thanks to hydroxide ions, reaching a total product yield of 2.21 w/w%, even without catalyst in contact with solution. Higher yields have been reached with 10

minutes tests, probably because vanillin and similar structures have not enough time to rearrange together.

Table 3.3 GC-MS results of blank tests

CONDITIONS	VANILLIN w/w%	GUAIACOL w/w%	ACETOVANILLONE w/w%	TOTAL w/w%
60 min	0.15	0.68	0.37	**1.20**
10 min	0.34	0.6	1.27	**2.21**

To overcome total yields of blank test, electrocatalytic reactions beyond the onset potential value, at 0.7 (Table 3.4) and 0.8 V (Table 3.5) vs SCE, were performed at 10 minutes. The best result was reached over Ni bare catalyst at 0.7 V vs SCE and 10 minutes, obtaining a total yield of 2.97 w/w%. Resembling the 0.5 V samples, Cu bare catalyst led to lower yields with respect to calcined catalysts and Ni bare (Ni bare > calcined Cu = calcined Ni > Cu bare).

Table 3.4 Lignin electrooxidation results at 0.7 V vs SCE

TIME	CATALYST	VANILLIN w/w%	GUAIACOL w/w%	ACETOVANILLONE w/w%	TOTAL w/w%
10 min	Cu calcined	0.38	0.54	1.23	**2.15**
10 min	Ni calcined	0.46	0.45	1.24	**2.15**
10 min	Cu bare	0.34	0.44	0.8	**1.58**
10 min	Ni bare	0.49	0.86	1.62	**2.97**

Increasing the potential to 0.8 V led to a decrease of total yield with Ni bare catalyst and an increase with Cu bare catalyst. The total yield of 2.97 w/w% obtained previously at 0.7 V with Ni bare was not reached by none of the catalysts at 0.8 V vs SCE.

TIME	CATALYST	VANILLIN w/w%	GUAIACOL w/w%	ACETOVANILLONE w/w%	TOTAL w/w%
10 min	Cu calcined	0.38	0.54	1.3	**2.22**
10 min	Ni calcined	0.4	0.7	1.32	**2.42**
10 min	Cu bare	0.38	0.5	1.51	**2.39**
10 min	Ni bare	0.38	0.53	1.45	**2.36**

Given the best result with Ni bare catalyst at 0.7 V, reaction time was increased again to 30 minutes. The total yield was not higher (2.55 w/w%) but an increase for vanillin yield was observed, reaching 0.5 w/w%. Acetovanillone and guaiacol yields were slightly lower, hence 0.7 V and 10 minutes were considered as the best reaction conditions.

Trend of products distribution are analyzed in relation to applied potential in Figure 3.11 for Ni bare catalyst and to reaction time in Figure 3.12 for calcined Cu catalyst. Acetovanillone production is generally higher than vanillin and guaiacol yield, which has intermediate values between vanillin and acetovanillone.
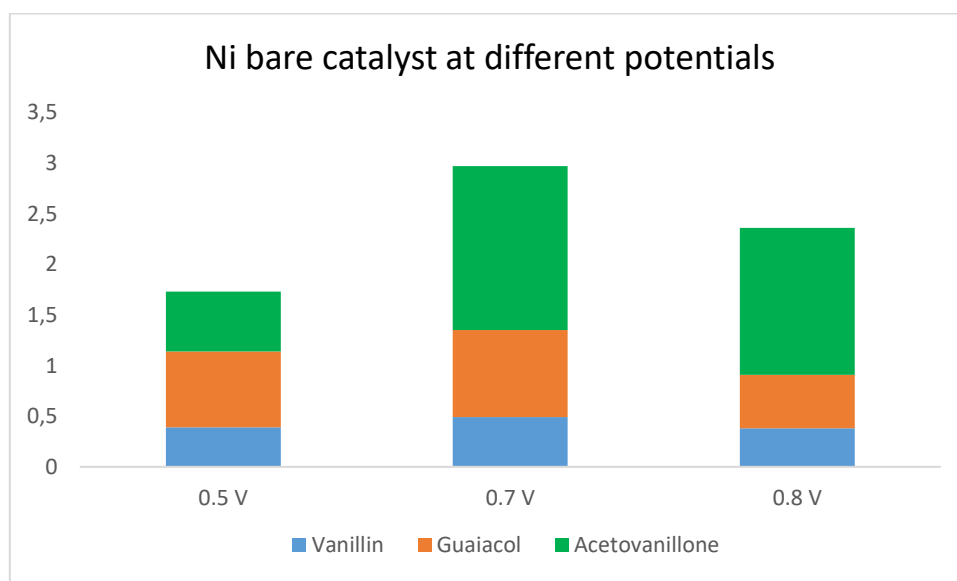

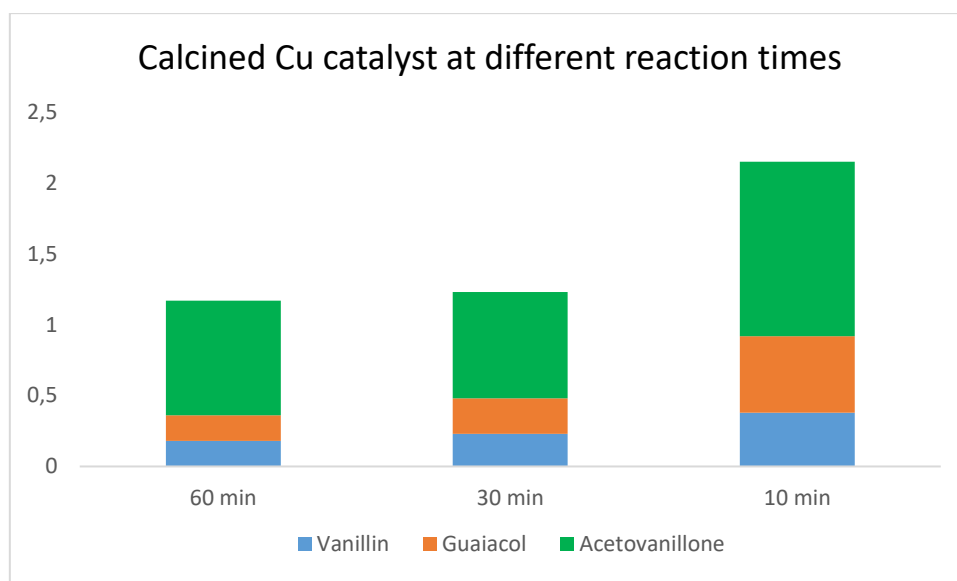Figure 3.11 Products yield and applied potential relationship

74

Figure 3.12 Products yield and reaction time relationship

There are other co-products and by-products in the product mixture from lignin depolymerization, such as acetic and formic acid, dimers and oligomers, hence it is not possible to perform an evaluation of the selectivity of electrooxidation. Moreover, only the organic phase of the extract has been quantified.

Aqueous phase was analyzed by ESI-MS, that did not reveal the presence of vanillin, but similar aromatic structures in the molecular weight range of 120-140 g/mol and some dimers.

3.4 Chemical-physical characterization of the catalysts after electrooxidation

Comparisons of SEM, XRD and Raman analyses of fresh and used catalysts are reported in this paragraph.

Cu bare catalysts comparison is shown in Figure 3.13, in which the used catalyst has more and smaller bubble cavities and its surface is damaged. Pre-reaction and post-reaction Ni bare comparison, in Fig. 3.14, did not reveal visible differences.
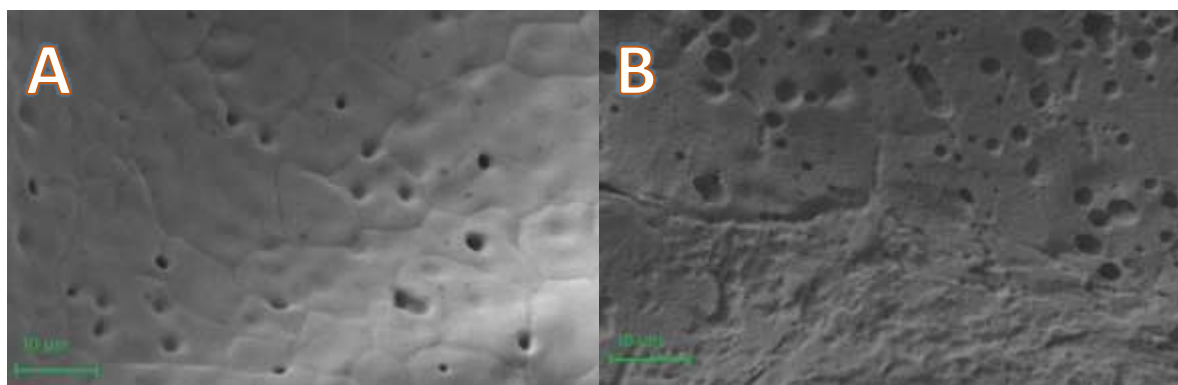
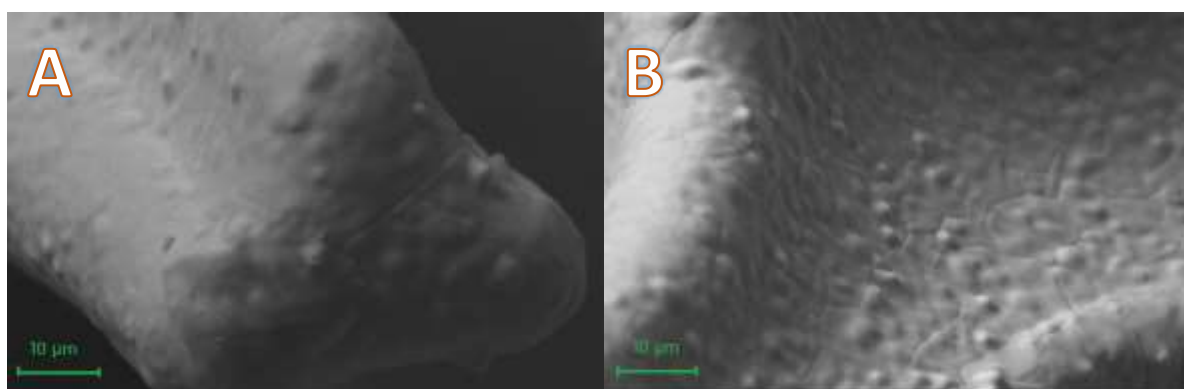*Figure 3.13 SEM secondary electrons characterization of fresh Cu bare (A) and post-reaction Cu bare (B).*

Figure 3.14 SEM secondary electrons characterization of fresh Ni bare (A) and post-reaction Ni bare (B).

In Figure 3.15 and Figure 3.16, pre- and post-reaction calcined Cu and Ni catalysts SEM comparisons are reported, observing the presence of darker regions in both Cu and Ni the post-reaction foams. By analyzing XRD pattern for post-reaction calcined Ni foam, no differences have been detected with respect to the fresh foam. XRD pattern of post-reaction calcined Cu foam in Figure 3.17 shows a tiny signal for carbon at 25 $2\theta°$ and oxide peaks intensities are bigger with respect to the fresh foam. Raman characterizations for calcined Ni foam (Fig. 3.17) highlighted the presence of D band at 1222 cm^{-1} and G band at 1566 cm^{-1}, of moderate intensity, typical of C-C aliphatic chains. Moreover, amorphous carbon band at 513 cm^{-1} was identified [63]. Hence the darker region noticed in SEM images have been identified as carbon. Raman characterization for calcined Cu foam was not reported because no characteristic shifts were detected.
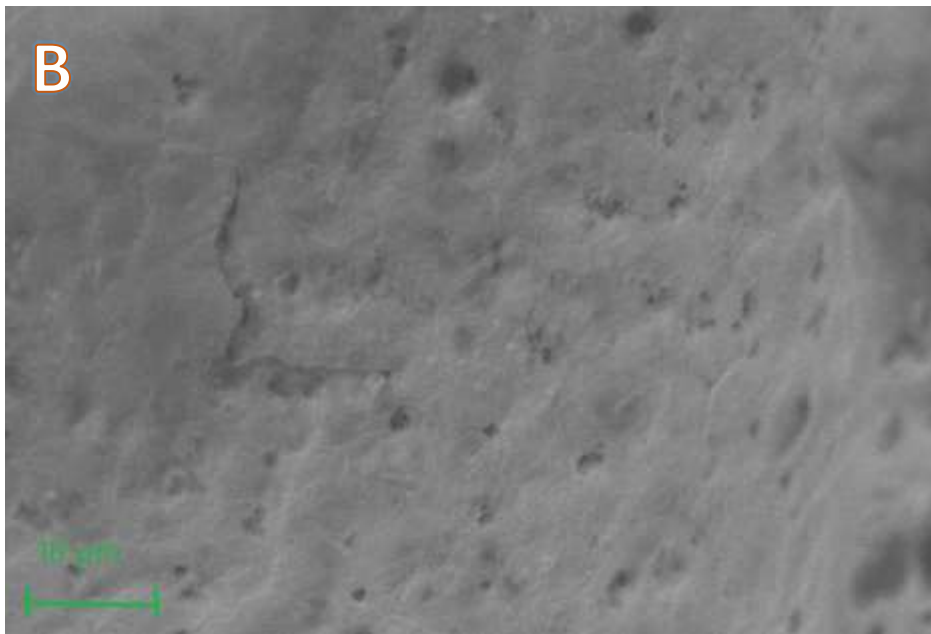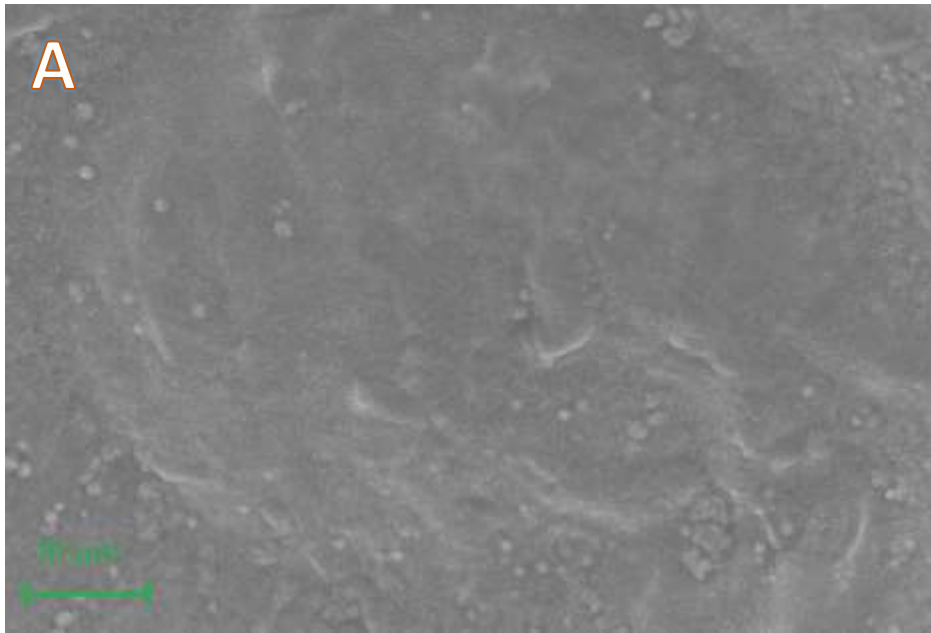
Figure 3.15 SEM secondary electrons characterization of fresh calcined Cu (A) and post-reaction calcined Cu (B).
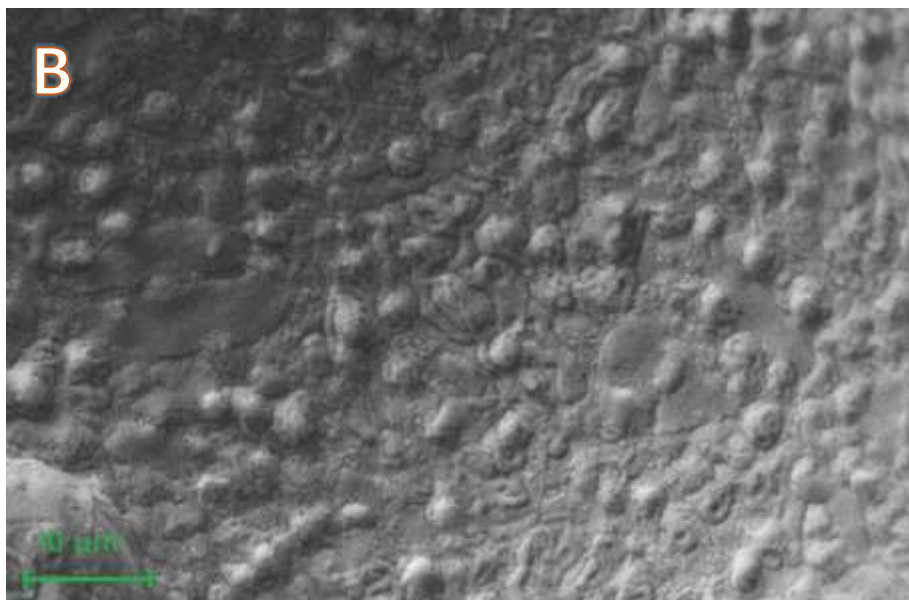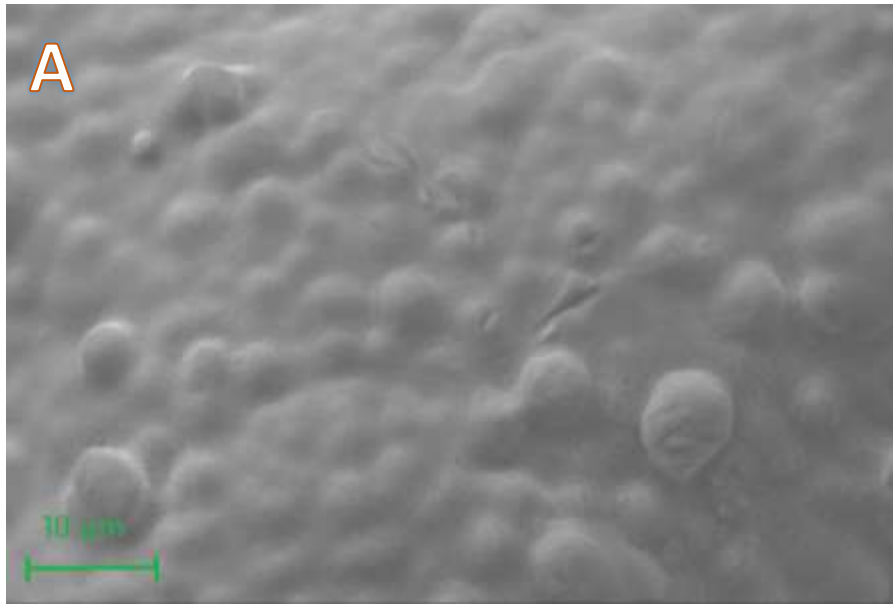
Figure 3.16 SEM secondary electrons characterization of fresh calcined Ni (A) and post-reaction calcined Ni (B).
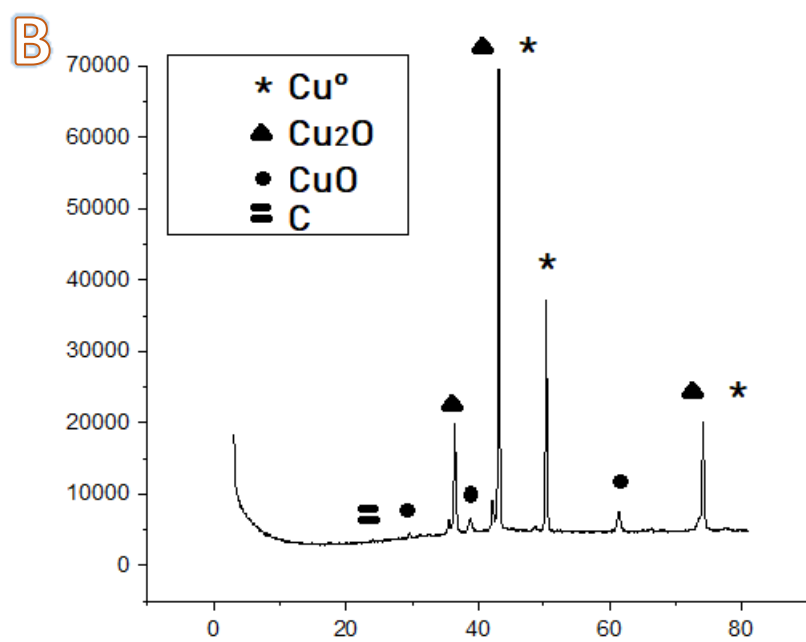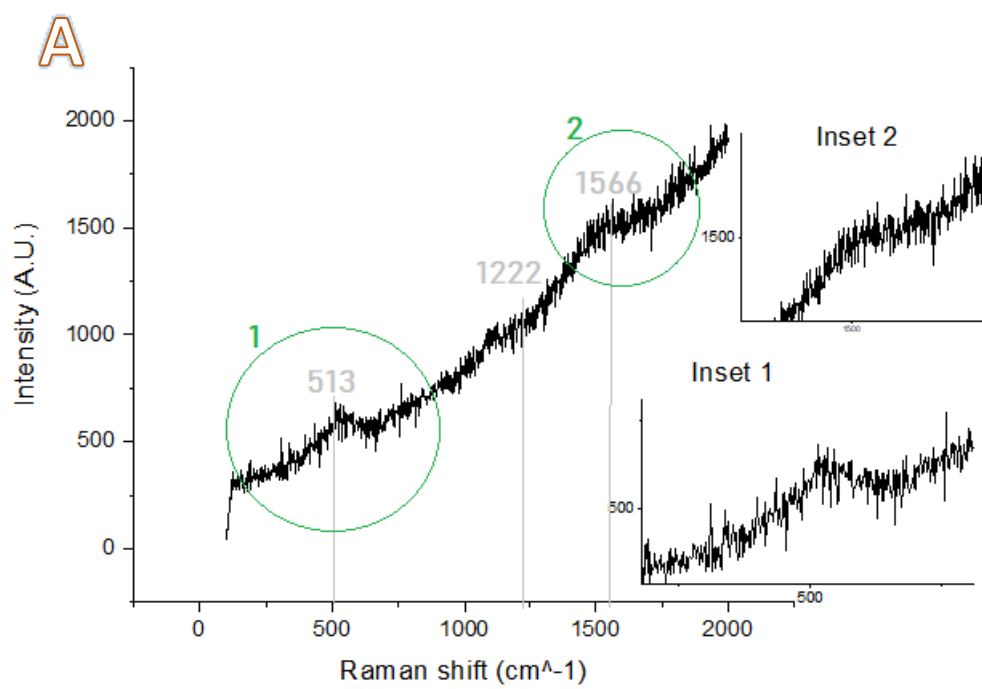
Figure 3.17 Raman characterization of post-reaction calcined Ni (A) and XRD characterization of post-reaction calcined Cu (B).

3.5 Electrochemical characterization of the catalysts after electrooxidation

Cyclovoltammetry scans after reaction are performed to electrochemically characterize the electrocatalyst after reaction. The procedure was identical to pre-reaction CV, but it is done by using the post-reaction catalyst.

From Figure 3.18 to Figure 3.25, post-reaction cyclic voltammograms are compared with pre-reaction ones for every catalyst type. In presence of Cu bare, the onset in post-reaction cyclic voltammogram is shifted to more anodic potential value in NaOH and the oxidation peak referred to Cu/Cu^+ oxidation results less intense. The opposite situation is observed with calcined Cu and calcined Ni, where the onset of post-reaction voltammogram falls at less anodic potential and the oxidation peak of the metal species is bigger. The shifting of the onset potential value to less anodic potentials could be explained as an activation toward lignin oxidation rather than OER. Pre- and post-reaction Ni bare in NaOH did not show differences. Performing only one catalytic cycle for every foam, no studies regarding the activation and deactivation of the catalysts have been conducted. Some differences between the pre- and the post- reaction cyclic voltammograms could be a reflection of the activation/deactivation of the electrocatalysts. Moreover, some trends could be a consequence of the different position of the electrodes in the cell setup during the catalytic cycle.
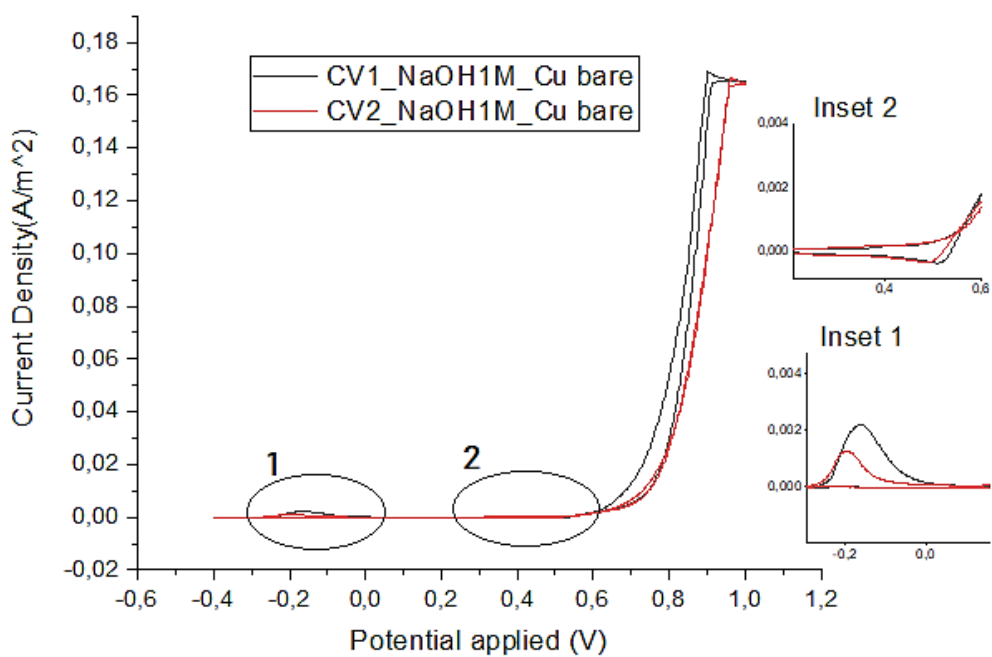
Figure 3.18 Cyclovoltammograms in NaOH 1M with Cu bare pre-reaction (black line) and post-reaction (red line).
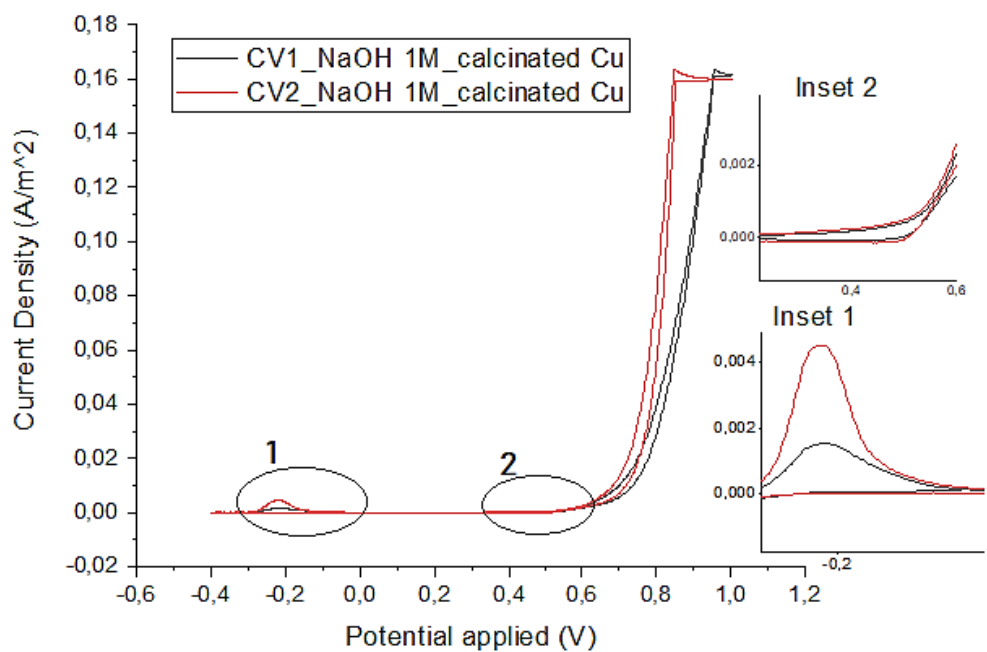

Figure 3.19 Cyclovoltammograms in NaOH 1M with calcined Cu pre-reaction (black line) and post-reaction (red line).

Figure 3.20 Cyclovoltammograms in lignin 10 g/L with Cu bare pre-reaction (black line) and post-reaction (red line).

Figure 3.21 Cyclovoltammograms in lignin 10 g/L with calcined Cu pre-reaction (black line) and post-reaction (red line).

Figure 3.22 Cyclovoltammograms in NaOH 1 M with Ni bare pre-reaction (black line) and post-reaction (red line).
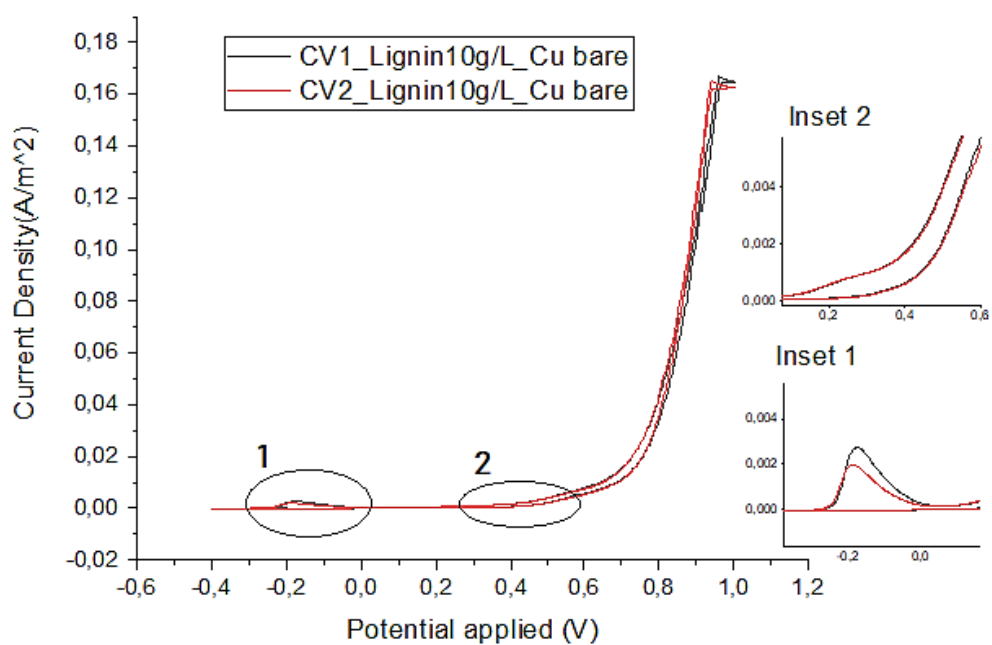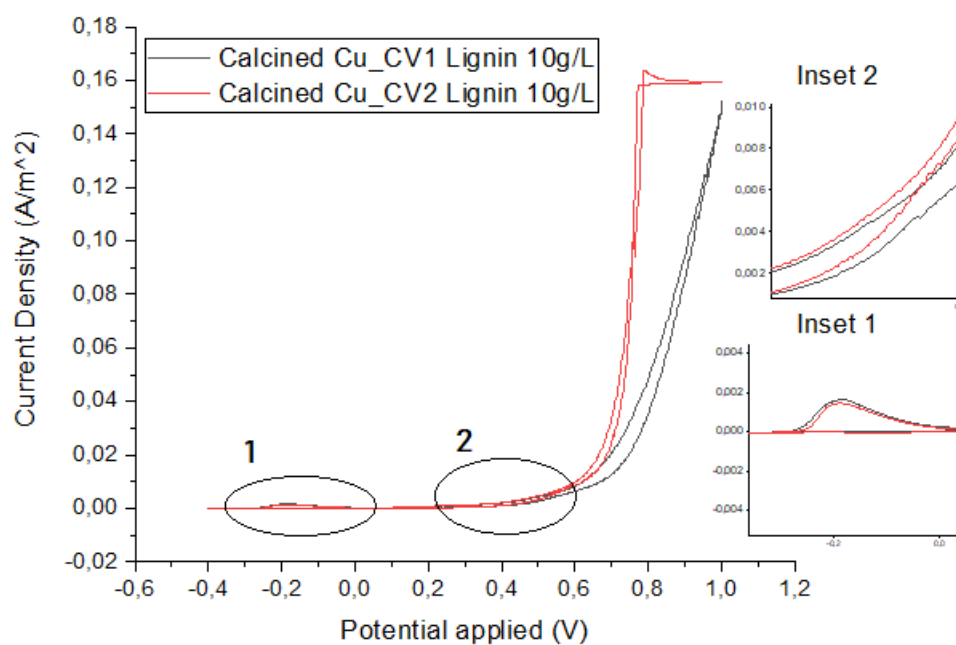

Figure 3.23 Cyclovoltammograms in Lignin 10 g/L with Ni bare pre-reaction (black line) and post-reaction (red line).

Figure 3.24 Cyclovoltammograms in NaOH 1 M with calcined Ni pre-reaction (black line) and post-reaction (red line).
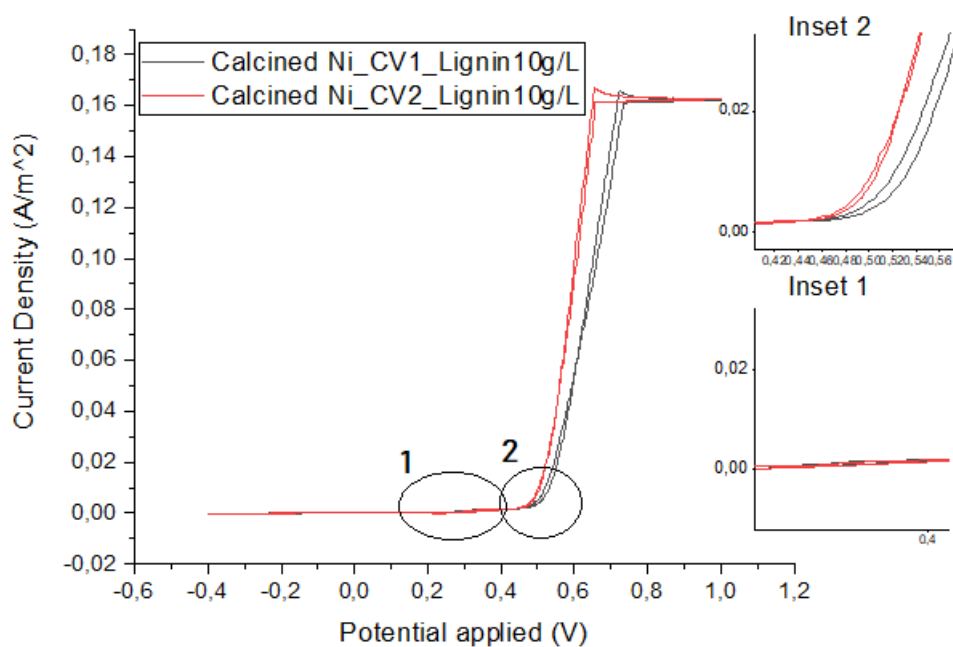
Figure 3.25 Cyclovoltammograms in Lignin 10 g/L with calcined Ni pre-reaction (black line) and post-reaction (red line).
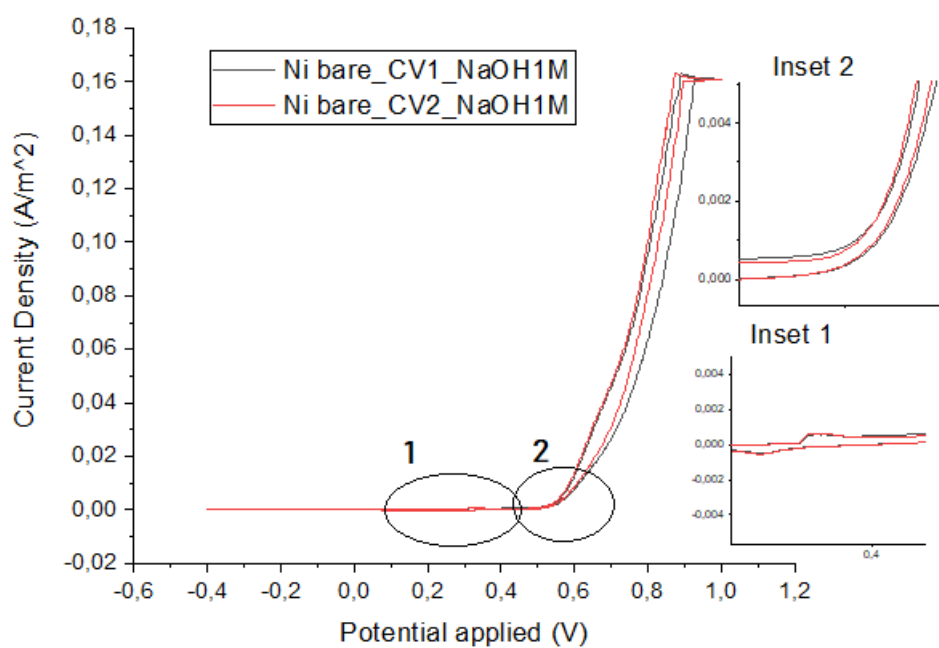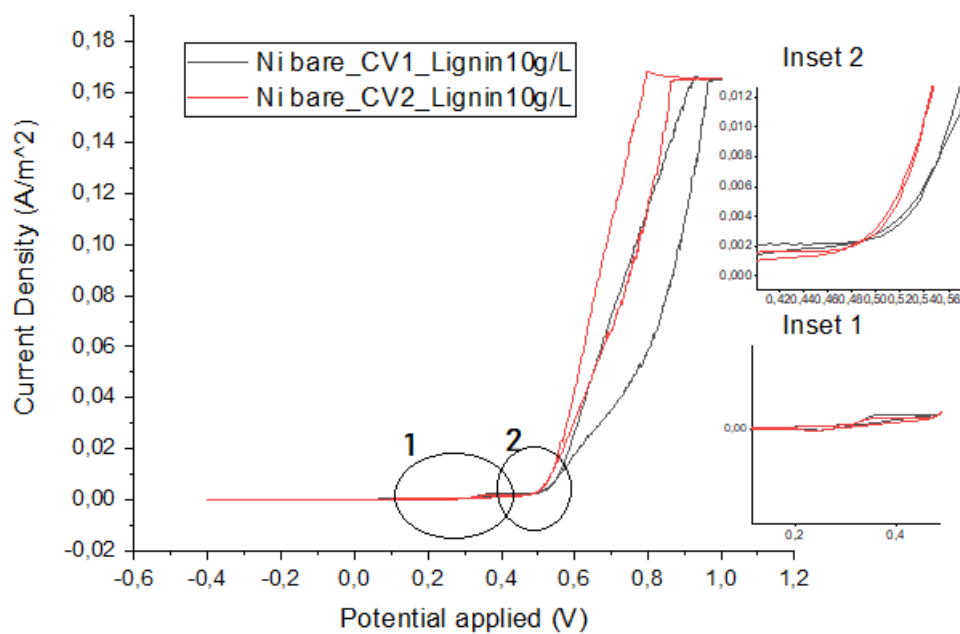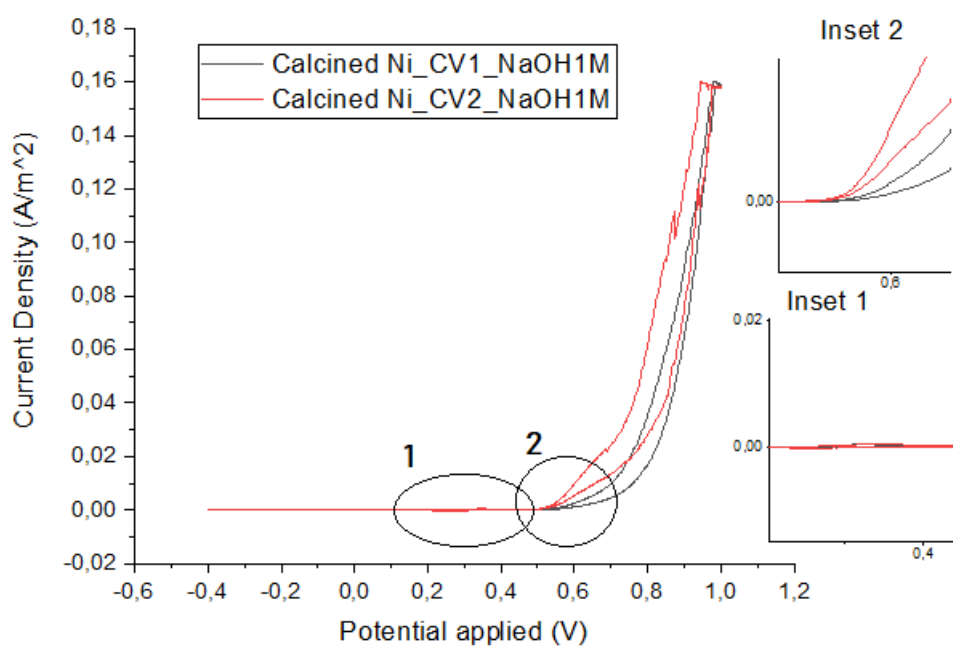
3.6 Lignin blank characterization

The same catalytic cycle simulation and extraction procedure were applied for ^{1}H NMR analysis of lignin blanks, prepared as it follows:

- Organic phase of lignin 10 g/L, in contact with Cu bare, in DMSO
- Organic phase of lignin 10 g/L, in contact with Ni foam, in DMSO

In both the samples, the presence of vanillin was detected, in line with GC-MS analysis (Table 3.3). The typical aldehydic and aromatic ring chemical shifts can be noticed respectively around 9.7 ppm and 7-8 ppm. Methoxy and hydroxyl groups are located around 4.5 and 7 ppm respectively.

4. Conclusions

The electrocatalytic oxidation of Kraft lignin in NaOH 1 M has been conducted into a three-electrode cell, over four different catalysts (Ni bare, Cu bare, calcined Ni and calcined Cu), to depolymerize lignin structure to aromatic building blocks. The most recurring products, vanillin, acetovanillone and guaiacol, were quantified by GC-MS, anyway some dimers and oligomers, acetic and formic acid were identified too.

Products yields depend on reaction conditions, applied potential, time and temperature, and on the electrocatalyst type. Electrocatalytic reactions were performed from 0.5 to 0.8 V vs SCE and from 10 to 60 minutes of reaction time. Blank tests were performed without applying potential, leaving 10 g/L lignin solution in NaOH 1 M for the required time, and analyzing the organic phase by GC-MS. Results on blank tests revealed that NaOH is able to depolymerize lignin structure, reaching a total yield of 1.20 w/w% in 60 minutes and a total yield of 2.21 w/w% in 10 minutes. It can be deduced that hydroxide ions in solutions can depolymerize the polymeric structure. Once depolymerized, the so-obtained products could rearrange and aggregate each other, hence increasing time of blank tests until 60 minutes, there is a decrease in vanillin, guaiacol and acetovanillone yield. By leaving lignin solution for only 10 minutes, fragments have not the necessary time to rearrange and total yield results higher.

The chosen best operating conditions (0.7 V vs SHE, 10 minutes) are based upon the blank tests results, in order to consider electrocatalysis effective on lignin oxidation and to associate the total product yield to the applied potential, together with NaOH action.

Electrocatalysts are characterized before and after electrocatalytic reactions and Ni bare was found to be the most active catalyst in lignin electrooxidation. The highest total yield of 2.97 w/w% was reached by means of Ni bare catalyst. Further studies on the selectivity toward a target product and on the catalytic runs could be conducted to better understand lignin electrooxidation behavior.

5. Bibliography

[1] Temperature Change and Carbon Dioxide Change, National Centers for Environmental Information NOAA

[2] CO_2 into atmosphere, ENEA

[3] National Centers for Environmental Information – National Oceanic and Atmospheric Administration (NCEI-NOAA)

[4] Le Quéré, C., Peters, G.P., Friedlingstein, P. *et al.* Fossil CO_2 emissions in the post-COVID-19 era. *Nat. Clim. Chang.* 11**,** 197–199 (2021)

[5] United Nations, The Sustainable Development Agenda

[6] Introduction to Climate Change, UNEP

[7] Environmental sustainability and the preservation of capacities. The case of ecological assimilative capacity in the economic analysis of optimal pollution, Marc Leandri, June 2009

[8] Office of Fossil Energy and Carbon Management, Carbon Utilization

[9] Carbon capture, utilisation and storage, European commission

[10] Biomass, R.A. Houghton, Encyclopedia of Ecology, 2008, 448-453

[11] Intro to photosynthesis, Khan Academy

[12] IEA. IEA bioenergy Task 42 on biorefineries: co-production of fuels, chemicals, power and materials from biomass. In: Minutes of the third Task meeting, Copenhagen, Denmark, 25–26 March 2007

[13] The biorefinery concept: using biomass instead of oil for producing energy and chemicals, Energy conversion and Management, Volume 51, Issue 7, July 2010, 1412-1421, Francesco Cherubini

[14] A comprehensive review on the implementation of the biorefinery concept in biodiesel production plants, Christian David Botero Gutiérrez, Daissy Lorena Restrepo Serna, Carlos Ariel Cardona Alzate, Biofuel research journal, Volume 4, Issue 3, 691-703

[15] An Overview of Biorefinery Derived Platform Chemicals from a Cellulose and Hemicellulose Biorefinery, Sudhakar Takkellapati, Tao Li, and Michael A. Gonzalez, Clean Technol Environ Policy. 2018 Sep; 20(7): 1615–1630

[16] Biorefinery, the future of chemical process industries, Alexandre C. Dimian, Research Gate

[17] The potential role of waste biomass in the future urban electricity system, Yu Jiang, Edwin van der Werf, Ekko C.van Ierland, Karel J.Keesman, Biomass and Bioenergy, Volume 107, December 2017, 182-190

[18] Lignocellulose, Advances in Bioenergy, 2019

[19] A review on common adsorbents for acid gases removal: Focus on biochar, June 2017, Renewable and Sustainable Energy Reviews 81, Hanieh Bamdad, Kelly Hawboldt, Stephanie MacQuarrie

[20] Lignin Degradation Processes and the Purification of Valuable Products, Stefan Schoenherr, Mehrdad Ebrahimi, Peter Czermak

[21] Antioxidant properties of lignin, G.L. Catignani, M.E. Carter, J. of Food Sci., Vol 47, 1745 (1982)

[21a] Chem. Rev. 2018, 118, 614−678

[22] Linger, J. G.; Vardon, D. R.; Guarnieri, M. T.; Karp, E. M.; Hunsinger, G. B.; Franden, M. a.; Johnson, C. W.; Chupka, G.; Strathmann, T. J.; Pienkos, P. T.; et al. Lignin Valorization through Integrated Biological Funneling and Chemical Catalysis. Proc. Natl. Acad. Sci. U. S. A. 2014, 111, 12013−12018.

[23] Chem. Eng. Technol. 2011, 34, No. 1, 29–41

[24] Nicholas J. Walton, Melinda J. Mayer e Arjan Narbad, Vanillin, in *Phytochemistry*, vol. 63, n. 5, pp. 505–51

[25] Dixon, R.A. (2014). "Vanillin Biosynthesis – Not as simple as it seems?" Archiviato il 14 giugno 2015 in Internet Archive. (PDF). Handbook of Vanilla Science and Technology: 292

[25a] Journal of Food and Frug analysis 23 (2015) 176-190

[26] American Chemical Society, What is Green Chemistry?

[27] CHEM-E4185 - Electrochemical Kinetics, 19.02.2018-23.05.2018

[28] An integrated electrochemical process to convert lignin to value-added products under mild conditions, May 2016, DOI: 10.1039/c6gc00878j

[28a] Nickel/Copper Plated Contacts as an Alternative to Silver Screen Printing for the Front Side Metallization of Industrial High Efficiency Silicon Solar Cells, Loic Tous

[29] Electrochemical Lignin Conversion, ChemSusChem 2020, 13, 4318–4343, Wiley Online Library

[30] Beilstein J. Org. Chem. 2015, 11, 473–480. doi:10.3762/bjoc.11.53

[31] An integrated electrochemical process to convert lignin to value-added products under mild conditions DOI: 10.1039/c6gc00878j, Green Chemistry, 2nd May 2016

[32] Electrochemical conversion of lignin to useful chemicals, Omar Movil-Cabrera, Allen Rodriguez-Silva, Christian Arroyo-Torres, John A. Staser, Biomass and Bioenergy, 88 (2016) 89-96

[33] International journal of hydrogen energy 40 (2015) 4519-4530, Omar Movil, Michael Garlock, John A. Staser

[34] ACS Omega 2020, 5, 31684−31691

[35] European Biomass Industry Association, Challenges related to biomass

[36] Aryama Raychaudhuri and Sadhan Kumar Ghosh. Biomass Supply Chain in Asian and European Countries. Procedia Environmental Sciences 35 (2016) 914 – 924

[37] IEA Bioenergy, 2011, Kankkunen, Miikkulainen

[38] T. Voitl, P.R. von Rohr, Demonstration of a process for the conversion of kraft lignin into vanillin and methyl vanillate by acidic oxidation in aqueous methanol, Ind. Eng. Chem. Res. 49 (2010) 520-525.

[39] ChemBioEng Rev 2015, 2, No. 6, 377–392

[40] Y. Zhao, Q. Xu, T. Pan, Y. Zuo, Y. Fu, Q.-X. Guo, Depolymerization of lignin by catalytic oxidation with aqueous polyoxometalates, Appl. Catal. A 467 (2013) 504-508.

[41] Bourbiaux D, Pu J, Rataboul F, Djakovitch L, Geantet C, Laurenti D, Reductive or oxidative catalytic lignin depolymerization: an overview of recent advances, Catalysis Today (2021), doi:https://doi.org/10.1016/j.cattod.2021.03.027

[42] J. Zhang, H. Deng, L. Lin, Wet aerobic oxidation of lignin into aromatic aldehydes catalyzed by a Perovskite-type oxide: LaFe1-xCuxO3 (x = 0, 0.1, 0.2), Molecules 14 (2009) 2747-2757.

[43] J. Luo, P. Melissa, W. Zhao, Z. Wang, Y. Zhu, Selective lignin oxidation towards vanillin in phenol media, Chem. Select 1 (2016) 4596-4601.

[44] L. Hdidou, L. Kouisni, B. Manoun, H. Hannache, A. Solhy, A. Barakat, Oxidative conversion of lignin over cobalt-iron mixed oxides prepared via the alginate gelation, Catal. Commun. 117 (2018) 99-104.

[45] Catalysis Today 352 (2020) 95–103

[46] Organic Process Research & Development 1999, 3, 330−340

[47] Chemical engineering research and design   8 7(2009)1276–1292

[48] Catalysis Today 189 (2012) 123– 128

[49] Pine research, Normal Pulse Voltammetry

[50] H. H. Girault, 2004, Analytical and Physical Electrochemistry

[51] Journal of Applied Electrochemistry (2021) 51:51–63

[52] ACS Sustainable Chem. Eng. 2018, 6, 7565−7573

[53] Electrochemistry Communications 00 (2017) 1–8

[54] J. Chem. Educ. 1972, 49, 8, A413

[55] Deformation and damage mechanisms of ODS steels under high-temperature cyclic loading, DOI:10.5445/IR/1000080339

[56] J. Chem. Educ. 1958, 35, 2, 80

[57] Bragg Condition/Law/Bragg Scattering/Bragg angle - Practical Electron Microscopy and Database

[58] Guide to raman spectroscopy, Bruker

[59] What is raman spectroscopy, Jasco

[60] J. Chem. Educ. 2018, 95, 197−206

[61] Electrochemical detection techniques in biosensor applications, Behzad Rezaei PhD, Neda Irannejad

[62] D. A. Skoog, J. F. Holler, S. R. Crouch, and L. Sabbatini, Chimica analitica strumentale. Napoli: Edises, 2009.

[63] Raman band correlation table, UCI, Department of Chemistry

[64] Fabrication of Nanosized Cuprous Oxide Using Fehling's Solution, Mohammad Kooti

[65] DOI: 10.1002/cctc.201901394

[66] ACS Catal. 2016, 6, 2473-2481